CLEAN WATER

WATER POLLUTION CONTROL RESEARCH SERIES ● 15080-EPL 04/70

PB192852

W 70-08163

SPREADING AND MOVEMENT OF OIL SPILLS

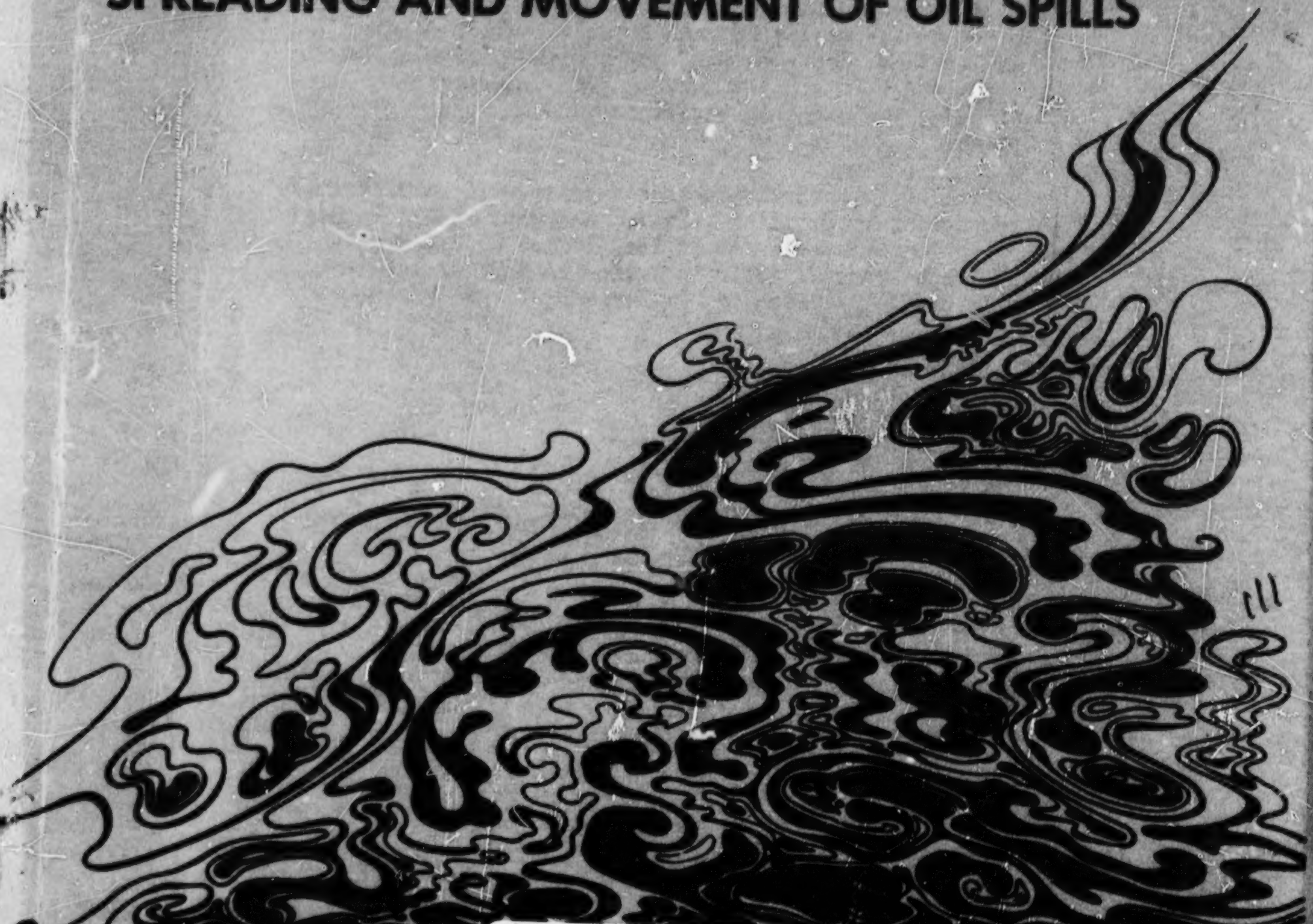

Reproduced by the
CLEARINGHOUSE
for Federal Scientific & Technical
Information Springfield Va. 22151

WATER POLLUTION CONTROL RESEARCH SERIES

The Water Pollution Control Research Reports describe the results and progress in the control and abatement of pollution of our Nation's waters. They provide a central source of information on the research, development and demonstration activities of the Federal Water Pollution Control Administration, Department of the Interior, through inhouse research and grants and contracts with Federal, State, and local agencies, research institutions, and industrial organizations.

[redacted]

SPREADING AND MOVEMENT OF OIL SPILLS

FEDERAL WATER POLLUTION CONTROL ADMINISTRATION
DEPARTMENT OF THE INTERIOR

by

Henry G. Schwartzberg
Chemical Engineering Department
New York University

Program Number 150 80
Contract Number WP 01342-01A

March 1970

FWPCA Review Notice

This report has been reviewed by the Federal Water Pollution Control Administration and approved for publication. Approval does not signify that the contents necessarily reflect the views and policies of the Federal Water Pollution Control Administration, nor does mention of trade names or commercial products constitute endorsement or recommendation for use.

ABSTRACT

The spreading and movement of oil spills on water were investigated. Areas for spills which form lenses were measured and correlated. ~~in Equations (8) and (51)~~. Most crudes tested formed thin films, not lenses; but lens formation could be induced and spreading greatly reduced by surfactant treatment.

Spreading rates for small spills were measured and correlated with spill volume, oil density and water viscosity ~~- Equation (53).~~ Field data and energy conservation, however, indicates ~~Equation (53~~) cannot be scaled up to large spill volumes.

Wind-water basin tests indicated that on quiet open water oil should drift windward at 3.66 ± .17% of the wind velocity. The percentage drift was not significantly affected by oil or water properties, depth, and wind speed, and agrees fairly well with field data. Waves caused significant reductions in wind drift, but in the shallow basin used did not induce significant drift themselves. Since wind causes waves, and deep water waves cause drift, further investigation of wind and wave drift interaction is recommended.

Wind drift was found to be confined to a thin surface layer. The use of 1 - 1 1/2 inch deep oil-confining drogues markedly reduced wind drift. Investigation of the use of nets of such drogues and of lens formation to reduce oil spread and movement is recommended.

Combined wind and current drifts were found not to be ~~directly additive, and were~~ roughly correlated by Equation ~~(72)~~.

This report was submitted in fulfillment of project WP 01342-01A between the Federal Water Pollution Control Administration and New York University.

KEY WORDS

Oil Spills
Oil on Water
Oil Spill Areas
Oil Spill Spreading Rates
Oil Spill Drift
Oil Lenses
Wind Drift
Wave Drift
Combined Current Wind Drift
Wind Wave Drift Interactions

CONTENTS

Page
Abstract iii
Section 1. Conclusions and Recommendations 1
Section 2. Introduction 4
Section 3. Body of Report 7
  Analysis of Prior State of Knowledge 7
    Spread 7
    Spreading Rates 18
    Drift-Wind Effects 22
    Drift-Current Effects 26
    Drift-Wave Effects 27
  Experimental 32
Section 4. Discussion of Results 47
    Lenses 47
    Crude Oils 59
    Crude Oil Spreading Rates 63
    Wind Drift 78
    Wave Drift 90
    Current Drift 92
    Combined Wind-Current Drift 93
References 96
Notation 100

TABLES

No.	Title	Page
1	Spill Volumes and Distances Traveled by Recent Oil Spills	5
2	Oil Drift vs Wind Speed	23
3	Estimated Wave Drift for Fully Developed Wind Waves	29
4	Lens Characteristics	51-52
5	Characteristics of Crudes	60
6	Area Spreading Rates as a Function of Oil Density	67
7	Area Spreading Rates vs Temperature for 100 cm^3 Pools of Fullerton Crude	72
8	Relative Drift Rates	89
9	Combined Wind and Current Drift	94

FIGURES

No.	Title	Page
I.	Lens Cross Section	7
II.	Neumann's Triangle	10
III.	Lens Angle	11
IV.	Test Basin Layout	37
V.	Wind Duct Support System	39
VI.	Transition Piece Arrangement	41
VII.	Wave Machine	42
VIII.	Wind-Water Tunnel	45
IX.	Different Lens' Shapes	47
X.	Log Volume vs Log Diameter for Light Paraffin Oil on Water	49
XI.	Log Volume vs Log Diameter for Water on Dibutyl Phthalate	50
XII.	Generalized Value vs Diameter Correlation for Lenses	57
XIII.	Pool Area vs Time for 100 cm^3 Pools of Various Crudes	65
XIV.	Spreading Rate vs Density Factor	66
XV.	Oil Spreading Rates (parameter volume of spill)	69
XVI.	Initial Spreading Rate vs Pool Volume	70
XVII.	Spreading Rates for 100 cm^3 Pools of Fullerton Crude vs Viscosity of Underlying Water	73
XVIII.	Disc Model of Spreading Pool	75
XIX.	Percent Drift vs Wind Speed	76
XX.	Velocity Profile of Air-Water System	81
XXI.	Draggers	91

SECTION 1

CONCLUSIONS AND RECOMMENDATIONS

1. The diameter of floating pools of oil which form lens (those for which $\sigma_L - \sigma_u - \sigma_i > 0$) can be approximately predicted as function of spill volume through the use of Equation (8), derived from Hardy's asymptotic lens thickness correlation.

2. Lens diameter vs volume can be more accurately predicted using Equation (53) a simple but fairly accurate approximation developed from Langmuir's more exact but complicated equations for lenses.

3. A fair number of crudes form lens like pools on water on which an oil film has previously been deposited, but most crudes will not form lenses on clean water. Crude oils which do not form lenses will ultimately form films roughly 0.013 to 0.041 mm (0.0005 to 0.0016 in.) thick.

4. Crudes can be induced to form lenses by treating the surrounding water with a surfactant which sufficiently lowers the water surface tension σ_L without excessively lowering the interfacial tension σ_i, (i.e. which causes $\sigma_L - \sigma_u - \sigma_i$ to become positive). Such lenses will be forty to one hundred times thicker than the thin films which would develop in the absence of lens formation, and the area of coverage and pollution will be reduced by a similar factor. Surfactant induced lens formation may represent a useful technique for minimizing the spread and area of pollution of oil films.

5. Small scale crude oil spills, will after an initial induction period (in which energy conversion limits the rate of spread), spread so that the pool area increases at a constant rate with respect to time. This constant rate is a function of oil and water density, spill volume, and water viscosity namely

$$\frac{dA}{d\Theta} = \frac{K}{\mu_w} \left[\left(1 - \frac{\rho_u}{\rho_L} \right) \rho_u \, V \right]^{1.8}$$

This constant spreading rate is ultimately followed by a lower spreading rate which has not yet adequately been correlated. For oils that are susceptible to the induction of lens formation the area of spread may approach a constant value.

The preceding equation predicts excessively rapid spreading rates for large volume spills, and another correlation - perhaps that characterizing the lower secondary spreading rate mentioned above - must apply to larger volume spills.

6. Wind will cause oil pools to drift on relatively calm water in the direction of the wind at a velocity equal to 3.66% ± .17% of the wind velocity - a figure which is in good agreement with those reported for the Torrey Canyon drift. Waves will cause significant reductions in the rate of wind induced drift, but this wave wind-drift interaction has not been adequately correlated yet.

7. Though negligible wave induced drift was noted in the present test work, on the basis of past work by other investigators it appears that significant wave induced drift is likely to occur in deep water. The measurement and correlation of wave drift and wave-wind drift interactions will require testing in deep water basins.

8. Wind induced drift and current induced drift are not simply additive. The data obtained to date is roughly correlated by the equation

$$T = W + 0.56\ C$$

where T is the total drift, W the wind drift and C the current drift. Though this equation must break down as W goes to zero, no significant change in the coefficient for C was observed when W was varied. The above correlation is suspect.

9. Oil tends to drift at a slightly slower speed than solid object floating in a current in the absence of wind. In the case of wind induced drift, oil will drift slightly faster than solid objects floating on the surface.

10. Wind induced drift is confined to a thin layer near the surface of the water, and shallow floats which confine the oil and have drag surfaces penetrating one or two inches down into the water will substantially reduce (e.g. by 50%) wind induced oil pool drift. Floating nets of such draggers may represent a feasible means of greatly reducing the drift and also the spread of oil spills.

It is recommended that:

1. The wind drift correlation be substantiated by testing in a longer (e.g. 40 ft. long) wind-water test basin of improved design. This should insure the attainment of steady conditions, the detection of fetch effects, and increased accuracy.

2. Wave drift and wave-wind drift interactions be investigated using a deep water (e.g. 6 ft. deep) wind wave test basin. Correlation of such drift and interaction appears necessary in order to adequately predict oil pool drift.

3. The drift correlations developed herein be verified by comparison with available field data.

4. Efforts be made to systematically obtain records of the wind, wave, current and tide conditions in the area of accidental spills and the corresponding travel and spread of such spills. This field data should be used for further improvement and verification in correlations for spreading and movement.

5. That the feasibility of surfactant induced lens formation, and drag networks for limiting the spread and movement of spilled oil be investigated.

6. That spreading rate measurements be made on spills of larger volume than tested in this work and that a spreading rate correlation suitable for large volume spills be developed.

SECTION 2

INTRODUCTION

The spillage of oil at sea and in estuarine and coastal waters has occurred with increasing frequency in recent years. To a certain extent deliberate spillage due to dumping, the pumping out of bilges and tank bottoms, has been curtailed by international convention (42) and the use of slop collection tanks at refineries and terminals. However the advent and increasing use of large tankers and off-shore drilling has greatly increased the probability of accidental large scale spillage.

Table I represents a list of major spills and some typical minor spills which have occurred in recent years. Also listed are the estimated spill volumes, and, where available, the longest distance which the spill traveled while still in a reasonably coherent or identifiable form. Detectable spills of some magnitude occur almost every week along the Northeast Coast of the United States.

Not only have very large spills occurred but these spills have often traveled considerable distances. In addition to those spills listed in Table I, spill travels of 500 miles have been reported by Egyptian authorities, 50 miles by Canadian authorities (42), and Stroop (71) has tracked oil slicks for up to ninety miles from the point of spillage.

In the case of very large spills oil concentration remains at a noxious level even when the spill is dispersed over a very large area. As the area of spread becomes larger, dispersion by the turbulent diffusive action of the sea becomes progressively less efficient; and greatly increased time is required for the oil concentrations to fall to a non-noxious level. Thus large spills persist as identifiable entities for long distances and times.

Until recently the use of detergents to induce and aid dispersion and to clean contaminated shorelines has been the primary method of combatting spills. For large spills this practice has proved increasingly ineffective. The oil, while dispersed into droplets or emulsified, persists at higher than tolerable concentrations until spatially dispersed by turbulent diffusion. For large spills this occurs so slowly that clean shorelines are frequently polluted or repolluted by redeposition of oil washed off previously fouled shores. In other instances the use of detergents led to the formation of persistent water in oil emulsions

Table I. Spill Volume and Distance Traveled for Recent Oil Spills

Date	Spill Source	Location	Spill Volume Gallons	Maximum Distance of Travel
3/18/67	Torrey Canyon (tanker)	Cornwall, England	49,200,000	350 miles [+]
3/7/68	General Colocotronis (tanker)	Eleuthra Island, Bahamas	610,000 to 1,250,000	10 miles
3/3/68	Ocean Eagle (tanker	San Juan, Puerto Rico	1,000,000 to 2,800,000	
3/57	Tampico Maru (tanker)	Baja, California	1,680,000	
2/1/69 to 4/69	Union Oil Well	Santa Barbara Channel	7,000,000 [0]	30 miles
3/16/69	Mobil-Newmont Oil Well	Louisiana Coast	?	5 miles
7/23/69	Unknown Ship	Atlantic City, New Jersey	?	45 miles
1/21/69	Unknown Ship	New London, Connecticut	?	20 miles
1955	Gerd Maersk (tanker)	North Sea near Germany	1,900,000	

[+] Gross distance traveled by oil which came ashore at Pointe du Raz and the Crozon peninsula on 5/19/67 and 5/20/67 52 to 55 days after 3/26-29/69 the probable dates of release from the Torrey Canyon.

[0] My estimate based on the reported area ultimately covered by the spill.

("mousses") and actually retarded dispersion. Further in many instances detergents have proved to be toxic and more injurious to marine life than the oil itself.

These facts clearly imply the need for new or revised techniques for combatting oil spills, for developing criteria as to which technique or techniques should be used, and for efficiently deploying the resources needed to implement these techniques.

The choice of technique and the efficient deployment of resources for combatting spills depends in a large measure on the rate and extent of spread and the direction and velocity of spill movement. Further, from the point of view of law enforcement, detection of the source of a spill of unknown origin can be greatly facilitated if rates of spread and movement are known and can be predicted.

Until recently very little was known regarding spread and movement. A few experiments (71) have been carried out on the rates of spread and movement, but most of these were qualitative and inconclusive.

The extent of spread of pure substances, particularly those forming either coherent monomolecular films or thick stable lens like pools can be predicted. Crudes and fuel oils, however, are complex mixtures and the spread correlations for pure substances cannot readily be used except to provide a theoretical framework for analysis.

Field records and observations for a number of major spills have recently become available (after the start of this investigation). Based on these records certain qualitative predictions can be made regarding spill spread and movement (66). But these predictions are rough and based on average values. Deviation from these average values are large and the causes for deviation are not readily apparent.

It therefore appears that, in spite of this new field data, considerable uncertainty remains regarding spill spread and movement, and that reliable predictive correlations are not yet available for such spread and movement. The work described herein aims at developing such correlations. It is directed towards empirically identifying, and at least roughly correlating all major factors influencing spread and movement. It is based on small scale test basin work, and in common with all scaled down experiments involves questions as to the validity of scale-up. Wherever possible attempts were made to resolve such questions experimentally or theoretically, but in many instances the ultimate test of validity will have to be made on the basis of comparison with available field data. Such comparison is recommended for future work.

SECTION 3

BODY OF REPORT

Analysis of Prior State of Knowledge

Spread

The spreading of a pure liquid or liquid mixture of stable composition on the surface of another liquid with which it is immiscible (e.g. oil on water) is determined primarily by the surface and interfacial tension imbalance set up between the liquids (32). If one considers a half cross section of a pool of floating liquid and its substrate, such as shown in Figure I, the nature of the surface tension imbalance can readily be seen. At some distance from the pool the surface of the lower layer is horizontal, and σ_L its surface tension acts horizontally. At the center of the pool σ_u, the surface tension of the upper layer and σ_i the interfacial tension also act horizontally.

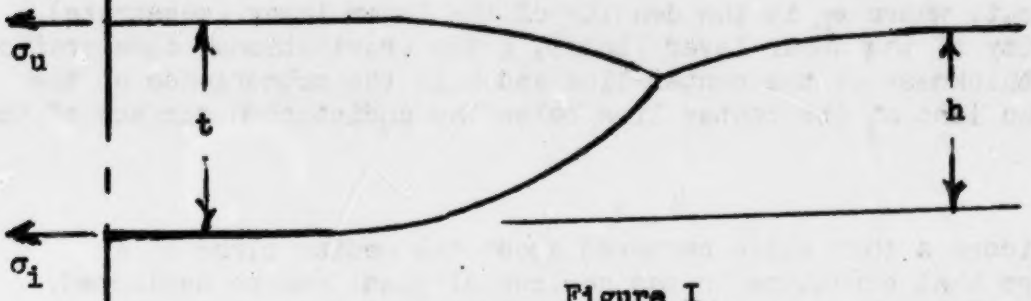

Figure I

σ_L acts to expand the pool, and σ_u and σ_i to contract it. Thus if the surface tension imbalance $(\sigma_L - \sigma_u - \sigma_i)$, sometimes also called the spreading force, is positive the pool will spread. If it is negative the pool will contract until the surface tension forces are counteracted by hydrostatic pressure, thus producing a pool which looks like a doubly convex lens. Such pools are therefore called lenses.

Lenses

The force balance which determines the equilibrium thickness of a lens provides insight into the type of forces which are operative in controlling both the equilibrium spread and the rate of spread of oil pools of all types, both lens forming and free spreading, and will therefore be considered in some detail.

In general a pressure difference exists across curved interfaces (3). This pressure difference is given by the equation

$$\Delta P = \sigma \left[\frac{1}{R_1} + \frac{1}{R_2} \right] \qquad (1)$$

where σ is the appropriate surface or interfacial tension and R_1 and R_2 the local radii of curvature of the interface. For relatively large pools, the surfaces at the center may be considered horizontal planes. In such a case, at the center line R_1 and R_2 are infinite and pressures are the same on both sides of the air-lens interface and also the lens-substrate interface. Thus $\rho_u gt$ hydrostatic pressure above the lens-substrate interface is equal to $\sigma_L gh$ the pressure below the interface; i.e. $\rho_L h = \rho_u t$, where ρ_L is the density of the lower layer (substrate), ρ_u the density of the upper layer (lens), g the gravitational acceleration, t the lens thickness at the center line and h is the submergence of the bottom of the lens at its center line below the undisturbed surface of the substrate.

If one considers a thin slice centered about the median plane of a lens so large that curvature in the horizontal plane can be neglected, a free-body force balance in the horizontal direction can be set up. The free body can be visualized as consisting of a thin slice parallel to the cross section shown in Figure I. The left hand edge of the slice terminates at the center line of the lens, and the right hand edge in the substrate at a point where the substrate surface is horizontal. The bottom of the slice is horizontal and just touches the bottom of the lens.

The net surface tension force acting to the left per unit length of lens perimeter is $-F_s$. The hydrostatic pressure forces per unit length are

$$F_{P_R} = \int_0^t P_u \, d_z = \int_0^t g \, \rho_u \, z \, d_z = \frac{g \, \rho_u \, t^2}{2} \qquad (2)$$

acting to the right, and similarly

$$F_{P_L} = g \, \rho_L \frac{h^2}{2} \qquad (3)$$

acting to the left. In the above, the local hydrostatic pressure P in each layer has been simply equated, the density ρ of the layer times the depth z and the gravitational acceleration g.

The net pressure force acting to the right is

$$F_P = \frac{g}{2} \left(\rho_u t^2 - \rho_L h^2 \right) \tag{4}$$

But since $\rho_L h = \rho_u t$ we can substitute $\left(\frac{\rho_u}{\rho_L} \right)^2 t^2$ for h^2 yielding

$$\frac{g}{2} t^2 \left(\rho_u - \frac{\rho_u^2}{\rho_L} \right) = \frac{g}{2} t^2 \rho_u \left(1 - \rho_u/\rho_L \right) \tag{5}$$

Equating the pressure force acting to the right to the surface tension force acting to the left and solving for t there is obtained

$$t = \left[\frac{-2 F_s}{g \rho_u \left(1 - \frac{\rho_u}{\rho_L}\right)} \right]^{1/2} \tag{6}$$

This assymptotic relationship for very large lens was derived by Hardy (32). This solution essentially applies to a lens so large that it can be treated as a two dimensional case. The above value of t is sometimes denoted t_∞.

For large lenses, the upper and lower surfaces are flat for a considerable portion of the lens diameter and the average lens thickness $\bar{t}$ should be moderately well approximated by t_∞. In such a case a given spill volume V should be related to the equilibrium lens diameter D by the following approximation

$$V = \frac{\pi D^2}{4} \bar{t} \doteq \frac{\pi D^2}{4} t_\infty \tag{7}$$

Substituting for t_∞ and solving for D yields

$$D \doteq \left[\frac{8 V^2}{\pi^2} \cdot \frac{g \rho_u \left(1 - \rho_u/\rho_L\right)}{- F_s} \right]^{1/4} \tag{8}$$

Thus if a spill tends to form lenses, as a first approximation the lens diameters should be proportional to the square root of the volume of oil contained in the lens. Alternatively stated, for moderately large lenses, the lens thickness should be approximately independent of the lens volume or diameter.

Real lenses of even moderately large size deviate somewhat from these assymptotic relationships. The diameter equation is intrinsically less subject to deviation than the thickness equation. As will be seen later, even for lens volumes as small as 1-cm^3 the actual diameter is usually only 20% larger than predictedby Equation (8) and even in the worst cases is only 33% larger.

Neumann's Triangle

In developing volume-thickness-diameter relationships for lenses of small to moderate volume, the angles the surfaces and interfaces form at the edge of the lens are significant intermediate variables. These angles are shown in Figure II.

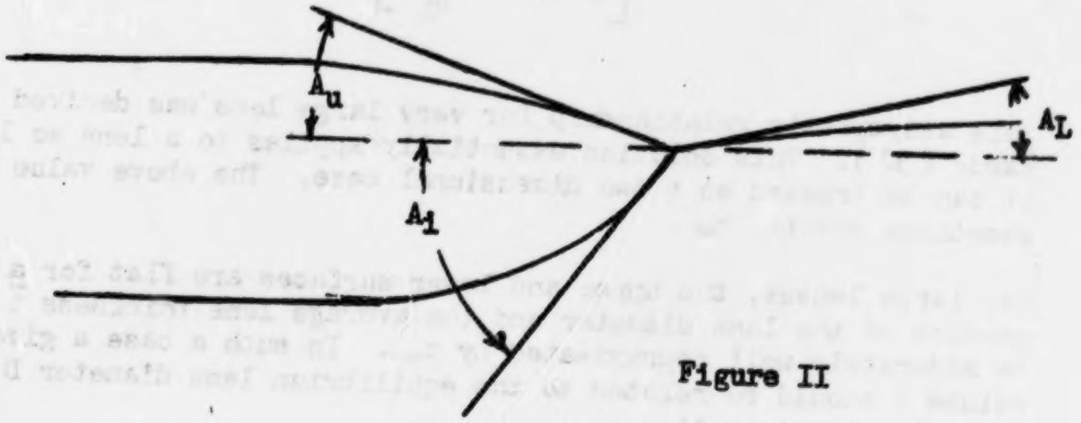

Figure II

Since the edge of the lens is in equilibrium,the vertical and horizontal components of the surface tension forces must satisfy the following force balances, sometimes known as Neumann's triangle.

(horizontal) $$\sigma_L \cos A_L = \sigma_u \cos A_u + \sigma_i \cos A_i \qquad (9)$$

(vertical) $$\sigma_i \sin A_i = \sigma_u \sin A_u + \sigma_L \sin A_L \qquad (10)$$

There are two equations in three unknowns, A_u, A_L and A_i. A third equation is needed to permit a solution. Such an equation can be provided by an overall vertical force balance for the lens

$$g V \rho_u = g V_L \rho_L + 2 \pi R \sigma_L \sin A_i \tag{11}$$

where V is the volume of the lens, V_L is the volume of substrate which it displaces, and the last term is the vertical component of the surface tension of the substrate times the peripheral length over which it is acting, R is the lens radius.

V and V_L can be determined as functions of R if equations are available or can be developed describing the shape of the liquid surfaces and interfaces of the lens. Unfortunately these equations usually involve angles A_u, and A_i and the solution of Equation (11) while possible is far from simple and, except in certain limiting cases, usually involves trial and error.

The ultimate solution for angles A_u and A_i is facilitated by solving for a related pair of angles shown in Figure III.

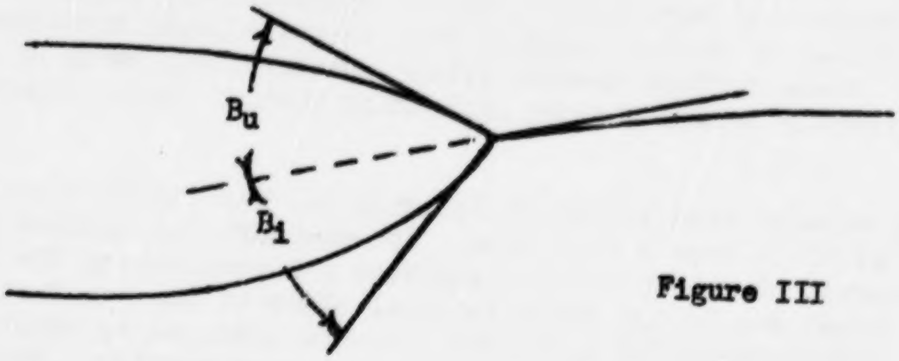

Figure III

Here we have the somewhat simpler component relationships

$$\sigma_u \cos B_u + \sigma_i \cos B_i = \sigma_L \tag{12}$$

$$\sigma_u \sin B_u + \sigma_i \sin B_i = 0 \tag{13}$$

B_i being taken as a negative angle.

These can be solved simultaneously to yield

$$\cos B_i = (\sigma_L^2 - \sigma_u^2 + \sigma_i^2)/ 2 \sigma_L \sigma_i) \qquad (14)$$

$$\cos B_u = (\sigma_L^2 + \sigma_u^2 - \sigma_i^2)/2 \sigma_L \sigma_u) \qquad (15)$$

And

$$A_u = B_u - A_L \qquad (16)$$

$$A_i = B_i + A_L \qquad (17)$$

Thus if A_L can be determined from Equation (11) A_u and A_i can be determined through the use of Equations (14) through (17).

Values of A_L, A_u, and A_i have been experimentally determined by Coghill and Anderson (18) and Lyons (41). The value of A_i is quite small usually 10° or less. Lyons claims that the angles do not necessarily satisfy Neumann's triangle, particularly for small lenses. However it can be noted that in those cases where significant deviations from Neumann's triangle exist Lyons has used the literature values for the surface tensions of pure liquids in his computations, rather than measured values of surface tension when saturated with the other liquid of the pair. These surface tension values, particularly those of water, can be significantly lower, thereby explaining most of Lyons' discrepancies.

The force balance used to derive Equation (6) essentially involves treating the lens as if it were a flat disk. It considers the surface and interfacial tension of the horizontal surfaces only, neglecting the surface tension forces due to the short vertical sides of the hypothetical disk. Improved correlations for t, $\bar{t}$, and D can be obtained by considering a more realistic model of the lens shape and cross section. Surprisingly, while two dimensional solutions are readily available, finite exact solutions for the three dimensional surfaces of revolution produced by the interaction of surface tension and gravitational forces do not exist. Tabular numerical approximations, of great accuracy, the Bashforth and Adams tables (7) do exist, but these are out of print and very rare.

Bashforth and Adams tables may be used for predicting lens volumes and diameters. A procedure for doing so was developed in the present investigation, but it is quite complex, difficult to apply, and therefore will not be discussed.

Simpler modified versions of the Bashforth and Adams tables, Dorsey's (27) and Porter's (59) tables for sessile drops and Sugden's (72) tables for meniscuses are used for correction purposes in surface and interfacial tension measurements. However use of these tables apply only to surfaces and interfaces which are vertical at their edge, and thus they cannot be used for predicting the characteristics of lenses.

Langmuir's Work

The most comprehensive work dealing with lenses is that of Langmuir (37). A fair number of intermediate steps are left out in the derivation of equations in Langmuir's article. Since these omissions can prove quite confusing, Langmuir's approach is recapitulated below.

In essence Langmuir uses a method of successive corrections. First he develops equations for the cross-section boundary curves of the surfaces and interfaces of a lens which is so large that it can be essentially treated as a two dimensional case (i.e. its curvature in the horizontal plane can be neglected). Using these equations for the boundary curves, he develops expressions for the extent to which the surface tension and hydrostatic pressure forces for the cross section so defined deviate from the corresponding forces in the simple disc model used to obtain t_∞.

Langmuir calls the total deviating force, obtained by integrating the local deviating forces over the entire width of the lens, the "linear tension", f. The "linear tension" appropriate to each surface or interface is shown to be equal to

$$f = \frac{2}{3}^{\,3/2} \sigma a \left[1 - \cos^3 \left(\frac{A}{2} \right) \right] \qquad (18)$$

where σ is the surface or interfacial tension, a is the capillary constant, $[2 \sigma/g (\rho_2 - \rho_1)]^{1/2}$, ρ_2 being the density of the lower liquid and ρ_1 the density of the upper liquid (or gas) bounding the interface, g is the gravitational acceleration, and A is the angle from the horizontal at which the surface intersects the edge of the lens.

Using values of f for the surfaces in question, Langmuir then corrects the equations for the cross section boundary curve so that f is taken into account. The equations for these corrected boundary curves are then solved simultaneously to obtain an equation for the thickness of the lens at its center line, namely

$$t^2 = \frac{2\,\rho_L}{g\,\rho_u(\rho_L-\rho_u)} \cdot \left[-F_s + \frac{f_L}{R + \frac{a_L}{\sqrt{2}}} + \frac{f_u}{R - \frac{a_u}{\sqrt{2}}} + \frac{f_i}{R - \frac{a_i}{\sqrt{2}}} \right] \qquad (19)$$

where the subscripts L refer to lower layer, u upper layer, and i interface.

Using the equations for the lens boundary curves Langmuir shows that for moderately large lens the lens volume V is given by

$$V = \pi R^2 t - \pi R (a_i^2 \sin A_i + a_u^2 \sin A_u) \qquad (20)$$

The various f terms are functions of the angles A_i, A_u and A_L. Thus both t and V are functions of these angles. The exact value of these angles cannot be determined solely from Neumann's triangle, but, as previously indicated, depends on A_L the angle of the substrate surface. Using the equations for the boundary curves, Langmuir was able to solve for A_L in the case where the various A were small enough for terms of order higher than $A^4/24$ to be negligible in the series expansion for 1-cos A. In this solution A_L is a fairly complex function of the capillary constants a_L and a_u, the lens radius R and thickness t, and the liquid densities. A_L thus varies as the lens volume varies. It approaches an assymptotic value $A_{L\infty}$ as R goes to infinity and t goes to t_∞. This is

$$A_{L\infty} = \frac{a_L\,B_u - (\rho_L - \rho_u)\sqrt{2}\,t_\infty}{a_u + a_L} \qquad (21)$$

From Langmuir's experimental data it appears that A_L differs from $A_{L\infty}$ by only 1% for lens as small as 1 cm. diameter. Thus negligible error is involved in using $A_{L\infty}$ for A_L. His calculated values for A_L are in good agreement with those experimentally measured by Coghill and Anderson (18) and Lyons (41).

Trial and error solution are required if one is to rigorously solve for V, t, and $\overline{t}$ as functions of R.

Direct approximate solutions, good for lenses of large diameter, can be obtained by using $A_{L\infty}$, and the corresponding value $A_{u\infty}$, and $A_{i\infty}$ in Equations (18), (19) and (20), $\bar{t}$ being given by the expression $V/\pi R^2$. Langmuir's approximate solution for $\bar{t}$ is about 9% in error for lenses of 2 cm^3 volume, and the error rapidly decreases as the volume increases.

Langmuir's Equations provide a significant improvement over the approximation $\bar{t} \doteq t_\infty$. They are however not rigorous and limited somewhat by assumptions made in their derivation. In some instances, particularly those where σ_u is greater than σ_L, the neglect of the $A^4/24$ term in the series expansions for 1-cos A can lead to an 8% error in the value of A. For very small lenses the radius of curvature of the lens surfaces at the center line is sufficiently small that the assumption $\rho_u t = \sigma_L h$ no longer holds. In Equation (19) the $a/\sqrt{2}$ correction terms which occur in the denominator are approximations which are true only when the respective angle A corresponding to the particular a is small. More exactly the term should be $a \sin (A)/(2)^{3/2} \sin (A/2)$; and when $\sigma_u > \sigma_L$, this more exact form deviates significantly (up to 29%) from $a/\sqrt{2}$ for the case of a_i, the most important of the correction terms. The assumptions upon which the $a_i/\sqrt{2}$ corrections in Equation (19) are derived appear to be somewhat arbitrary. Equation (20) appears to be strictly applicable only for large lenses, otherwise the term multiplying $a_i^2 \sin A_i$ should be of the order $\pi (R - a_i \sin A_i/(2)^{3/2} \sin A_i/2)$ and that multiplying $a_u^2 \sin A_u$ of the order $\pi (R - a_u \sin A_u/(2)^{3/2} \sin A_u/2)$ rather than πR in each case. Despite this fault finding the errors in question apply mainly to correction terms, and their overall effect is probably not significant.

Lens Stability

Very little information appears to be available on the ability of lens to resist deformation and breakup under the influence of externally applied stresses, such as might arise from wind or wave action or turbulent eddies. Bradley (13) has derived an equation for the period T with which a lens will oscillate when distorted horizontally from a circular to an elliptical shape. This equation is

$$T = 2\pi \left[\frac{R^2 \rho_u t}{g \sigma_u t^2 - 2 F_s + 4 f/R} \right]^{1/2} \tag{22}$$

where f represents the summation of the linear tensions f_u, f_L, and f_i.

From this equation it can be seen that the time required for a deformation to relax increases as the lens radius increases, and for lenses of large size this relaxation time is proportional to R. The terms in $-F_s$ and t^2 dominate the denominator for large values of R, and for large lenses t^2 is almost directly proportional to $-F_s$. Thus if we substitute for $-F_s$ in terms of t or vice versa it can be shown that for large lenses T is inversely proportional to $t^{1/2}$ or $-F_s{}^{1/4}$. Thus it appears that deformations in large radius lenses or lenses of small thickness or those with small values of $-F_s$ should take a long time to relax. Since relaxation is brought on by the action of forces opposing deformation, lenses which take a long time to relax must possess less deformation resisting capability. Therefore large lenses, thin lenses, and lenses with low values of $-F_s$ should be more susceptible to breakup.

Non Lens Formers

Pure materials for which F_s is positive do not form lens and in theory will spread to form layers of near monomolecular thickness. Oils, which are complex mixtures, exhibit more complicated behavior but will nevertheless form films which are very thin. The few thickness measurements in the literature and estimates based on spill spread areas reported by Blokker (11), Sigwalt (65), Stroop (10) and Smith (66) indicate average thicknesses ranging from 0.013 to .041 mm (0.0005 to 0.0015 in) compared to thicknesses of the order of 1.25 to 12.5 mm (0.05 to 0.50 in) for lenses.

Induced Lens Formation

If the surface tension of the water is sufficiently lowered without lowering the interfacial tension of the oil by an equal amount the spreading force F_s can be changed from a positive value to a negative value. Thus it should be possible to convert a spreading oil into a lens former and greatly reduce the extent of spread of a spill.

This idea in effect has been investigated by Sigwalt (63) and Garrett (31) and briefly by Blokker (11). Garrett showed that a wide variety of substances which tended to form monomolecular films could, when spread on water, induce lens formation, and that the thickness of the resultant lenses is roughly predictable by Equation (6) with $(F_{s1}-F_{s2})$ substituted for F_s, where F_{s1} is the spreading force for the oil-water system, and F_{s2} is the spreading force for the monolayer-water system. It will be shown later that this is equivalent to lowering the surface tension of the water by an amount equal to $-F_{s2}$. It can be seen that if F_{s1} is positive, F_{s2} must also be positive and greater than F_{s1} to induce lens formation.

Sigwalt showed that the spreading of oil film could be checked and the oil film driven back by the spreading of a film of fatty acid which tended to spread at a more rapid rate than the oil, but his ideas were embodied in a less general, less quantitative form than Garrett's. Since Garrett showed that the spreading rate for monomolecular films tends to be proportional to thé spreading force, Sigwalt's spreading rate criterion is essentially equivalent to Garrett's ($F_s - F_{s2}$) criterion.

Blokker showed that traces of sodium alkyl sulfate by lowering the surface tension of water induced the formation of a 1 to 1.5 mm thick lens in a middle Eastern crude which normally spread to a thickness of 0.015 mm - i.e. reduced the area of spread by a factor of 100.

Water in Oil Emulsions

Under certain circumstances, e.g. sloshing of oily ballast, and water-containing oil, detergent treatment of spills, etc., water in oil emulsions will form, and, if these are discharged or found at sea, they exhibit markedly reduced spreading as compared to the oil from which they are formed. Emulsion film patches several inches thick have been reported (71). In one instance (66) the data indicates a sea area of roughly 140,000 ft.^{2} was covered by a emulsion layer averaging 90 mm (3.6 in) thick. Following the Torrey Canyon incident, 100 to 150 mm (4 to 6 in) thick grease like patches, presumably emulsion, were reported by the French Navy.

Such emulsion patches tend to gradually thin out, thin films spreading from the edge of the patch, carrying away their patch oil content. If the patch is broken up by sea action the thinning out process appears to be accelerated. Such breakup appears to be favored by choppy waves and not greatly influenced by swells (71).

It is interesting to note that the formation of stable emulsion patches represents a method for keeping spilled oil pools in a compact form if desired. Since in a water in oil emulsion, oil, the continuous phase, can not occupy less than 26% of the volume, the oil volume per square foot of pool area is even greater than that of a thick lens. Based on the reports of the French Navy following the Torrey Canyon spill such emulsion patches have persisted for as long as two months.

Spreading Rates

The spreading rates of floating liquid pools has been studied by a number of investigators, Reynolds (62), Brinkman (14), Cary and Rideal (15), Ramdas (61), Wooly (79), Garrett (31), Blokker (11), Lippok (28), Sigwalt (65), Abbott (1) and Stehr (69). Of these only the last five are concerned with large pools such as those resulting from spills. The remaining are concerned with the spreading of monomolecular films from droplets.

Blokker derives a relationship for the spread of oil down a long straight sided channel. He assumes that the instantaneous rate of spread is proportional to excess hydrostatic pressure in the pool which he assumes is proportional to $(t - t_\infty)\ \rho_u\ (1 - \rho_u/\rho_L)$,

$$\frac{d\ell}{d\Theta} = K\ \rho_u \left[1 - \frac{\rho_u}{\rho_L} \right] (t - t_\infty) \qquad (23)$$

where ℓ is the length of the pool, Θ time and K the constant of proportionality. This is not quite according with the hydrostatic force equations developed for lenses, according to which this expression should be $[\ (t^2 - t_\infty^2)/2\ t\ ]\ \rho_u\ (1 - \rho_u/\rho_L)$ i.e. the hydrostatic force per unit length divided by the pool thickness. However as t_∞ becomes very small (as is the case in Blokker's work) the two expressions become exactly proportional to one another.

In Equation (23) Blokker substitutes V/b, the spill volume divided by the channel width for t, and integrates the rate expression for the case where t_∞ is negligible, thereby obtaining

$$\ell^2 - \ell_o^2 = 2\ K \left(1 - \frac{\rho_u}{\rho_L} \right) \frac{\rho_u\ V\ \Theta}{b} \qquad (24)$$

where ℓ_o is the original pool length. Blokker verified that ℓ^2 did increase linearly with time. The constant K varied from system to system though. K and the rate of spreading were not inversely proportional to the oil viscosity. For all the materials tested K only varied by a factor of 3 ranging from 9,800 to 30,000 min^{-1}, even though the viscosity varied by a factor of 600. This lack of influence of oil viscosity on spreading rates was also reported by Stehr (69) and Morlock (44).

On the other hand in Sigwalt's experiments on spreading, which were carried out over a temperature range of 7°C to 25°C, the rate of spreading was found to decrease as the temperature decreased. Both the viscosity of the oil and that of the underlying water increase as the temperature decreases, and thus the effect produced by the change of temperature may well have been due to the concomitant change in viscosity of either the oil or the water.

If viscosity regulates the spread rate , as in laminar flow, the time required to spreading a given distance should be proportional to the viscosity. If one looks up water viscosities corresponding to Sigwalt's experimental temperatures it can be seen that these viscosities are roughly proportional to the spreading times reported by Sigwalt. For example in one instance a 1.73 fold increase in spreading time is accompanied by 1.60 fold increase in water viscosity. In another instance a 1.62 fold increase in spreading time is accompanied by a 1.55 fold increase in water viscosity. Sigwalt only identifies his test oil as an "huile grasse activee", and therefore it is not possible to determine its variation in viscosity. Sigwalt's temperature vs spreading time data and Blokker (11), Stehr (69) and Morlock's (44) observation that spreading time does not vary greatly with oil viscosity appears to indicate that oil pool spreading rates are roughly inversely proportional to the viscosity of the underlying water. Unfortunately we cannot tell from Sigwalt's spreading rate data whether he was working with hydrostatically driven spreading (thick pools) or surface tension driven spreading (films). Since the mechanism determining spreading distance may be different for these two cases, an inference as to the influence of water viscosity on spreading rate may be invalid or may apply only to one form of spreading.

Though the linear increase of ℓ^2 with time is verified by Blokker's tests, the validity of the factor $\left(1 - \frac{\rho_u}{\rho_L}\right) \rho_u \frac{V}{b}$ cannot be regarded as experimentally verified. Blokker varied the initial pool thickness of the oil in several of his experiments, but it is not apparent whether he did so by varying the volume V, or whether he used the same volume and varied the original length ℓ_o. Thus on the basis of the data as reported in the Blokker article we cannot decide whether the rate of increase in ℓ^2 is truly proportional to V. Somewhat similarly because K varied significantly in the one series of tests where Blokker varied $\left(1 - \frac{\rho_u}{\rho_L}\right) \rho_u$ without markedly varying the other factors, the proportionality of $d\ell/d\theta$ to $\left(1 - \frac{\rho_u}{\rho_L}\right) \rho_u$ cannot be regarded as experimentally established.

Blokker on similar grounds derived an expression for the spreading of a circular pool. For the case where the final pool thickness can be regarded as negligible this is:

$$D^3 - D_o^{\,3} = \frac{24}{\pi} K \left(1 - \frac{\rho_u}{\rho_L}\right) \rho_u V_o \theta \tag{25}$$

This postulated behavior of the pool diameter D predicted by this relationship was not subjected to experimental test. Since only a fragmentary hydrodynamic model was used by Blokker in deriving his equations, it is by no means certain that K should be the same for the circular pool case as it is for the linear spreading case. If one attempts to apply Blokker's equation for the spreading of circular pools to the spread data reported by Stroop (71) for the spread of non-emulsified oil at sea Blokker's formula, using his largest K value, predicts values of D^3 which are 65 times too small. Evaluating D, (i.e. taking the cube root of D^3) reduces the error so that the predicted values of D are only 4 times too small.

It might be noted that for monomolecular films spreading from droplets or small lenses floating on the films Garrett (31) showed that the spreading rate was proportional to F_s rather than the $\left(1 - \frac{\rho_u}{\rho_L}\right) \rho_u$.

For such films the spreading rates range from roughly 4 to 13 cm/sec. Based on Garret's data it appears that the spreading rates of monomolecular films can be roughly (i.e. within ± 39%) correlated by $\frac{d\ell}{d\theta} \doteqdot .38\, F_s$.

Diffusive Spread

Diffusive spread must be considered in addition to hydrostatic and surface tension drive spread in determining the gross area of coverage of an oil spill. Under the stresses developed by the wind and sea, oil pools when thinned out sufficiently will usually break up into smaller patches. The probability of recoalescence of these patches will be low, and driven by the turbulence of the sea they will tend to diffuse away from one another.

For a small spill this breakup and diffusion process ultimately spreads the oil over so much space that its concentration falls below the nuisance level. Detergent treatment of small spills is designed to accelerate this diffusion driven dispersive process.

Diffusion at sea has been the subject of much study (30, 49, 50, 51, 52). It is a matter of considerable practical interest in that it helps regulate gradients in salinity and temperature and the dilution of sewage outfalls and radioactive wastes. Unfortunately neither the theoretical nor the empirical study of diffusion at sea is as yet well resolved. In particular the effective turbulent diffusivity appears to vary with time and distance in a not wholly predictable way.

The classical (Fickian) solution for diffusion from a point source (48) is

$$C = \frac{M}{4 \pi K \theta} e^{-r^2/4 K \theta} \qquad (26)$$

where C is the concentration of the diffusing substance as a function of r the radial distance from the source and θ the time elapsed after release of the source. M is the source strength and K is the effective diffusivity.

If one makes various assumptions as to how the effective diffusity varies with time and distance different solutions similar in form to Equation (26) are generated but with r and θ raised to different powers (49, 50, 51, 52). Dye tracer studies at sea and in bays show that the Fick's law solution is not applicable and though there is considerable scatter in the data, solutions in which θ^2 or θ^3 appear in the denominator of the non exponential term fit the dye concentration data best. This means that concentrations should decay considerably faster than predicted by the Fick's law expression.

Typical values of K obtained from a dye tracer study , Foxworthy et al. (30) range from 1.6 ft^2/sec. after 490 sec. and 14 ft^2/sec. after 4130 sec. the lack of constancy in this case indicating the diffusion is non-Fickian.

In any case, the concentration at any given time and distance is proportional to the source strength (i.e. the oil spill volume). For points reasonably distant from the spill, the oil concentration will be proportional to the initial spill volume and will thus take longer to decay to a tolerably low concentration. The rate of decay varies with the effective diffusivity K, but for Fickian diffusion there are two limiting cases when K or t is very large and when K or t is very small. In the first case the concentration will be inversely proportional to time and in the second C will be inversely proportional to time squared. For the first case the time required for oil concentration to reach a non noxious level at a given distance r , remote from the center of the spill, will be proportional to the spill volume and in the second case to the square root of the spill volume.

close to the spill, the spill can no longer be treated as a point source but must be treated as an area source. The sources corresponding to each point in the original spill area must be added, i.e. the sources integrated over the spill area. This source addition or integration process leads to slower decay of concentration near the center of the spill. Essentially because diffusion is a "random walk process", when the spill concentration is uniform, oil from the edge of the spill is just as likely to walk towards the center as oil from the center is to walk towards the edge. It is only when the concentration near the center decays that the center concentration can begin to decay, and the larger the spill the longer this process takes.

Drift-Wind Effects

Until recently very little quantitative information has been available about the drift of oil deposited at sea.

Stroop (71) followed a series of test spills. Analyzing his oil drift data it appears that oil drift over a given period of time averaged 3.98% of the total wind travel during the same time. The scatter about this average was very great the percentage drift ranging from 1.38% to 6.58%. It is impossible to tell from Stroop's reported data whether any appreciable currents were present - the tests were in mid ocean near Hawaii, - and whether the wind direction had shifted significantly during the course of the tests. The slicks were tracked for a considerable period of time - between 23 and 117 hours.

Following spillage of oil from the Gerd Maersk in 1955 the German Hydrographic Institute of Hamburg tracked the spill and concluded that it moved at about 4.2% of the wind velocity (Tomczak). This movement occurred in the shallow coastal waters off Germany and Denmark and tides and coastal currents may have been complicating factors.

During the course of the present study, the book 'Torrey Canyon' Pollution and Marine Life edited by J.E. Smith appeared. Chapters 8 and 9 of this book are valuable though somewhat fragmentary sources of information concerning the drift oil spilled from the Torrey Canyon. On the basis of the drift of recognizable patches of oil which were charted using aerial photographs taken by the Royal Air Force, Smith concluded that the oil moved in the direction of the wind at an average velocity equal to 3.4% of the wind velocity. The following table is adapted from

Table 26 in Smith's book and presents the data upon which he based his conclusions.

Table 2. Oil Drift vs Wind Speed

Path Segment	Vector Distance Traveled (Nautical Miles)		Elapsed Time (hrs)	Percent Drift †	Wind Velocity (knots)	Direction of Movement	
	Oil	Wind				Oil	Wind
A	23.3	834	48	2.79	17.4	116°	120°
B	23.8	911	102	2.61	8.1	69°	73°
C	29.9	633	43	4.72	14.8	81°	98°
D	20.3	556	97	3.65	5.7	145°	152°
E	27.1	849	73	3.19	11.6	63°	70°
F	41.7	1081	98	3.86	11.1	153°	123°
Total	166.1 ‡	4864 ‡	461	3.41 ‡	10.6	91°	95°

† Percent Drift = (Oil Velocity/Wind Velocity) x 100

‡ Our corrected figures. These values appear to be in error in Smith's table

It can be seen that the percent drift varies widely about the average, ranging as low as 2.61% and as high as 4.72%. This variation does not appear to correlate with wind velocity or with fetch, the distance over the wind has blown without markedly shifting direction. The cause of variation may be due to tidal and current influences not reported by Smith.

For all path segments except F, the last, the oil moved at a slightly less clockwise angle than the wind. The oil movement for segments A through E averaged 7.8° less clockwise than the wind.

The counterclockwise shift in oil movement may have been due to the current in the English Channel which though weak and rather variable tends to run in the East North East direction (35), the correct direction for producing the shift noted. In contrast to all the other segments the wind direction during segment F was less clockwise than the direction of oil movement and differed fairly markedly in angle, i.e. by 30°. However during segment F the oil was in the Gulf of St. Malo, a region noted for large tides, and these tides may have caused the deviant behavior.

Thus barring other influences Smith's conclusion that oil patches will move in the direction of the wind seems reasonably correct (i.e. at least within roughly 8°).

As noted currents in the English Channel are weak and rather variable in direction. This low degree of influence of current may explain part of the success of Smith's correlation of oil patch drift with wind velocity. Although there is a great deal of scatter in the data, it is noteworthy that when the oil movement direction deviates most markedly from the wind direction, the percentage drift tends to be high. This suggests that the directional deviation and the percentage drift increment might both be due to current induced drift.

On the open ocean far from shore currents are usually moderately weak, e.g. 0.4 to 0.6 knots and quite variable in direction. Current induced drifts of this magnitude, or smaller, aiding or opposing wind induced drift could have caused the variability in percentage drift calculated for Stroop's open ocean work and also the difference between Stroop's percentage drift results and those for the Torrey Canyon. Similar factors could explain the difference between the Gerd Maersk percentage drift and the Torrey Canyon drift.

Smith pointed out that the movement of the oil which came ashore at Pointe du Raz and the Crozon Peninsula 52-55 days after its estimated release from the Torrey Canyon was also reasonably well predicted by utilizing a 3.3% percentage drift figure. Here the predicted distance moved was 20% greater than the actual movement. Smith noted that this difference could have been caused by a slow northerly current having a speed of only .05 knots.

The percentage drift found by Smith agrees well with measurements made by Hughes (33) of the drift of plastic envelopes floating close to the surface of the Atlantic Ocean. Hughes found that the envelopes drifted in the direction of the wind at a velocity equal to 3.3% of the wind velocity. Hughes recommended that in the absence of direct wind velocity data, that the wind velocity be estimated as 2/3 of the geostrophic wind obtained from isobaric plots. Where necessary, i.e. on the open sea in the absence of wind monitoring stations, Smith used this procedure to calculate the wind velocities on which his percentage drift figures were calculated. In all cases but one, where checks could be made, the wind velocity calculated in this manner agreed with that obtained by direct measurement of nearby wind monitoring stations.

It should be noted that though the agreement between Hughes and Smith's results is good, the question of wind induced surface drift is a subject of debate in Oceanography and results deviating from those of Hughes have been reported. For example Thorade(73) reports that the surface drift V (in centimeters/sec.) is given by the following equations

$$V = \frac{2.59\sqrt{W}}{\sqrt{\sin\beta}} \qquad \text{for } W \leq 6 \text{ meters/sec.} \qquad (26)$$

and

$$V = \frac{1.26\,W}{\sqrt{\sin\beta}} \qquad \text{for } W > 6 \text{ meters/sec.} \qquad (27)$$

where W is the wind speed in meters/sec. and β is the latitude. It is obvious that this relationship must break down as the Equator is approached. If we substitute the latitude of the English Channel (50°), the second of Thorade's equations predicts a percentage drift of 1.43% which is much lower than that noted by Smith and Hughes.

The question of wind induced surface drift depends in large measure on the shear stress developed by the wind in blowing over the water. This stress in turn depends on the drag coefficient C, and the drag coefficients for such flow are subject to a great deal of uncertainty and debate. Figure 8.18, page 209 in Neumann and Pierson's Principles of Physical Oceanography indicates some of the highly scattered drag coefficient data and two of the principal proposed correlations, namely: 1 that the drag coefficient is independent of the wind velocity and 2 that the drag coefficient is inversely proportional to the square root of the wind velocity (48). There are many complicating factors, i.e. the waviness of the sea surface and air turbulence which may account for some of the scatter and preclude a simple drag coefficient correlation.

Further it appears, following Ekman, that Coriolis forces should cause surface currents to deflect to the right of the wind in the Northern hemisphere and to the left in the Southern hemisphere. Deflections of about 45° have been reported for the open ocean Krummel. In shallow seas the deflection is significantly smaller and has been found to decrease with increasing wind velocity. A typical correlation, Witting(77) relates α the angle of deflection to the wind speed W (in meters/sec.) by the following equation

$$\alpha = 30^\circ - 7.5\sqrt{W} \qquad (28)$$

This, for the range of wind speeds encountered following the Torrey Canyon incident, would predict a deflection of 14°, clockwise. Other similar correlations, Neumann (47) indicate deflection of about 10° clockwise. Except for the last portion of drift in the Gulf of St. Malo the Torrey Canyon drifts average 8° counterclockwise from the wind direction. This moderately large 18° to 22° deviation as previously noted may have been due to prevailing currents flowing towards the North.

Drift-Current Effects

It is commonly assumed, either explicitly or complicitly, that oil drift will occur at the same rate as the drift of water at the surface of the sea. This surface drift and thus that of floating oil will be the sum of drift due to wind, wave current and tide action. This assumption, while plausible and providing a good working hypothesis, is by no means proven. J.E. Smith (as shown in Figure 33 page 152 of "Torrey Canyon" Pollution and Marine Life) makes this assumption when vectorially adding the tidal current to the calculated wind drift in an effort to trace the path of an oil spill near the Torrey Canyon. The results in Figure 33 qualitatively support Smith's assumption, but quantitative agreement is not demonstrated - even taking into account local variations in tidal strength which Smith neglected.

The assumption that drift will tend to occur at the same velocity as surface currents was also used by the British Ministry of Transport and Civil Aviation (42) in devising boundaries for zones near the British Isles in which the dumping of oil ballast was prohibited.

Maps and charts presenting average current data as a function of position in the ocean are available (35). These currents are fairly variable and though the variability can in part be specified through the use of current roses and stability indices, the prediction of current induced drift involves undertainty because of this variability. Current induced oil drift is therefore best predicted using current measurements taken near the time and place of the spill rather than current charts. In most instances ocean currents are about 0.5 knots but in some instances (e.g. near the northeastern coast of South America) currents of about 2 knots will occur. Since for winds of moderate intensity (i.e. 10 to 20 knots) wind induced drift should be of the order of 0.35 to 0.7 knots it can be seen that current induced drift can not be neglected in most instances.

In shallow waters surface flow due to tides can reach rather high velocities, much greater than that produced by currents on the open ocean and wind drift. Tidal amplitude tables and tidal current tables are usually available for most coasts. Where tidal current data is not available currents can be predicted from tidal amplitude and period data and topography using the method of Defant (22). In general tidal flows can be predicted with much more accuracy than ocean currents.

Drift-Wave Effects

Stokes has shown that there is a steady second order mean forward velocity $\overline{U}$ associated with free surface wave motion. Based on the assumption of irrotational flow and a sinusoidal wave form he developed the following equation for this forward velocity

$$\overline{U} = \frac{\frac{\pi A^2 \omega}{\lambda} \cosh \left[\frac{4\pi(Z-h)}{\lambda} \right]}{\sinh^2 \left(\frac{2\pi h}{\lambda} \right)} - \frac{A^2 \omega}{2h} \coth \left(\frac{2\pi h}{\lambda} \right) \qquad (29)$$

where cosh is the hyperbolic cosine, sinh the hyperbolic sine, coth the hyperbolic cotangent, A the wave amplitude (1/2 the wave length), Z the distance below the mean surface elevation, h the water height, ω the angular frequency,(i.e. $\omega = 2\pi/T$, where T is the wave period), and λ is the wave length. For the free surface, $Z = 0$, and the expression for $\overline{U}_o$ the surface drift becomes

$$\overline{U}_o = \frac{\pi A^2 \omega}{\lambda} \left[1 + \coth^2 \left(\frac{2\pi h}{\lambda} \right) - \frac{\lambda}{2\pi h} \coth \left(\frac{2\pi h}{\lambda} \right) \right] \qquad (30)$$

For $h/\lambda \gg 1$, i.e. for deep water, this reduces to

$$\overline{U}_o = 2\pi \frac{A^2 \omega}{\lambda} \qquad (31)$$

or alternatively

$$\overline{U}_o = \frac{(2\pi A^2)}{\lambda T} \qquad (32)$$

For deep water, wave velocity depends on wave length and because of the interdependence of wave velocity, frequency and wave length these expressions reduce to

$$\overline{U}_o = \left(\frac{2\pi}{\lambda}\right)^{3/2} A^2 g^{1/2} \qquad (33)$$

or

$$\overline{U}_o = \left(\frac{2\pi}{T}\right)^{3} \frac{A^2}{g} \qquad (34)$$

This would appear to imply that wave induced drift in deep water increases as the period and wave length decrease. This is true if the amplitude A remains constant. However the maximum value of A is limited to one-fourteenth of the wave length and when this maximum value or its equivalent period is substituted for A there is obtained

$$\overline{U}_{o\,max} = \frac{(2\pi)^{3/2}}{196} (\lambda g)^{1/2} \qquad (35)$$

or

$$\overline{U}_{o\,max} = \frac{2\pi g T}{196} \qquad (36)$$

However it is extremely rare that waves of maximum amplitude are generated. In a fully developed sea for a twenty knot wind the average wave height is only about 40% of the maximum height corresponding to the wave period (8 sec.) in which most wave energy is concentrated. In a fully developed sea for a 30 knot wind the average wave height is only 5.2% of the maximum for the period (12 sec.) where most energy is concentrated and for a 40 knot wind 5.9% (period 16 sec.). Thus for wind waves in a deep sea, drifts will range between 0.27% and 16% of the maximum values.

Based on average wave heights taken from the wind wave spectra of Pierson, Neumann, and James (55), and the equations derived above from Stokes formulas, the following table of estimated wave drift for fully developed seas corresponding to various wind speeds has been compiled.

Table 3. Estimated Wave Drift for Fully Developed Wind Waves

Wind Speed (knots)	Period Where Most Energy is Concentrated (Sec.)	Average° Wave Height (ft.)	Estimated Drift Speed (knots)	Percent + Drift	Conditions Required for Full Development	
					Fetch (nautical miles)	Time (hrs.)
10	4	0.9	0.042	0.12	10	2.4
15	6	2.5	0.033	0.22	34	6
20	8	5	0.056	0.28	75	10
25	10	9	0.092	0.37	160	16
30	12	14	0.129	0.43	280	23
40	16	28	0.217	0.54	710	42
50	20	48	0.326	0.65	1420	69

o Average wave height = 2 A

+ Percent Drift = (Estimated Wave Drift Speed/Wind Speed) x 100

The above table only has qualitative significance and may only be used for very rough estimation. The distribution of wave heights and periods in the wave spectrum was not considered - 10% of the waves have heights roughly twice the average height, and one-third have heights roughly 1.5 to 1.6 times the average height; the wave periods in which there is significant wave energy content range roughly from twice to one half the period where most wave energy is contained. Since the drift depends on the amplitude squared (A^2) and the inverse of the period cubed ($1/T^3$), the use of simple average values for A and periods of maximum energy content for T is not strictly valid. Further wave spectra are somewhat variable, and somewhat different spectra, e.g. Moskowitz (45) and Pierson and Moskowitz (54) have been reported for fully developed wind waves.

Nevertheless it appears that wave induced drift should be of significantly lower magnitude than the direct wind induced drift (roughly 20% of the wind induced drift or less). This is however subject to debate. Computer studies are under way elsewhere at New York University (in the Meteorology and Oceanography Department) in which the spectral characteristics of the waves are considered, (17). These studies indicate that much of what is thought to be wind induced drift may be drift induced by wind generated waves. (Note: Our experimental results do not agree with these computer based results.)

It might be noted that the average wind speed during Stroop's drift tests was 19.5 knots whereas the average wind speed during the tracking of the Torrey Canyon oil patches was 10.5 knots. The effect of this difference in wind speed on wind-wave induced drift may account for roughly 0.16% of the 0.57% difference between Stroop's average 3.98% drift and the 3.41% average drift for the Torrey Canyon oil.

Test basin results, Mitchim (43) and the U.S. Beach Erosion Board (76), indicate that Stokes equations are valid for deep water waves. However other tests, Coligny (19), U.S. Beach Erosion Board (76) and Bagnold, indicate that Stokes equations do not hold for shallow water. In fact in some instance, Bagnold (5), backward motion has been observed at the surface.

Longuet - Higgins (40) taking into account the viscosity of the fluid - i.e. abandoning the assumption of irrotational flow - developed drift equations which differ from those developed by Stokes. These equations provide better agreement with shallow water test work, but since in most instances we will be dealing with deep water waves, they will not be discussed further.

Real waves are not sinusoidal as assumed by Stokes and Lonquet-Higgins in their analyses of wave drift, and wind waves as previously noted consist of a broad spectrum of wave frequencies. Chang (16) building on the wave spectrum analyses of Tick and Pierson derived expressions for drift in terms of these wave spectra. Making suitable substitutions Chang's expression for drift at the free surface can be shown to be

$$\bar{U} = 4 \int_{0}^{\infty} \frac{\omega^3}{g} S_Z(\omega)\, d\omega \qquad (37)$$

where $S_Z(\omega)$ is the spectral distribution factor of wave energy (proportional to the square of the displacement Z from the mean surface level) as a function of the frequency ω.

Chang obtained good agreement with this equation in tests using random mixed waves in a deep water test basin. This equation reduces to Stokes equation for waves of a single frequency.

If one substitutes for $SZ(\omega)$, Pierson and Moskowitz's generalized wind-wave spectra expression

$$S(\omega) = \frac{\alpha g^2}{2\omega^5} e^{-\beta (g/W\omega)^4} \qquad (38)$$

where W is the wind velocity, and carries out the indicated integration one obtains

$$\overline{U} = .022\ W \qquad (39)$$

for the wave induced drift velocity. This result indicates that for fully developed wind waves the wave induced drift velocity should be 2.2% of the wind velocity. This is substantially higher than indicated by our previous method of estimation and substantially higher than obtained for wind drift measurements at sea. It should be noted that there are fairly large quantitative differences between the Pierson and Moskowitz spectrum equation and the spectra used to obtain the amplitude data for the calculations in Table 3.

Both sets of wave drift results computed so far have been for fully developed wind waves. As indicated in Table 3 it takes a considerable fetch and period of blow for full wave development to occur at high wind velocities. In the case of the Torrey Canyon drift and even in Stroop's tests the wind velocities were low enough that full development was probably present most of the time.

Because winds give rise to wind waves, and wind waves give rise to wave induced drift, it should be apparent that the separation of wind induced drift from the drift caused by waves generated by the wind can be a difficult problem. The problem is further complicated by the fact that wind induced drift should depend on the drag coefficient for wind flow over water. This drag coefficient is very likely to be a function of the waviness of the water. To the extent that wind drag induces waviness (essentially turbulence) it is less likely to directly induce a uniform directed drift. That is as greater amounts of waviness are generated, more of the momentum transferred from the wind is likely to go into maintaining the waviness rather than directly maintaining a mean forward drift velocity. The complexity of interaction between wind and waves is great. Similar interactions may exist with respect to combined wave motion and current motion, and current induced drift and wind drift, and the principle of additivity of drifts, while initially plausible, may now be seen to be subject to serious questions.

The use in the present program of a relatively short wind wave test basin precludes full wind-wave development, and to that extent the tests are not representative of conditions at sea. On the other hand the relative absence of wind waves allows a separate clear-cut evaluation of wind induced drift without the complicating effects of wind waves.

Experimental

Lens Measurements

The substrate liquid was generally deposited in a shallow (1 inch deep by 24 inches long x 18 inches wide) rectangular tray made of fiberglass reinforced melamine plastic. If the substrate liquid was expensive or was likely to react with or dissolve the plastic, a smaller glass, aluminum or teflon coated aluminum tray was used. Prior to depositing the substrate liquid the tray was washed and rinsed ten times with tap and then ten times with distilled water. If a non-aqueous substrate was to be used, the tray was dried and then rinsed ten times with the substrate liquid prior to use.

Various amounts of the lens forming material were then deposited from calibrated pipets or burets onto the substrate surface. The pipets and burets were previously cleaned by a procedure similar to that used in cleaning the trays, except that they were first subjected to a wash with H_2SO_4, $K_2Cr_2O_7$ cleaning solution.

The diameter of the deposited lens was measured with a transparent centimeter scale calibrated to the nearest millimeter. Care was taken to minimize parallax. The scale was generally rested on wooden blocks alongside the tray so as to avoid disturbing the tray. The lenses were quite mobile, and gentle air currents, and vibration tended to greatly disturb them and caused them to move about, so that measurement was difficult. Two lens diameters at right angles to one another were measured in each instance so as to insure that lens was at equilibrium and was truly circular.

Additional measured volumes of lens forming liquid were added to that previously deposited and the resulting new diameters measured. Check runs showed that the same lens diameter was obtained using this incremental method of addition as was when the same total volume was added all at once.

As the lens diameter increased the lens became progressively more susceptible to distortion by minor disturbances. Not only did small disturbances tend to produce greater distortion, but these distortions took a longer time to disappear, and often a relatively minor disturbance produced distortion which propagated through the lens breaking it into two or more parts. Thus as the lens became larger it became progressively more difficult to measure, and it became progressively more difficult to successfully add, without lens breakup, the additional material required to produce further increases in lens volume.

There are slight end effects associated with the use of small trays. If the small tray was well wetted by the substrate liquid so the substrate meniscus curves upward at the tray edge, the size of the lens tended to decrease slightly. If the tray wall was poorly wetted so that the substrate meniscus curves downward at the tray edge the size of the lens tended to increase slightly, and further the lens tended to drift to the side of the tray. These difficulties were circumvented by using large trays wherever possible.

The surface tensions of the substrate and lens forming liquid and their interfacial tension were measured using a Du Nuoy ring tensiometer. The raw tension measurements were corrected using Zuidema and Water's correction factor charts (82). In all cases the tensions were measured using liquids which had been mutually saturated with one another. Difficulty was experienced in measuring the interfacial tension for liquid pairs which differed only very slightly in density. In such cases the ring tended to pull the interface up to the top liquid surface. If the top liquid level was raised to prevent this, it tended to wet the ring support brace, thus interfering with the measurement. Further when the density difference was small corrections had to be extrapolated a considerable distance beyond the range of Zuidema and Water's charts. The liquid densities were measured both by the weighing of liquid samples in pycnometer bottles, and by means of a Westphal balance.

Because of the difficulties involved in measuring large lenses attempts were made to photograph such lens and then measure the photographs. Because of shadows cast by the lens edges, and the continued problem of maintaining the lens undistorted, this did not prove to be any more convenient than direct measurement.

Motion pictures were taken of lens which were deliberately distorted by means of styluses and by impulse waves in the substrate fluid. These pictures were reprojected, tracings made of the lens boundary, and the lens areas measured by running a planimeter around the boundary trace.

Spreading Rate Measurements

A three inch deep by six foot square plywood test basin was constructed. This basin was painted light gray to provide photographic contrast, and was lined with polyethylene film. A new sheet of polyethylene film was used for each run, and the old sheet was discarded, thus providing a clean basin surface for each run.

A six foot high bridge was set up over the basin. A 16 mm Kodak motion picture camera pointing downward was mounted at the center of the bridge. Two 150 watt floodlights each pointing downward at a 45° angle and at the center of the basin were mounted on the bridge support towers.

A phonograph motor turning a turntable at 78 r.p.m. or 45 r.p.m. was mounted over one corner of the pool. A radial line was inscribed on the turntable, so that when pictures were taken including the rotating turntable the rotating line provided an elapsed time reference.

The polyethylene lined basin was filled to a depth of two inches, generally with cold tap water, though in some instances the water temperature was varied for experimental purposes, i.e. to change the viscosity of the water . A sign identifying the nature of the run was positioned over the basin and a short sequence of motion pictures was taken. The sign was removed and a ring dam was inserted at the center of the basin. This dam consisted of a vertical cylinder with an open top and bottom. The dam was allowed to rest on the bottom of the basin, its upper edge protruding several inches above the surface of the water. A predetermined, measured volume of oil (a natural crude oil) was deposited inside the ring, the motion picture camera was started and the ring dam lifted. Pictures were taken of the spreading pool of oil until the spring motor of the camera ran down (38 feet or 1520 frames could be exposed per winding). An exposure rate of 32 frames/ second at f 4.0 was used in some instances. In other cases a 8 frames/second rate at f 4.0, with the shutter opened only one quarter to provide equivalent photographic exposure, was used so as to obtain pictures of the spreading oil over a longer period of time. Tri X, positive reversal film, Kodak type 7278 was used.

The pictures were projected, and the major and minor axis of the pool measured usually at five, ten or twenty frame intervals. The area A of the pool was calculated on the basis that it was an ellipse. That is $A = \pi D_1 D_2/4$ where D_1 and D_2 are the major and minor diameters respectively. In a number of instances the area was checked by using a planimeter and making a traverse around the pool's outline. Good agreement was obtained between the areas as measured by planimeter and those calculated using the ellipse formula, even though in some cases the periphery was locally distorted. The difference between the two areas was less than 2% in all instances in which a check was made. It is possible, though, that poor agreement would have occurred if checks had been made in cases of more extreme distortion.

Drift Test Basin

Tests involving wind and current drift and the influence of waves were carried out in a 20-ft. long by 8-ft. wide wind water test basin. Because of the thickness of wooden walls and support beams, the actual inside dimensions of the basin were 19-ft. 1 1/2-in. long, 7-ft. 1 1/2-in. wide by 11 3/4 in. deep. The basin was lined with 10 mil polyethylene film. Return ducts were created on each side of the test basin by installing 17-ft. long by 11 1/2-in. deep by 3/4-in. thick redwood planks, their long side parallel to the long walls of the basin, each plank standing 12 in. away from the neighboring wall. 18-in. spaces which formed the entrance and exit port to the return ducts were left between each end of the redwood planks and the ends of the test basin. The space between the lower edge of the redwood plank and the bottom of the test basin was sealed by a lip of polyethylene film tacked onto the redwood plank. The redwood planks were held in place by slotted angle iron beams to which their top edges were fastened. These angle iron beams ran the length of the basin and were in turn fastened to the end wall of the basin. With the installation of the return ducts, the width of the main channel of the test basin was reduced to 5-ft.

The bottom of the basin was formed by 4-ft. by 8-ft. sheets of 3/4 in. plywood. These were supported off the floor by five evenly spaced 2 in. x 6 in. wooden beams lying flat, and running the length of the basin. The beams provided clearance between the basin bottom and the floor sc that any leakage could drain away.

Variable speed propeller-type mixers were mounted with their propellers in the return ducts at the downstream end of the test basin. The shafts of these mixers were inclined at a slight angle to the horizontal. Thus the propellers when turning would drive water down the return duct; and the mixers functioned as high velocity - low head pumps. This pumping action was used to create currents by return flow in the main duct. The current speed was varied by varying the rotational speed of the propeller.

The flow created by the propellers when discharged into the main duct was not uniformly distributed and created strong eddies which gave rise to abnormal and non-reproducible drift. This condition was corrected by the insertion of an egg-crate grid and fiber mat flow distributor. The grid was 1/2-in. deep and had 3/4-in. square openings. The fibrous mat was made of loose random array of rubberized fibers and was roughly 2-in. thick. Though this distributor greatly improved the flow uniformity and eliminated eddying, it tended to greatly reduce the maximum current speeds that could be produced by the propellers. The discharge capacities of the propellers fall off rapidly as the head (or pressure drop) they have to overcome increases. Flow uniformity was achieved by increasing resistance and pressure drop and flow capacity was consequently greatly reduced. No simple way has as yet been found to circumvent this difficulty. Pumps capable of providing high flow rates and overcoming the required pressure drop without loss in capacity can be obtained but their cost and that of the associated electrical installation and piping would greatly exceed the total cost of the present test setup.

The return ducts, in addition to providing a means for creating currents in the main duct, helped to minimize some of the main channel end effects. Any drift in the main channel has to come to a halt at the channel's downstream end. If the main channel were closed off, no net flow could occur within it. Thus any surface flow, such as might be induced by wind, would have to be accompanied by a return flow presumably in the lower layers of the water in the channel. The zone of transition between the surface and the return flow occupies a fairly long length at the end of the channel, preventing that length from being used for drift measurements. These effects, which occur in a closed channel, would not occur in most situations at sea. The two side ducts allow the drift induced flow to return outside of the main channel, thus providing a more normal flow profile and minimizing the length of the main channel which could not be used because of drift termination end effects.

The overall layout of the test basin is shown in Figure IV. For clarity the angle iron supports for the redwood planks are not shown.

A variable height wind duct was mounted over the main channel of the test basin. The walls and top of the wind duct were formed of 10 mil polyethylene film attached by pressure sensitive tape to supporting slotted angle-iron cross beams. The cross beams supporting the top of the duct were in turn attached to vertical slotted angle iron pillars bolted to the side wall of the test basin. The support beams could be fastened at various elevations on these pillars thus changing the height of the duct. The side walls of the wind duct were fastened at their lower edge to the

FIGURE IV

TEST BASIN LAYOUT

P : PROPELLOR TYPE PUMPS
D : EGG CRATE FIBER MAT FLOW DISTRIBUTOR

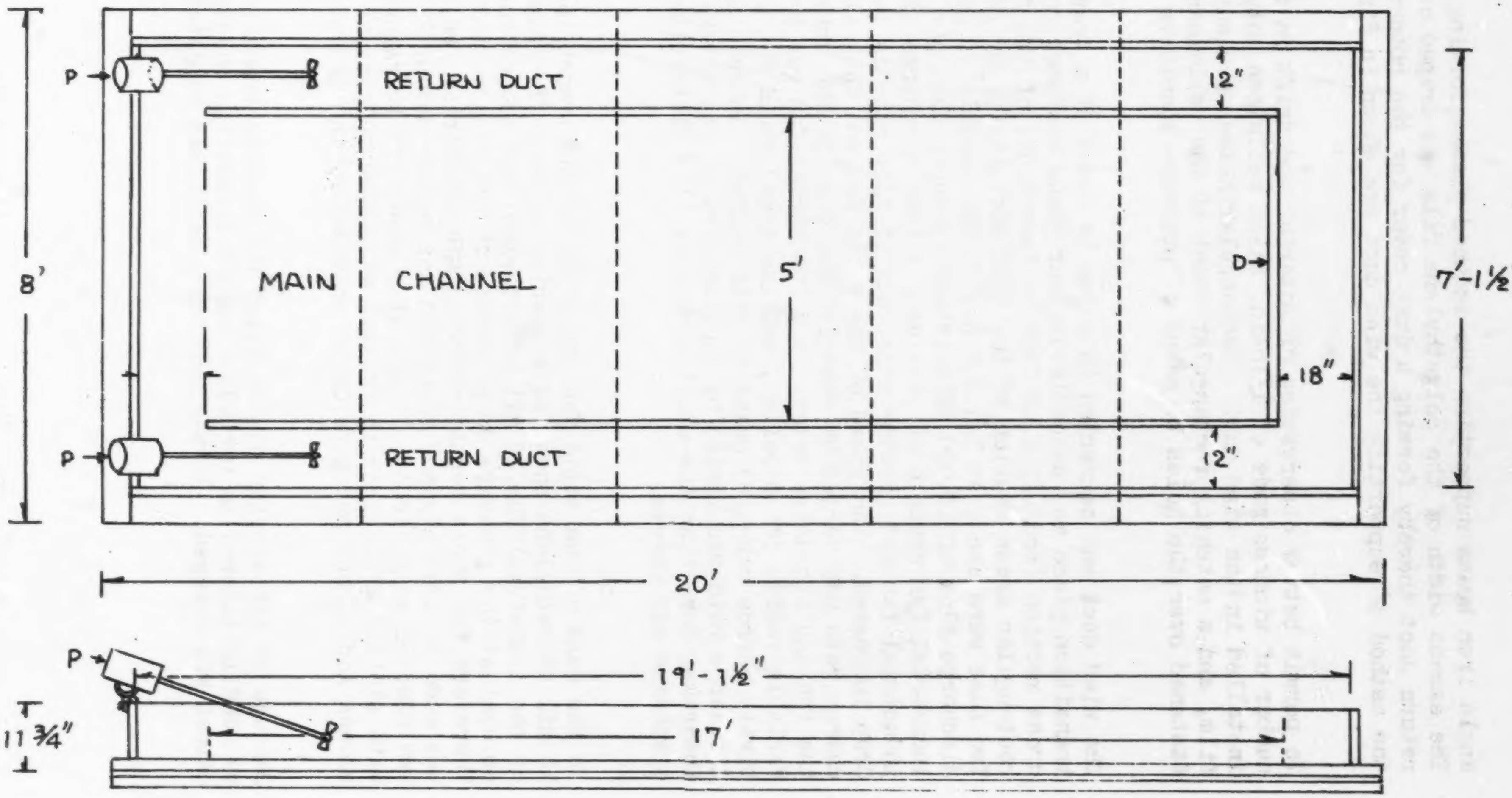
P
P
P
RETURN DUCT
RETURN DUCT
MAIN CHANNEL
D
5'
8'
12"
12"
18"
7'-1½"
20'
19'-1½"
17'
11 ¾"

angle iron beams supporting the redwood planks forming the return duct. The excess width of the polyethylene film was draped over the top of the return duct thereby forming a dust cover for the return duct. Details of the method of supporting the wind duct are shown in Figure V.

To permit better observation of material and drift in the test basin, a number of windows made of 1/16-in. thick cellulose butyrate sheeting were installed in the wind duct. Rectangular holes were cut in the polyethylene film, and a matching rectangular sheet of the cellulose butyrate was fastened over the holes by means of pressure sensitive polyethylene tape.

The wind duct was connected to a fan by means of a transition piece. This transition piece was essentially four plane surfaces connecting the square cross section (roughly four feet by four feet) of the fan housing to the rectangular cross section of the wind duct (5-ft. by 22-in. in most tests). Two fans were used, an 1/4 H.P. attic fan capable of providing a free discharge flow of 12,000 SCFM (standard cubic feet per minute) and a 3 H.P. industrial fan capable of providing a free discharge of 30,000 SCFM. The industrial fan had greater constancy of flow rate as the discharge pressure drop increased. The speed of the attic fan and thus its volumetric discharge rate was varied by changing the size of the drive pulleys connecting the fan and its drive motor. The industrial fan was provided with a variable radius drive pulley, and its speed could be varied over a relatively narrow range by means of this pulley. In some instances the fan discharge rate was varied by closing part of its intake area, or by inserting more than the usual number of flow distributor grids in the fan discharge air stream.

In the case of the attic fan, the walls of the transition piece were made of 10 mil polyethylene sheeting supported on an angle iron frame. In the case of the industrial fan, 10 mil polyethylene was not strong enough to stand up against the pressure drops caused by the higher wind velocities. Therefore, for those tests involving the industrial fan, the transition piece was made of 1/4" plywood supported and reinforced by 2" x 4" wooden beams and slotted angle iron. It was also necessary to reinforce the wind duct with slotted angle iron to prevent excessive bulging at the higher wind speeds and higher pressure drops provided by the industrial fan.

Because of its simpler construction the plastic transition piece could be readily altered to provide a smooth transition whenever the wind duct height was changed. It was much more difficult to alter the wooden

FIGURE V

WIND DUCT SUPPORT SYSTEM

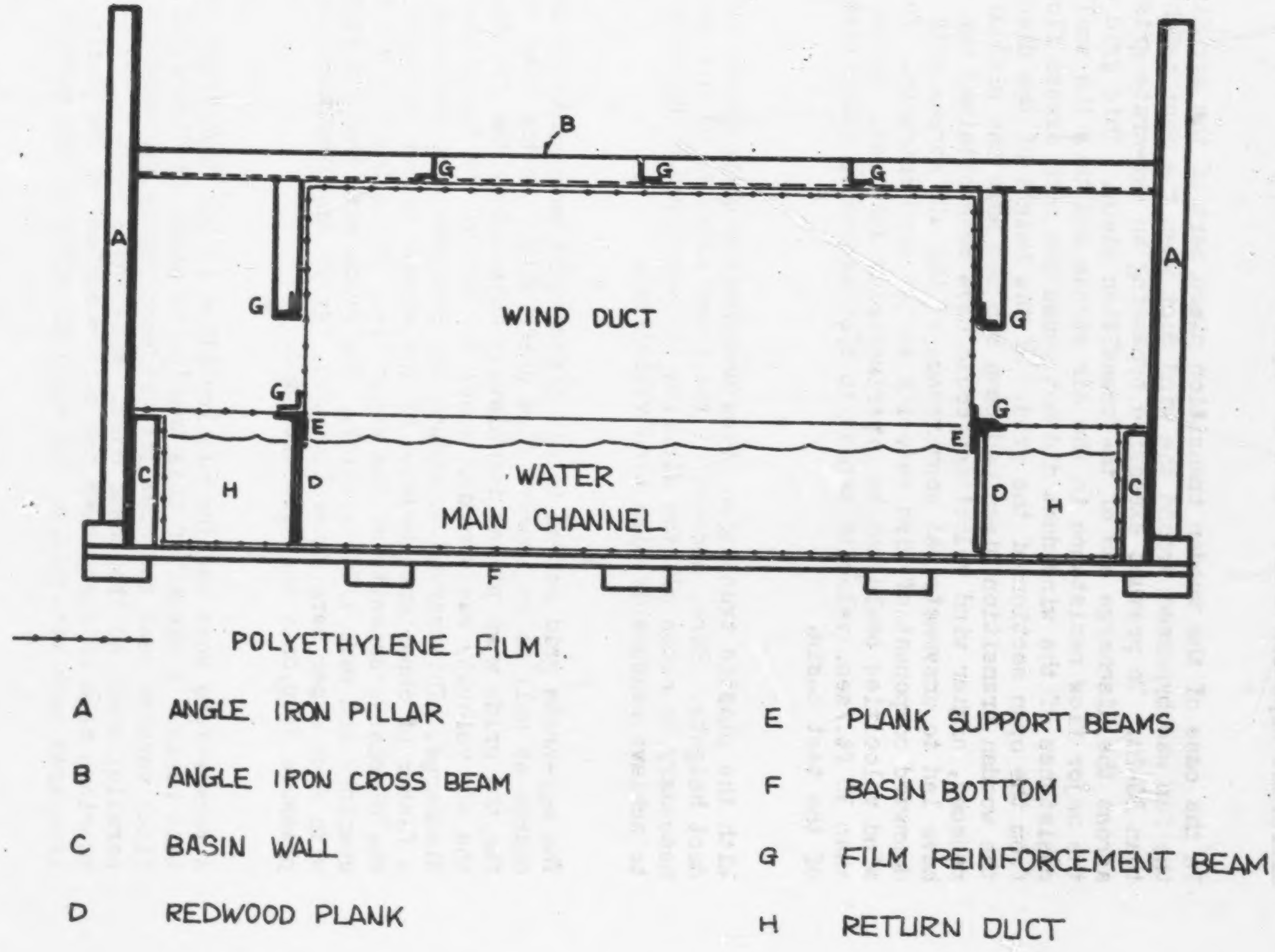
B
G
G
G
A
A
G
WIND DUCT
G
G
G
E
E
C
H
D
WATER
MAIN CHANNEL
D
H
C
F
POLYETHYLENE FILM
A ANGLE IRON PILLAR
B ANGLE IRON CROSS BEAM
C BASIN WALL
D REDWOOD PLANK
E PLANK SUPPORT BEAMS
F BASIN BOTTOM
G FILM REINFORCEMENT BEAM
H RETURN DUCT

transition piece. Therefore with the wood transition piece a somewhat different expedient was used when the duct height was altered. These different expedients are shown in Figure VI.

In the case of the wooden transition piece, part of the air discharged by the fan was bypassed around the wind duct when the duct height was lower than 30-in. To prevent excessive bypassing an egg-crate grid was placed across the discharge end of the transition piece. This grid constituted the major flow resistance in the air stream and thus the smaller added resistance of the wind duct did not cause too much excess flow to escape from the open section of the grid. If the height of the discharge and of the wooden transition piece had been reduced when the wind duct height was reduced, higher wind velocities could have been obtained but this would have led to unsymmetrical convergence of the air stream with a consequent downward component of wind velocity at the wind entrance. Further, higher wind velocities could not be experimentally utilized. Winds of higher than 30 ft./sec. velocity tended to blow excessive quantities of water out of the test basin.

With the plastic transition piece unsymmetric convergence did occur at low duct heights. Here, because of the lower capacity of the attic fan it was necessary to cause all the air flow to pass through the wind duct in order to achieve reasonably high wind velocities.

The egg-crate grid served to eliminate swirl components in the fan discharge as well as to improve flow uniformity. In the case of the attic fan, the grids were placed immediately adjacent to the fan frame where the air velocity was somewhat lower and not at the transition piece discharge. This served to reduce the pressure drop produced by the grid, a factor of importance because of the marked effect pressure drop had on the discharge capacity of the attic fan. The grids had 3/4-in. square openings and were 1/2 in. thick. Two grids with their openings in line with each other were generally used, but in some instances, to minimize pressure drop, only one grid was used.

A rocker-type wave machine was installed at the downstream end of the test basin. A sketch of this machine is shown in Figure VII. In the final version used, the slat like redwood paddle was attached to a parallel shaft at its lower edge. This shaft could pivot in two wooden bearings held in place near the bottom surface of the basin. Two angle iron arms were attached to the vertical sides of the paddle. These arms

FIGURE VI

TRANSITION PIECE ARRANGMENT

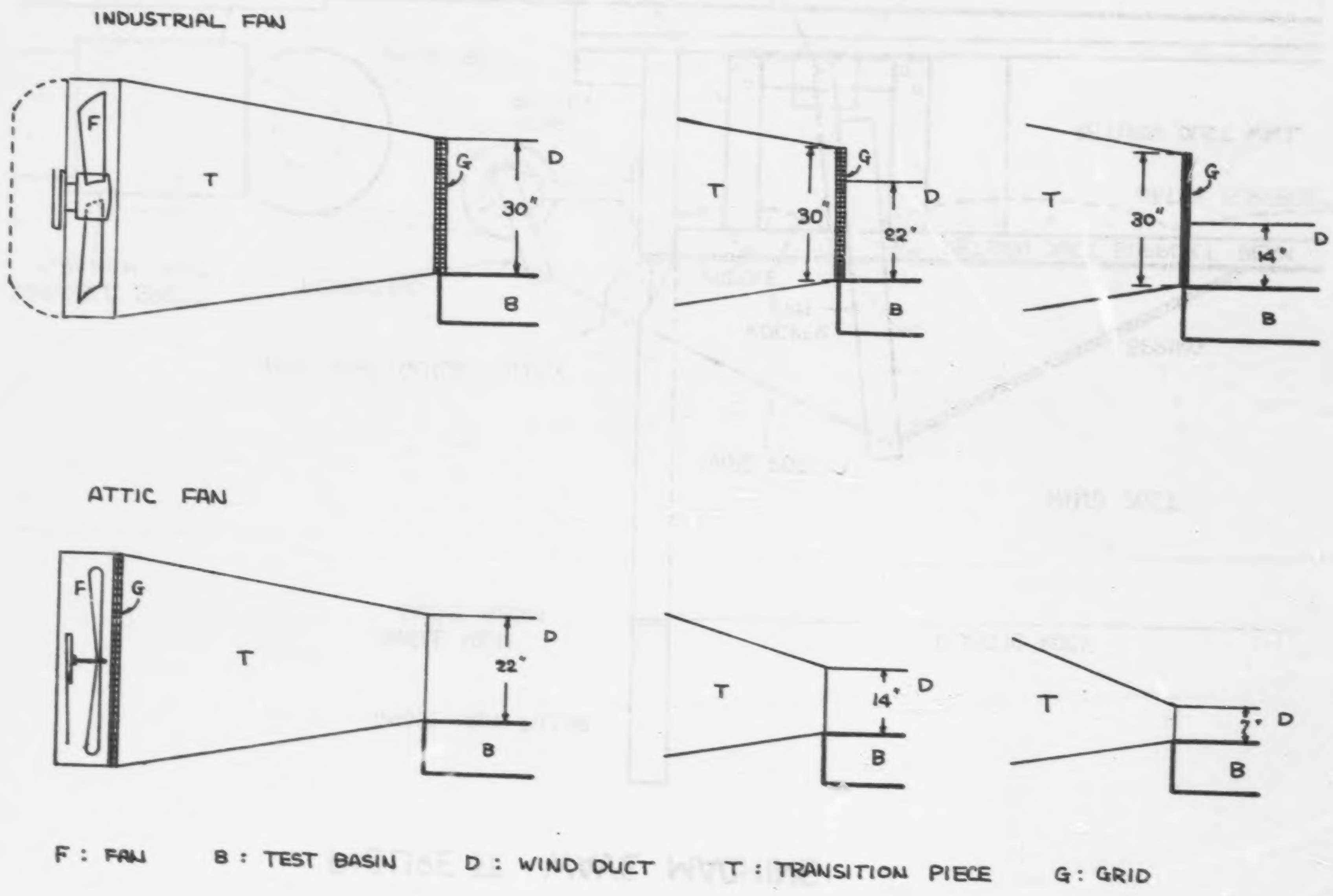
INDUSTRIAL FAN
F
T
G
D
30"
B
T
30"
G
D
22"
B
T
30"
G
D
14"
B
ATTIC FAN
F
G
T
D
22"
B
T
D
14"
B
T
D
7"
B
F : FAN
B : TEST BASIN
D : WIND DUCT
T : TRANSITION PIECE
G : GRID

FIGURE VII WAVE MACHINE

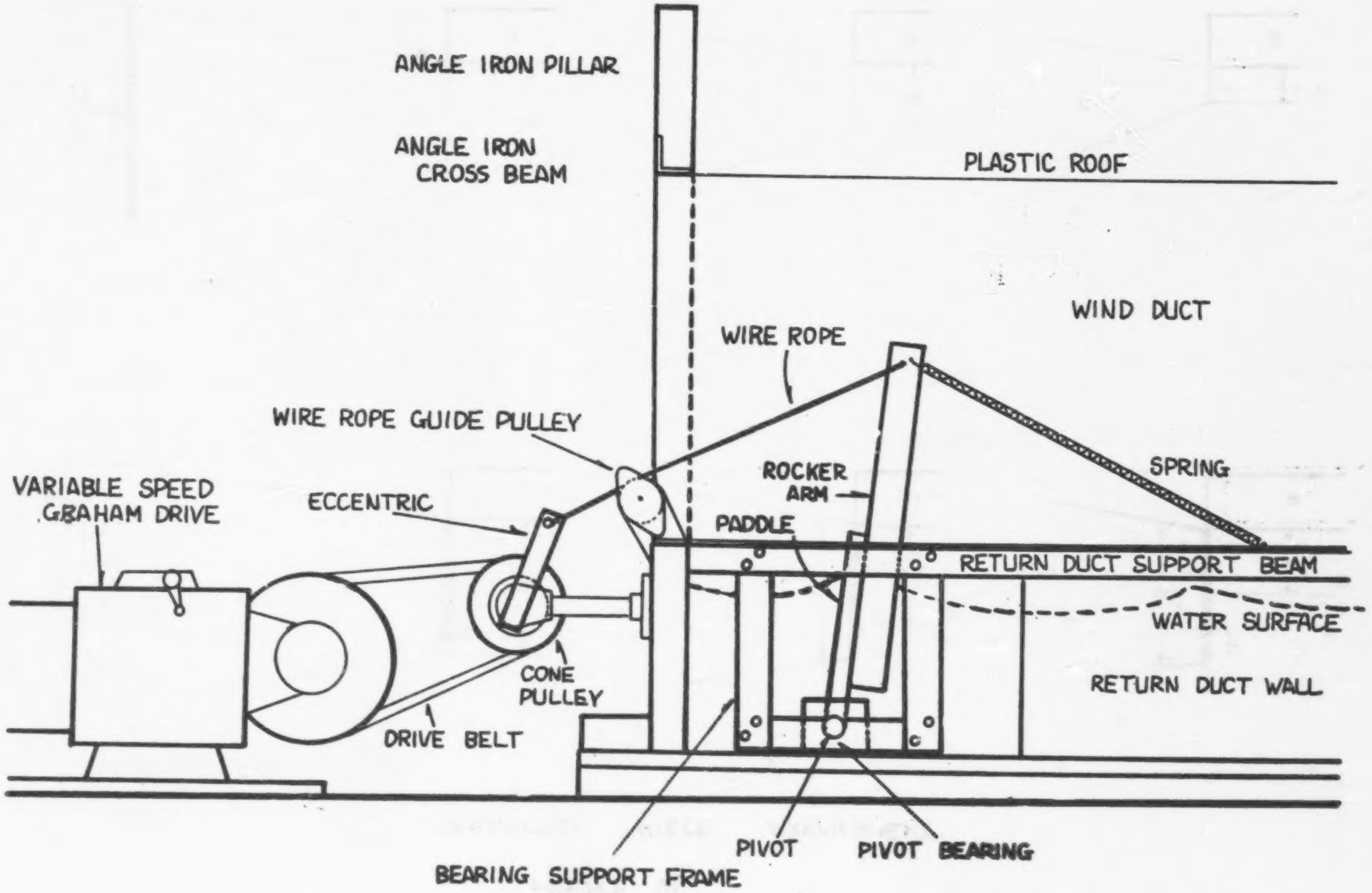
ANGLE IRON PILLAR
ANGLE IRON CROSS BEAM
PLASTIC ROOF
WIND DUCT
WIRE ROPE
WIRE ROPE GUIDE PULLEY
VARIABLE SPEED GRAHAM DRIVE
ECCENTRIC
ROCKER ARM
PADDLE
SPRING
RETURN DUCT SUPPORT BEAM
WATER SURFACE
RETURN DUCT WALL
CONE PULLEY
DRIVE BELT
PIVOT
PIVOT BEARING
BEARING SUPPORT FRAME

projected vertically about 12-in. above the upper edge of the paddle. A wire rope and a spring were attached to the upper ends of these arms. The spring was attached to angle iron beams supporting the return duct redwood wall about two feet in front of the paddle and thus tended to force the paddle forward. The wire rope was attached to a rotating eccentric, driven by a shaft which was held in rocker bearings cantilevered out from the rear wall of the test basin. As the eccentric rotated it alternately pulled and slacked up on the wire rope which in turn pulled and slacked up on the shaft. The combined action of the spring and wire rope thus imparted a reciprocating motion to the wave paddle.

The eccentric shaft was turned by a belt driven, triple-step cone pulley mounted on the shaft. The belt in turn was driven by a 10-in. diameter pulley driven by a 1/4 H.P. Graham variable speed drive capable of producing speeds from 0 to 60 RPM. In general the 5-in. step on the cone pulley was used and thus the paddle rocked at a frequency which was twice the rotational speed of the Graham drive.

In an earlier version of the wave machine the paddle had been pivoted at the top rather than the bottom. The bottom pivot arrangement was finally resorted to because it produced greater amplitude of motion at the water surface where motion should be the greatest if it is to conform to the usual pattern of wave motion. Though the wave machine was designed to produce a wide variety of wave frequencies by varying the drive pulley arrangement and the speed of the Graham drive, and amplitudes by varying the throw of the eccentrics, it functioned most efficiently when producing with a period of about one second (i.e. one wave per second). The wave amplitude depended on the frequency of rocking as well as the stroke length of the paddle; and when the frequency was reduced much below one stroke per second, the wave amplitude fell off markedly even though the stroke was lengthened by increasing the throw of the eccentric. Frequencies significantly higher than one cycle per second tended to overload the wave machine drive.

Wave reflection tended to occur at the upstream end of the test basin, particularly if the current flow distributor was not being used. This reflection, if not minimized, caused the formation of standing waves of large amplitude. The current flow distributor when placed 1/4 wave length away from the upstream end of the test basin was most efficacious in minimizing standing formation. Part of the wave passed through the distributor, part was absorbed, and part was reflected 180° out of phase with the incident wave. The part passing through the distributor changed phase 90° in traveling to the upstream wall, 180° upon reflection from the upstream wall, and 90° in traveling back to the distributor. Thus when it arrived back at the distributor it was 180° out of phase with that part of the wave reflected at the distributor. The two reflections therefore tended to cancel each other, minimizing the total reflection and standing wave formation.

An overall view of the wind-wave-current test basin setup is shown in Figure VIII.

Drift Test Procedure

A ring dam, a vertical circular cylinder open at both ends, (roughly 5-in. in diameter and 4-in. high) was mounted about two to three feet from the upstream end of the test basin. This ring dam when partially immersed formed a trap within which oil could be contained. A known volume of oil (usually 50 or 100 cc) was fed into the ring dam from a plastic hose connected to a separatory funnel mounted above the basin. Whatever drift producing device (i.e. fan, propellers, or wave machine) being used was turned on and conditions in the basin were allowed to equilibrate. By means of a projecting arm attached to the dam, the ring dam was then lowered below the surface of the water, thus releasing the oil. The oil moved downstream in the basin under the influence of whatever drift action was being tested. Marker strings were strung across the basin every two feet. The time required for the oil to travel between two of these strings, two or three gaps apart, (i.e. four or six feet) was timed to the nearest 0.1 second using a stopwatch.

It was noted that the oil required a certain time to accelerate after being released. Thus timing was usually not started until the oil had reached a string three to five feet away from the point of deposition. The flow termination which occurred at the downstream wall caused oil drift to slow down as the downstream wall was approached. To eliminate this end effect, the last five feet of the basin were not used in making drift rate measurements.

Drift tests were carried out under wind action, current action, and under various combinations of these actions. In certain cases the drift rate of wooden chips or polyethylene film squares were also measured for comparison purposes.

FIGURE VIII

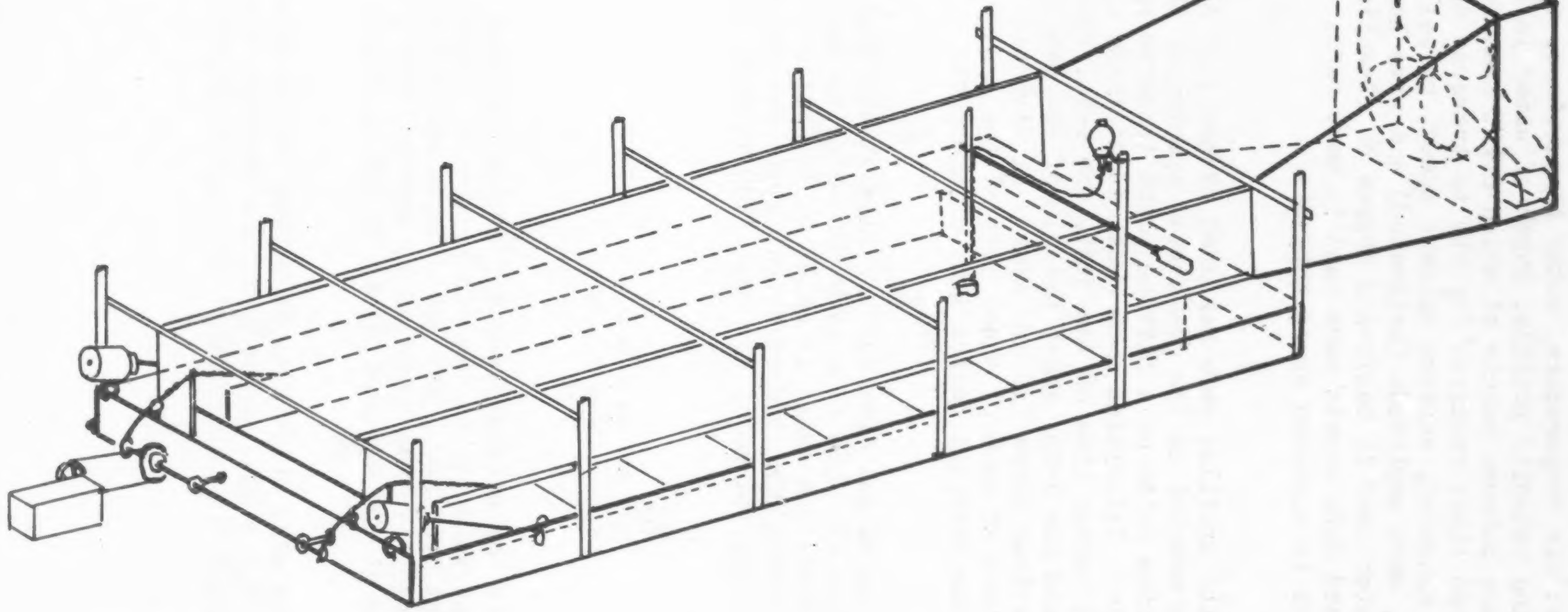

In carrying out the various tests, the following data were taken where applicable: air temperature, water temperature, oil type, oil spill volume, wind velocity profile, depth of water in basin, location and distance between points at which drift measurements were carried out, elapsed times required for oil to traverse distances over which drift was measured, surface current speed, propeller speed, wave frequency, wave amplitude (estimated) and wave length (estimated), type of water used in basin and degree of cleanliness of the water. Standardized data sheets were used in most runs. A copy of these data sheets is enclosed as an appendix.

Air velocity profiles were measured by means of a moving vane anemometer mounted in the downstream opening of the wind duct. Either a nine point or a fifteen point traverse was used in measuring the profile. Velocities were measured at three heights, one at the horizontal center line of the duct, one 4-in. below the top edge of the duct and one 4-in. above the rim of the basin. Measurements were taken at either three (18-in. apart) or five (12-in. apart) evenly spaced points at each of these levels, the center point at each level being at the vertical center line of the duct.

The cross sectional area for air flow at the duct discharge opening is less than air flow area over the water in the test basin. The ratio of these two areas is equal to the ratio of the duct height above the basin rim to duct height above the water surface. Thus since the same volume of air must flow through the two areas

$$\frac{\overline{V}_W}{\overline{V}_D} = \frac{H}{H + T - W} \qquad (37)$$

where $\overline{V}_W$ is the average velocity of the air over the water, $\overline{V}_D$ is the average velocity of the air in the duct opening, H is the height of the duct opening, T the basin depth and W the depth of the water in the basin. $\overline{V}_D$ was computed by arithmetically averaging the velocities at the various points in the discharge traverse.

Most of the wind drift data is correlated in terms of percentage drift $(\overline{V}_o/\overline{V}_w) \times 100$, where $\overline{V}_o$ is the average velocity of the oil as determined from a series of drift rate measurements.

Section 4

DISCUSSION OF RESULTS

Lenses

Eleven lens forming systems covering a wide range of surface and interfacial tensions and liquid densities were tested. Lens diameters were measured vs volume up to volumes of 100 cc or more in most instances. Lenses ranging in thickness from 1.4 mm to 12 mm, and having a variety of shapes were formed. In the case of those lenses where the surface tension of the upper phase was greater than that of the lower phase, the bottom of the lens curved around so the interfacial tension aided the lower layer surface tension in opposing the upper layer surface tension at the edge of the lens. Such a lens, which usually occurred for water floating on a denser organic layer, is shown in Figure IX-A.

Figure IX.

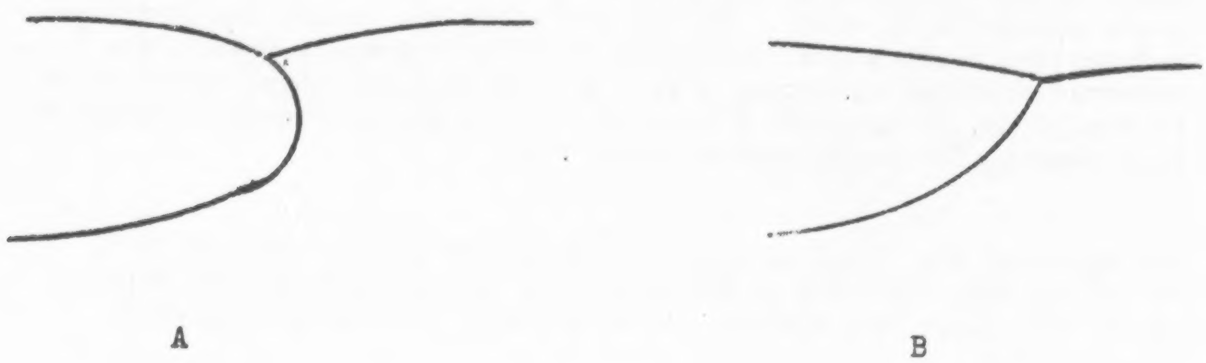

A

B

In a more typical case with an organic upper layer floating on water, the surface tension of the upper layer was smaller than that of the lower layer and the lens formed was similar to that shown in Figure IX-B.

The lens diameters when plotted vs volume on log-log paper form smooth curves which are, in many instances, almost straight lines, and, if care is not taken, may easily be mistaken for straight lines. Actually the slope of the curves gradually increases as the volume increases until the slope reaches an asymptotic value of 0.5 at large volumes - thus satisfying Hardy's and Langmuir's asymptotic relationship for large lenses. Some typical log diameter vs log volume curves are shown in Figure X and XI.

At a lens volume of 100 cc, the lens diameter can be moderately well predicted by assuming that $t = t_\infty$ and that Equation (8) holds

$$D \doteq \left[\frac{8\, V^2}{\pi^2} \cdot \frac{g\, \rho_u (1 - \rho_u/\rho_L)}{- F_s} \right]^{1/4} \tag{8}$$

The measured lens diameter at a volume of 100 cc, the lens diameters predicted using Equation (8) and the properties of the lens forming systems are presented in Table 4. The average deviation between the predicted value of D and the observed value is 4.4%, and the greatest deviation is slightly less than 11%.

The deviations are usually largest where $-F_s$ or $\rho_L - \rho_u$ is small. In each of these cases, the predicted value of D depends on taking a small difference between two large numbers, which is a computation quite conducive to error. In all cases but one, where the deviation between the predicted and observed value is extremely small, the observed diameter is larger than the predicted diameter, which is as it should be, if Langmuir's prediction that the thickness t should be less than t_∞ for small lenses is correct.

The slope of the log D vs log V curve in the solume range of 1 to 10 cm^3 is also included in Table 4. It can be seen that in this range this slope can deviate quite markedly from the asymptotic value of 0.5.

If Langmuir's expression (Equation 20) for the lens volume is expanded there is obtained

$$\begin{aligned} V = {} & \pi R^2\, t_\infty + \frac{\sqrt{2\pi R t_\infty}}{-3F_s} \Big[\sigma_L\, a_L (1 - \cos^3(A_L/2)) + \sigma_i\, a_i\, (1-\cos^3 (A_i/2)) \\ & + \sigma_u\, a_u\, (1-\cos^3(A_u/2)) \Big] - \pi R\, (a_i^{\,2} \sin A_i - a_u^{\,2} \sin A_u) \\ & + \frac{\pi t_\infty}{-3F_s} \Big[-\sigma_L a_L^{\,2} (1-\cos^3(A_L/2)) + \sigma_i a_i^{\,2} (1-\cos^3(A_i/2)) + \sigma_u a_u^{\,2} (1-\cos^3(A_u/2)) \Big] \end{aligned} \tag{38}$$

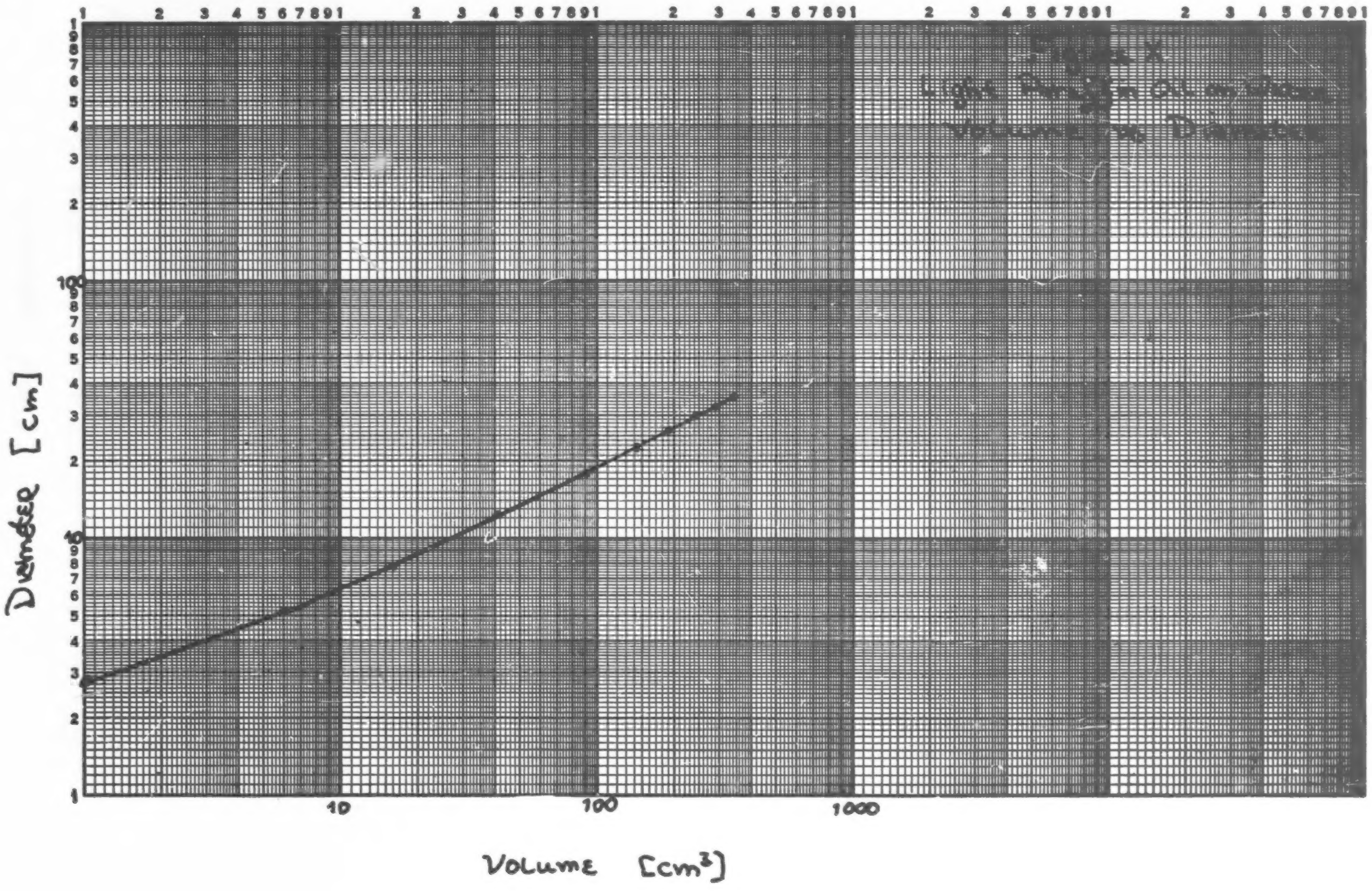

Figure X
Light Paraffin Oil on Water
Volume vs Diameter

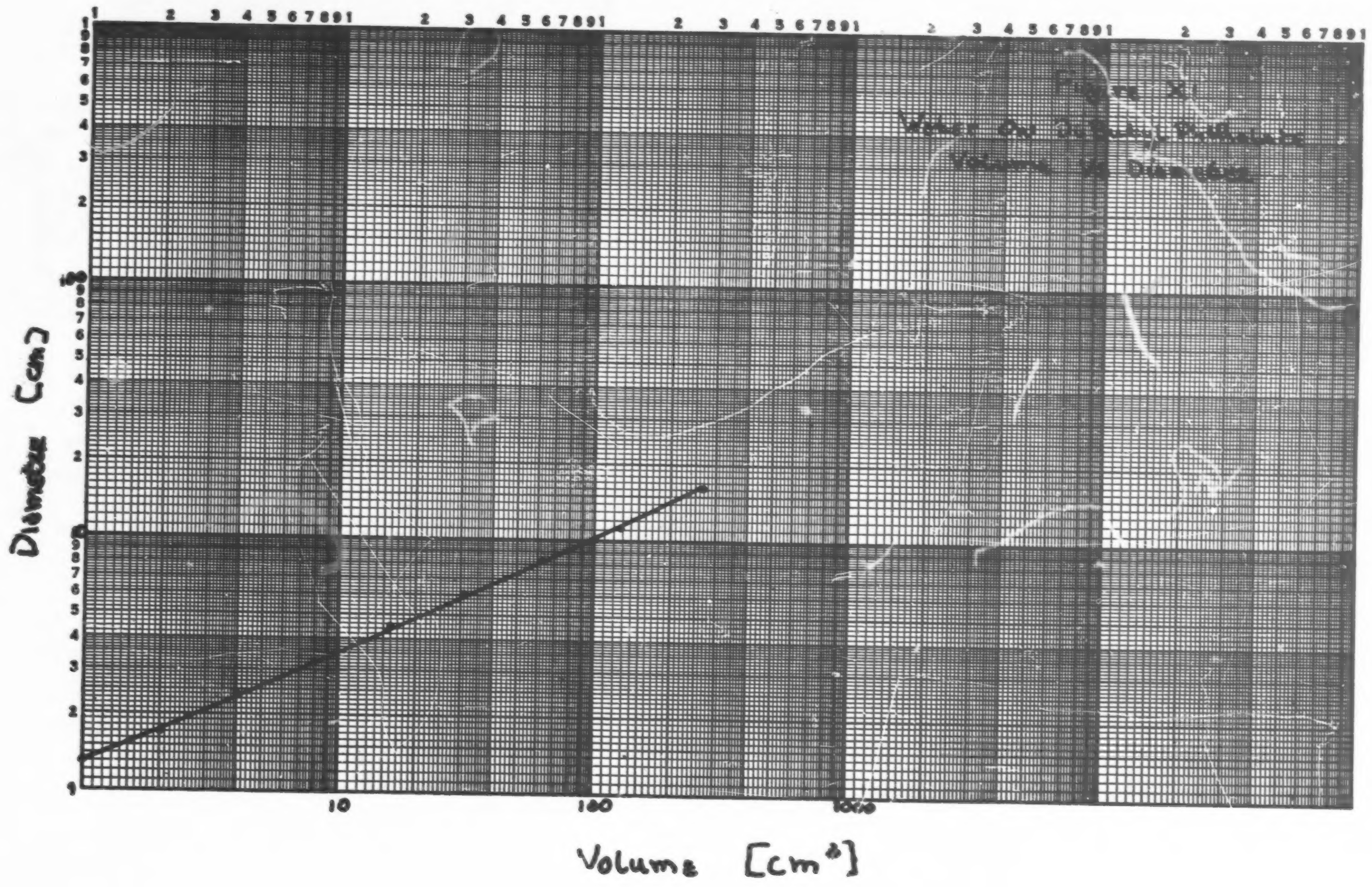

Figure XI
Water on Dibutyl Phthalate
Volume vs Diameter

Table 4. Lens Characteristics

System Code	Upper Phase	Lower Phase	ρ_u	ρ_L	σ_u	σ_L	σ_I	$-F_s$	D_{100} Actual	D_{100} Predicted	$\frac{d \log D}{d \log V}$	t_∞	$\frac{a_I}{t_\infty}$
			(gr / cm^3)		(dynes/cm)				(cm)			(cm)	
LPO	Light Paraffin Oil	Water	0.8599	0.9928	29.8	69.3	50.3	10.8	18.6	17.2	.410	.368*	2.28
HPO	Heavy Paraffin Oil	Water	0.8830	0.9980	30.8	69.3	47.5	9.0	17.4	17.3	.470	.426^o	2.15
LPO SW	Light Paraffin Oil	Synthetic Sea Water	0.8599	1.0186	29.4	66.3	49.6	12.7	18.5	17.1	.439	.373*	2.05
DEC	Decalin	Water	0.8744	0.9968	29.2	69.4	47.8	7.6	18.4	18.1	.416	.388^o	2.29
DOD	Dodecane	Water	0.7415	0.9965	24.3	69.5	47.3	2.1	30.3	28.9	.498	.138*	4.48
BB LPO	0.2 Vol. Bromobenzene 0.8 Vol. Lt. Paraffin Oil	Water	0.9739	0.9965	30.7	68.8	45.7	7.3	16.0	15.7	.391	.519^o	3.99
TET	Tetradecane	Water	0.7569	0.9965	24.8	68.7	47.8	3.9	27.0	24.6	.464	.175*	3.62
DBP	Water	Dibutyl Phthalate	0.9982	1.0453	52.6	32.7	21.8	41.7	10.2	9.6	.432	1.390^o	0.70

Table 4. Lens Characteristics

System	Upper Phase	Lower Phase	ρ_u	ρ_L	σ_u	σ_L	σ_I	$-F_s$	D_{100}		$\frac{d \log D}{d \log V}$	t_∞	$\frac{a_I}{t_\infty}$
									Actual	Predicted			
			(gr / cm^3)		(dynes / cm)				(cm)			(cm)	
DEM	Water	Diethyl Malonate	0.9982	1.0680	49.0	33.4	9.6	25.2	11.80	11.85	.421	.905^{o}	.583
DMP	Water	Dimethyl Phthalate	0.9952	1.1840	49.5	27.4	10.3	32.4	15.7	14.0	.476	.651^{o}	.516
BB	Water	Bromo-benzene	0.9971	1.4863	68.7	35.2	22.7	56.2	15.3	14.6	.470	.591^{o}	.520

* Based on observed D_{100} rather than Equation (6)

o Based on Equation (6)

The term $\pi R^2 t_\infty$ is the asymptotic relationship between the volume radius and thickness, and the other terms essentially correct this asymptotic relationship for pools of moderate diameter. If one examines the relative magnitudes of these correction terms, it can be seen that for other than very small lenses the last bracketed term is negligibly small, and that of the remaining terms those involving a_i^2 or $\sigma_i a_i$ are the dominant corrections.

Retaining only the dominant correction terms there is obtained after some rearrangement

$$V = \pi R^2 t_\infty \left[1 + \frac{\sqrt{2}}{3} \left(\frac{\sigma_i}{-F_s}\right)\left(\frac{a_i}{R}\right)\left(1 - \cos^3\left(\frac{A_i}{2}\right)\right) - \left(\frac{a_i}{t_\infty}\right)\left(\frac{a_i}{R}\right) \sin A_i \right] \qquad (39)$$

It can be shown by substitution that

$$\frac{\sigma_i}{-F_s} = \left(\frac{a_i}{t_\infty}\right)^2 \left(\frac{\rho_L}{\rho_u}\right) \qquad (40)$$

Using this expression for $\sigma_i/(-F_s)$ in the simplified expression for V there is obtained

$$V = \pi R^2 t_\infty \left[1 + \frac{\sqrt{2}}{3} \left(\frac{\rho_L}{\rho_u}\right)\left(\frac{a_i}{t_\infty}\right)^2 \frac{a_i}{R}\left(1 - \cos^3\left(\frac{A_i}{2}\right)\right) - \left(\frac{a_i}{t_\infty}\right)\left(\frac{a_i}{R}\right) \sin A_i \right] \qquad (41)$$

It can be clearly seen from this expression that the magnitude of the correction will depend largely on a_i / t_∞. It will be shown later that if a_i / t_∞ is large the angle A_i will be small. For small values of A_i it can be shown that expansion of the term $1 - \cos^3\left(\frac{A_i}{2}\right)$ will yield a term equal to $0.18 \frac{a_i}{t_\infty}\left(\frac{a_i}{R}\right) \sin A_i$. Thus if the correction is large, the term 0.82 $(a_i/t_\infty)(a_i/R)$ sin A_i will be the dominant correction term. That is for small A_i the correction due to the $(1 - \cos^3 (A_i/2)$ term will be of opposite sign and 18% as large as the term containing sin A_i. If a_i/t_∞ is not too small and A_i not too large, the term containing $1 - \cos^3 (A_i/2)$ will, because of its smaller coefficient and the fact that it is multiplied an additional time by the small factor a_i/t_∞, still remain smaller than the term containing sin A_i. Thus when $A_i = 120^\circ$, $(a_i/t_\infty = .58)$ the term containing sine A_i will be roughly 3.4 times as great as that containing $1 - \cos^3 (A_i/2)$, and at $A_i = 150^\circ$ $(a_i/t_\infty = .52)$, roughly 2.0 times as great.

For all the systems tested a_i/t_∞ was never less than 0.55. As an approximation, the terms in $1 - \cos^3 (A_i/2)$ and sine A_i will be combined to yield 0.82 $(a_i/t_\infty)(a_i/R)$ sin A_i. The error in this approximation is significant only when the correction is small, i.e. when a_i/t_∞ is small, and the actual error introduced by the approximation should therefore always be small. Thus we will write:

$$V \doteq \pi R^2 t_\infty \left[1 - 0.82\left(\frac{a_i}{t_\infty}\right)\left(\frac{a_i}{R}\right) \sin A_i\right] \tag{42}$$

The angle A_i equals $B_i + A_L$ (refer to Equation 16). Most of the time A_L is small, and for the purposes of approximation it will be assumed $A_i \doteq B_i$. An alternative form to Equation (14) for B_i is:

$$\sin^2 (B_i/2) = -F_s\,(\sigma_L + \sigma_u - \sigma_i)/4\,\sigma_L\,\sigma_i \tag{43}$$

Making the assumption that $\sigma_u \doteq \sigma_i$ we get as a rough approximation

$$\sin^2 (B_i/2) \doteq -F_s/4\,\sigma_i \tag{44}$$

Referring back to Equation (40) it can be seen that

$$-\frac{F_s}{\sigma_i} = \left(\frac{t_\infty}{a_i}\right)^2 \frac{\rho_u}{\sigma_L} \tag{45}$$

Substituting for $-F_s/\sigma_i$, we obtain upon taking square roots:

$$\sin\left(\frac{B_1}{2}\right) \div \frac{t_\infty}{2\,a_1}\left(\frac{\rho_u}{\rho_L}\right)^{1/2} \div \sin\left(\frac{A_1}{2}\right) \qquad (46)$$

For small angles sin $A_1 \div 2 \sin \frac{A_1}{2}$. Further $\left(\frac{\rho_u}{\rho_L}\right)^{1/2}$ rarely differs from 1.0 by more than 10%. Therefore

$$\sin A_1 \div \frac{t_\infty}{a_1} \qquad (47)$$

verifying our previous assumption that A_1 is small when a_1/t_∞ is large. Substituting the above for sin A_1 in Equation (42) there is obtained

$$V \div \pi R^2\, t_\infty \left[1 - 0.82\, \frac{a_1}{R} \right] \qquad (48)$$

Putting this in dimensionless form by dividing through by πt^2_∞ there is obtained:

$$\frac{V}{\pi\, t_\infty^3} \div \left(\frac{R}{t_\infty}\right)\left[\left(\frac{R}{t_\infty}\right) - 0.82 \left(\frac{a_1}{t_\infty}\right) \right] \qquad (49)$$

Thus we see that the dimensionless volume $V/\pi\, t_\infty^3$ should be a function of the dimensionless radius R/t_∞ with the dimensionless capillary constant as a parameter. As a_1/t_∞ goes to 0, or R/t_∞ goes to infinity the relationship reduces to the assymptotic t_∞ volume-radius equation, as it should. Putting this in the somewhat more convenient diameter form

$$\frac{V}{\pi\, t_\infty^3} \div \frac{1}{4}\left(\frac{D}{t_\infty}\right)\left[\frac{D}{t_\infty} - \frac{1.64\, a_1}{t_\infty} \right] \qquad (50)$$

The coefficient for a_1/t_∞ is somewhat in error due to the dropping of various terms and the simplifying assumptions used. These errors were evaluated for typical lenses. Based on the calculations it was found that these errors could be roughly compensated for by changing the coefficient of a_1/t_∞ to 1.35, thus yielding

$$\frac{V}{\pi t_\infty^3} \doteq \frac{D}{4 t_\infty} \quad \frac{D}{t_\infty} \quad \frac{-1.35 a_i}{t_\infty} \tag{51}$$

$V/\pi t_\infty^3$ as calculated from the above equation is plotted versus D/t_∞ in **Figure XII** for various values of the parameter a_i/t_∞. Experimentally obtained $V/\pi t_\infty^3$ and D/t_∞ points for the various systems tested are plotted on the same curve. Where there was a large discrepancy between D as obtained from Equation (8) and the measured value of D for a 100 cm^3 volume, the value of t_∞ used was not that obtained from Equation (6) but rather the t_∞ value obtained by extrapolating a $\overline{t}$ vs $\frac{1}{R}$ plot to $\frac{1}{R}$ equals zero (after the fashion of Langmuir (37)).

It can be seen that this method of plotting, unifies in a single plot a **wide** variety of data with only a single added parameter a_i/t_∞ being necessary to fit most of the data with fairly good accuracy. Therefore it appears that either Equation (51) or Figure XII, in conjunction with Equation (6), can be used for predicting the non-asymptotic volume vs diameter behavior of lens forming systems. **From Figure** XII it can be seen that at D/t_∞ values of 20 or greater all systems tend to approach the assymptotic D vs V behavior within 10%. This corresponds roughly to 100 cm^3 pool values for most systems, thus explaining why the relatively good agreement between D observed at 100 cm^3 volume and that predicted by Equation (8) and why the observed diameter averaged 4.4% higher than the predicted values.

It should be noted that the **asymptotic** Equation (8) and Equation (51) for the non-**asymptotic** case, apply to systems based on sea water (simulated) and oil, as well as for fresh water and oil systems.

A procedure based on the Bashforth and Adams' tables (7) was developed for computing lens value vs diameter behavior but it is much more awkward and time consuming than the previously described method. Because of this awkwardness the procedure was not investigated extensively.

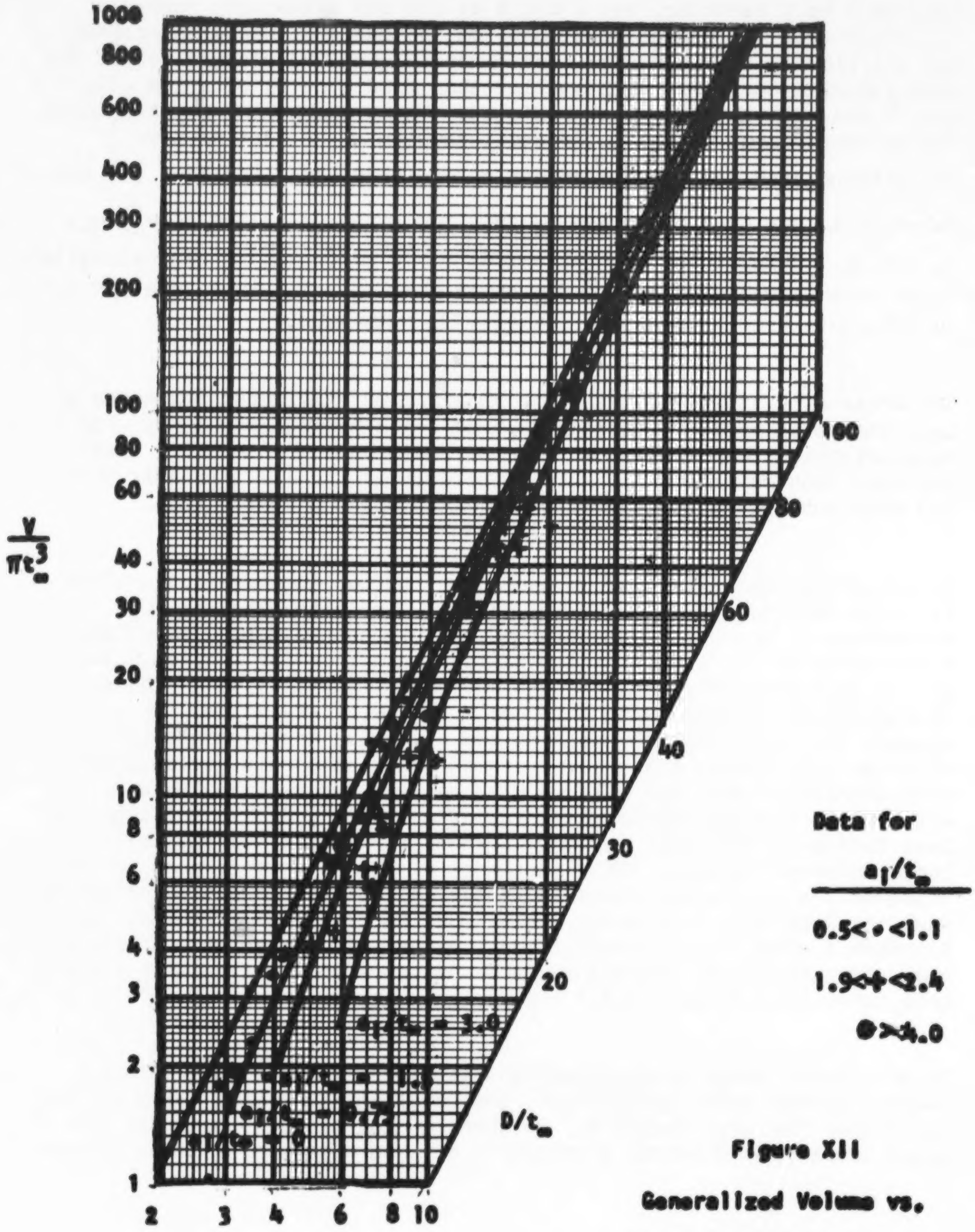

Figure XII

Generalized Volume vs.

Diameter Correlation for

Lenses

Tests were carried out using light paraffin oil, and water containing various levels of detergent (0.5% and 1.0%). These systems showed typical D vs V behavior, but D and $\bar{t}$ at 100 cm^3 value were markedly different from the values predicted, on the basis of measured surface and interfacial tensions, from Equations (8) and (6) respectively. The observed diameters were much smaller than predicted by Equation (8), i.e. $\bar{t}$ was much thicker than predicted. The disagreement appears to be due to measurement of the interfacial tension σ_i. A plot of $\bar{t}$ vs $\frac{1}{R}$ was extrapolated to $\frac{1}{R} = 0$ to obtain t_∞ and then using Equation (6) this value of t_∞ was used to obtain σ_i from the measured values of σ_u, σ_L, ρ_u and ρ_L. Using this value of σ_i, $a_i = \sqrt{2 \sigma_i/(\rho_L - \rho_u)g}$ was calculated. Based on this value of a_i and the extrapolation value of t_∞ the $V/\pi \, t_\infty^3$ vs D/t_∞ data fit the curves of Figure XII very well.

The areas of distorted lenses were measured by planimeter traverses of lens images on motion pictures taken of relaxing deformed lens. For eccentricities (major diameter/minor diameter) as great as 2:1 these deformed lens covered areas which were only 1.6 to 1.7 % greater than the area covered by the corresponding undeformed circular lens.

As noted previously, the larger the lens diameter, the more susceptible it is to deformation and breakup. It was also noted that as $-F_s$ approaches 0, the more susceptible a lens is to breakup. Essentially a low value of $-F_s$ implies a low t_∞ value, and thus for a given value of D a lens characterized by a low value of $-F_s$ will have a higher dimensionless diameter D/t_∞ than one with a high $-F_s$ value. Thus it appears that D/t_∞ may very well be the criterion for lens stability. At large D/t_∞ values $\bar{t}$ approaches t_∞ closely and barely varies at all with diameter. Thus for a large D/t_∞ lens, a deformation (which effectively changes the local radius of curvature, does not change the lens thickness very much (as also seen by our area measurements on large deformed lenses). This smallness of change in thickness in turn cause only a very small increase in the hydrostatic forces which act to push the lens into a circular form. Thus as D/t_∞ becomes large, lenses approach a condition of neutral equilibrium with respect to deformation, and deformation, once started, tends to continue with very little resistance, permitting breakup under very slight stress.

In wind drift tests it was observed that lenses tended to break into smaller lenses under wind action, the resultant lens size being smaller the higher the wind velocity. At about 10 knots, light paraffin oil would break up into lenses of roughly 3 or 4 cm diameter, and at 20 knots lenses of roughly 1 to 2 cm diameter would be obtained.

Since over the range in question the lens diameter varies roughly as the 0.45 power of the lens volume, t varies roughly as $V^{0.1}$. This is a breakup induced change from a 1000 cm^3 pool to 1000, 1 cm^3 pools would only cause a two-fold decrease average lens thickness, and a consequent two-fold increase in net area of coverage. Lens breakup therefore is not likely to be accompanied by large increase in net area of coverage. The gross area of coverage may well increase due to turbulent diffusion and spreading apart of the individual small lenses with respect to one another.

Crude Oils

The spreading characteristics of four typical crudes were tested. Some of the properties of these crudes are listed in Table 5.

These crudes vary widely in their spreading character. The Fullerton spreads out uniformly and rapidly. It quickly covers the surface of small test basins. Upon standing, dispersed small beads form upon the surface. This behavior may be akin to that observed in confined monolayer forming systems, where the excess film material gathers in beadlike little lenses upon the monolayer, Adam (3). The bead formation may also be due to progressive changes in composition induced by evaporation.

The Tia Juana,Safaniya and Urania when initially deposited in small quantities disperse very rapidly, covering the entire surface of a small test basin. Subsequent additions spread more slowly often forming a diffuse, but readily discernible pool. When still further oil is added, irregular somewhat thicker and more deeply colored pools form in the case of the Tia Juana and Safaniya crudes. The thickness of such a pool of Safaniya crude will be roughly 0.013 cm. On the other hand Urania crude upon further deposition forms a lens-like pool on top of the previously deposited thin film. Such pools had thicknesses ranging from 0.14 to 0.18 cm, larger thicknesses being obtained at larger spill volumes. The diameters of these lens like pools vary roughly as the 0.45 power of the deposited volume, somewhat similar to the case of regular lens formers.

The behavior of the crudes seemsto form a progression where high viscosity, high density, high carbon to hydrogen ratio all indicate

Table 5. Characteristics of Crudes

Type	Point of Origin	Density gr/cm^3	σ_u	σ_L dynes/cm	σ_i	$-F_s$	Viscosity Saybolt Seconds	Boiling Point at Vol. % distillate
Fullerton	Texas	0.8114(c) 0.8090(d)	24.9(a)	44.8(a)	18.7(b)	-1.2 -26.4(g)	45.8(h)	246(e)
Tia Juana	Venezuela	0.8961(c) 0.8876(d)	20.9(a)	58.7(a)	34.3(b)	-3.5 -14.8(g)	297 (h)	404(e)
Urania	Louisiana	0.9260(c) 0.9202(d)	31.5(a)	58.1(a)	17.5(b)	-9.1 -21.6(g)	2591(h)	515(e)
Safaniya	Saudi Arabia	0.8927(c) 0.8588(d)	27.3(a)	53.3(a)	30.1(b)	-4.1 -20.8(g)	270(h)	480(f)

(a) After mixing and separating oil and water.
(b) Letting oil and water quietly contact each other in Tensiometer dish.
(c) At 20°C, provided by the Mobil Oil Company.
(d) At 27°C, measured in our laboratory.
(e) Hempel
(f) ASTM
(g) Based on a clean water surface tension of 70 dynes/cm
(h) At 60°F

a greater tendency towards ultimately displaying lens-like behavior, with intermediate values of these factors being associated with irregular pool formation, and low values with uniform film formation.

The group $\sigma_u - \sigma_i - \sigma_L$, (i.e. $-F_s$) is negative for each of the crudes. Each of the crudes appreciably lowers the surface tension of the water, the reduction being most marked in the case of Fullerton crude. This lowering is presumably produced by the extractive transfer of rate-soluble components from the crude into the water, and therefore may depend on the relative quantities of crude and water in contact with each other. In a dynamic spreading situation, the pool may spread faster than such extraction can take place, and σ_L the surface tension of the water may well be closer to that of pure water uncontaminated by material extracted from the crude. Based on a clean water surface tension of 70 dynes/cm, a set of alternative values of $-F_s$ have been calculated and are also tabulated in Table 5. In the case of $-F_s$ calculated in this manner, Fullerton has the greatest $-F_s$ value, and the $-F_s$ values vary from system to system by less than a factor of 2. In the case where σ_L is that for oil contaminated water, $-F_s$ is least for Fullerton, is significantly lower for all systems, and varies from system to system by a factor of almost eight.

Since $-F_s$ is negative for all the crudes tested, none should ordinarily form lenses. Yet the Urania forms a lens-like pool when deposited on a previously formed Urania film. By measuring the surface tension of water covered with this film it was found that it decreases as the amount of oil in the film increases and that it ultimately levels off at a value 18 dynes/cm below that of water saturated with Urania crude. (It is perhaps a coincidence but the interfacial tension of Urania Crude and water is also about 18.0 dynes.) In any case when the saturated water surface tension lowered by this 18 dynes is substituted for σ_L, $-F_s$ becomes positive (9.4 dynes/cm) indicating that a lens should be capable of forming. That is, since the lens rests on this thin film, the surface tension of the film rather than that of water should be used for σ_L. The lens like pools that do form are significantly larger, (29 cm diameter for a 100 cm^3 pool) than predicted using the t_∞ approximation, and the 9.4 dyne/cm $-F_s$ value based on maximum surface tension lowering (16.2 cm diameter for a 100 cm^3 pool). This may be because we are not using the correct interfacial tension for oil in contact with the film. Actually we have no means of measuring this film-oil interfacial tension, and can only measure and therefore use the water-oil interfacial tension. Alternatively, the water surface tension may not have been lowered by the maximum amount that Urania film deposition could induce. It was previously noted that up to a leveling off point the lowering of the water surface tension was dependent upon the amount of film forming material that had been deposited.

In the case of the Safaniya and Tia Juana crudes, similar low surface tension film formation takes place. But here the value of $-F_s$ though positive at the minimum film surface tension is small, and the tendency towards film formation is marginal - which is in qualitative accord with the pool forming behavior of these crudes.

It appears that the spreading process for crude oil lenses and pools may depend largely on the rapidity of the convective and diffusive breakup and thinning of the thin oil films adjacent to these pools. For small spills on the ocean, such thinning should be rapid and lens-like pools are not likely to remain stable for any prolonged period of time. For large pools however lens-like pools may persist for considerable periods of time.

When traces of surface active agents, capable of lowering the surface tension of water, are added to water adjacent to the oil spill boundary, all of the crudes tested will form lens, reducing the area of pool coverage by a factor of 3 to 10. If the surface active agent is added five to ten minutes after crude deposition some case hardening of the oil pool appears to have taken place, and while the pool volume contracts it retains vestiges of its former shape. Often it has shard-like jagged edges and will not form a circular lens in many cases. Thus by adding suitable surface active agents it should be possible to greatly reduce the area of spread of spilled oil. Though this idea was developed independently, it was subsequently found that Sigwalt (65), Blokker (11) and Garrett (31) had previously developed somewhat similar ideas. The use of external films, monolayers or surfactant treatment to prevent pool spreading at sea may not be feasible under unfavorable weather conditions. Sigwalt noted that oil pool spreading was not retarded by fatty acid films when winds of greater than 2 to 4 knots were blowing in the direction of spreading. Garrett noted that the ability of monolayers to resist wind induced deformation depended on their spreading pressure F_s The higher F_s was, the more resistant the monolayer was to deformation, but even at the largest F_s value tested, 41.1 dynes/cm, the film could not resist deformation at wind speeds in excess of 10 knots. However in both Sigwalt's and Garrett's test the monolayer was restrained on its downward side and thus could not move downwind as a whole. It is possible that in an open sea situation, the oil spill and the surrounding monolayer or surfactant treated surface water could move downwind together - the zone of modified surface still continuing to maintain the oil in lens-like pools.

It was noted that partial vaporization of the crudes tended to make them more susceptible to lens formation. In a spill at sea the spreading will be so rapid that very thin films will usually be obtained before any evaporation induced lens forming tendencies manifest themselves. Evaporation will also cause stable skin formation. The oil, through loss of its more volatile components, is converted into a tarry non-deformable film. As spreading of fluid oil continues, the surface area available for evaporation increases. Continued evaporation, aided by the increase in avaporation area, but slowed down by the depletion of the more volatile fractions, should ultimately lead to a degree of tarryness which will prevent further spreading. Except for thin highly volatile oils, the time in which stable skin formation is induced will tend to determine the ultimate thickness and area of spread of the spill. For a typical Mid Eastern crude, due to the nearly complete loss of the more volatile fraction, evaporation is likely to virtually cease after thirty percent of the crude has evaporated. For large spills Blokker has estimated that this may take from 7 to 14 hours under near quiescent wind conditions, and 2 to 4 hours with 29 knot winds.

If tarryness sets in at this 30% evaporation level, it can be estimated from Blokker's data that the resulting tarry films will be 0.14 to 0.23 mm thick (.0055 to .009-in. thick).

Crude Oil Spreading Rates

Using motion pictures, as described in the Procedures Section, the areas of oil pools spreading on quiet water were measured vs elapsed time. In all cases, after an unsteady state period of about 0.2 seconds, the pool area initially increased at a constant rate. For the Fullerton crude (the one least likely to form a lens in the presence of a film contaminated surface) the rate of increase in area remained constant over the entire range of times tested (20 seconds). During this time the pool thinned down to an average thickness of 0.017-cm (0.0065-in.) in some instances.

At the other extreme, for the Urania crude the constant rate period persisted for only roughly 1.5 seconds, after which the rate of expansion gradually decreased, and the pool appeared to asymptotically approach a thickness of 0.15 cm, the thickness previously noted when Urania forms a lens-like pool on top of a previously deposited Urania film.

Leveling-off of the rate of increase in area also occurred for the Tia Juana and Safaniya crudes, but the constant rate of expansion period persisted for more time - usually eight seconds or more. The time at which leveling-off started was very variable. In one case the area increase rate for a Tia Juana pool started leveling-off after only two seconds; in another case only after 13 seconds. Though the rate of increase in area gradually decreased after the onset of leveling-off, the Tia Juana and Safaniya pools did not appear to approach an asymptotic thickness. Rather they appeared to approach a new but markedly lower constant rate of expansion. The Tia Juana and Safaniya pools were measured until they reached thicknesses of .029-cm (0.011-in.) in some instances.

Typical pool area vs time curves are shown in Figure XIII. Though the initial rate of increase in area is clearly a constant in any given test, the reproducibility of the rate data in duplicate tests is poor. In multiple tests, at the presumably same conditions, deviations from the average spreading rate have ranged up to 14%. The cause for this variation may be partly due to variation in temperature, but more likely it is due to variations in the amount of oil released. It is difficult to accurately measure and release a known volume of the stickier more viscous oils. On the basis of volume vs rate of spread correlation to be discussed later, it is anticipated that a 7.5% difference in volume would be required to produce a 14% change in the rate of spread.

Since the pools tested were initially quite thick, it was anticipated that the hydrostatic pressure force, $\frac{g\ t^2}{2} [1 - \frac{\rho_u}{\rho_L}]$, would be more important than $-F_s$ in promoting initial spreading. Initial spreading rates $(dA/d\theta)_o$ for 100 cm^3 pools of the four different types of crudes were measured. These rates and the corresponding values of $[1 - \frac{\rho_u}{\rho_L}] \rho_u$, $([1 - \frac{\rho_u}{\rho_L}] \rho_u)^2$, and $(dA/d\theta)_o$ are tabulated in Table 6, and $(\frac{dA}{d\theta})_o$ is plotted vs $[1 - \frac{\rho_u}{\rho_L}] \rho_u$ in Figure XIV.

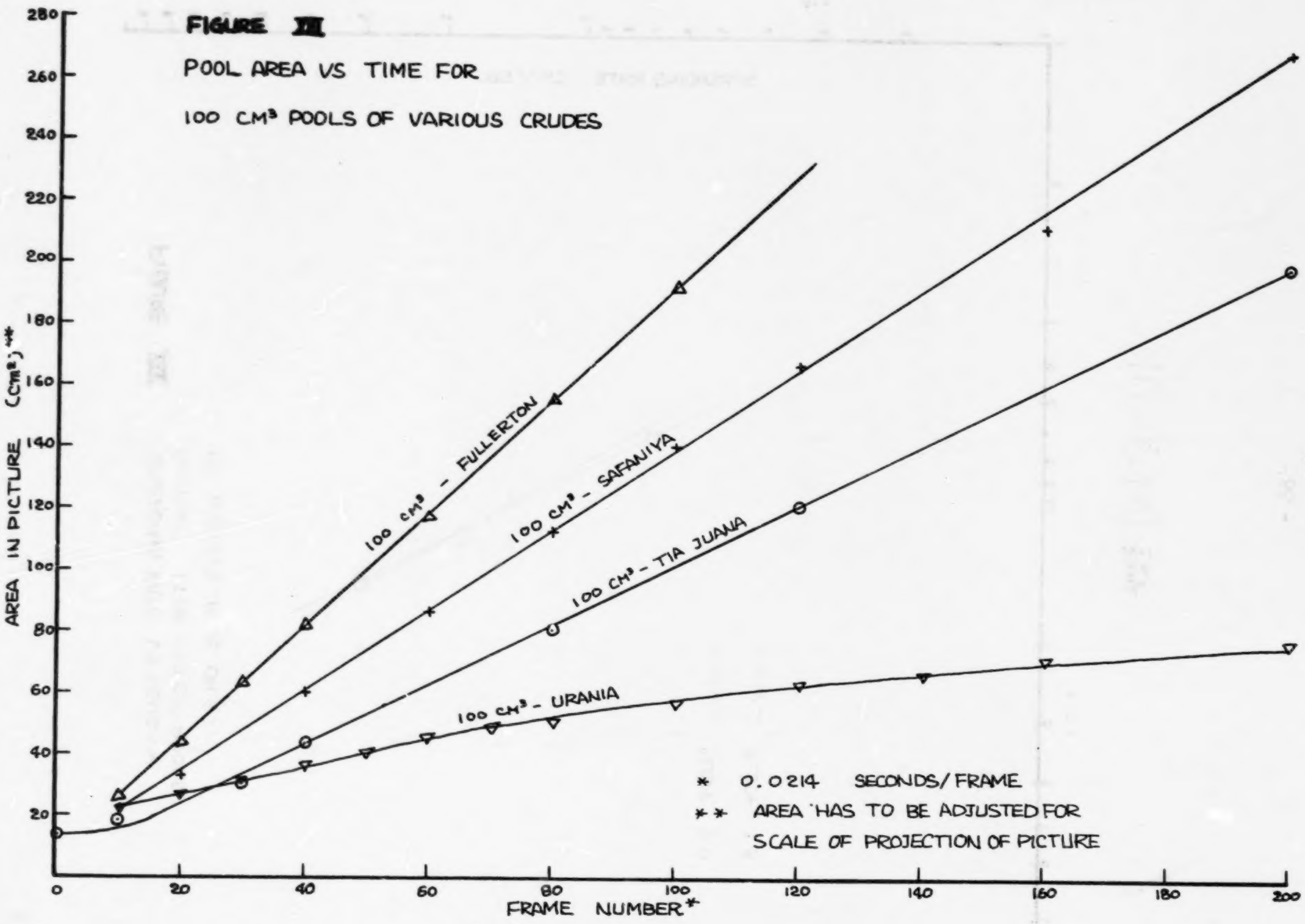

FIGURE XII

POOL AREA VS TIME FOR

100 CM³ POOLS OF VARIOUS CRUDES

* 0.0214 SECONDS/FRAME

** AREA HAS TO BE ADJUSTED FOR SCALE OF PROJECTION OF PICTURE

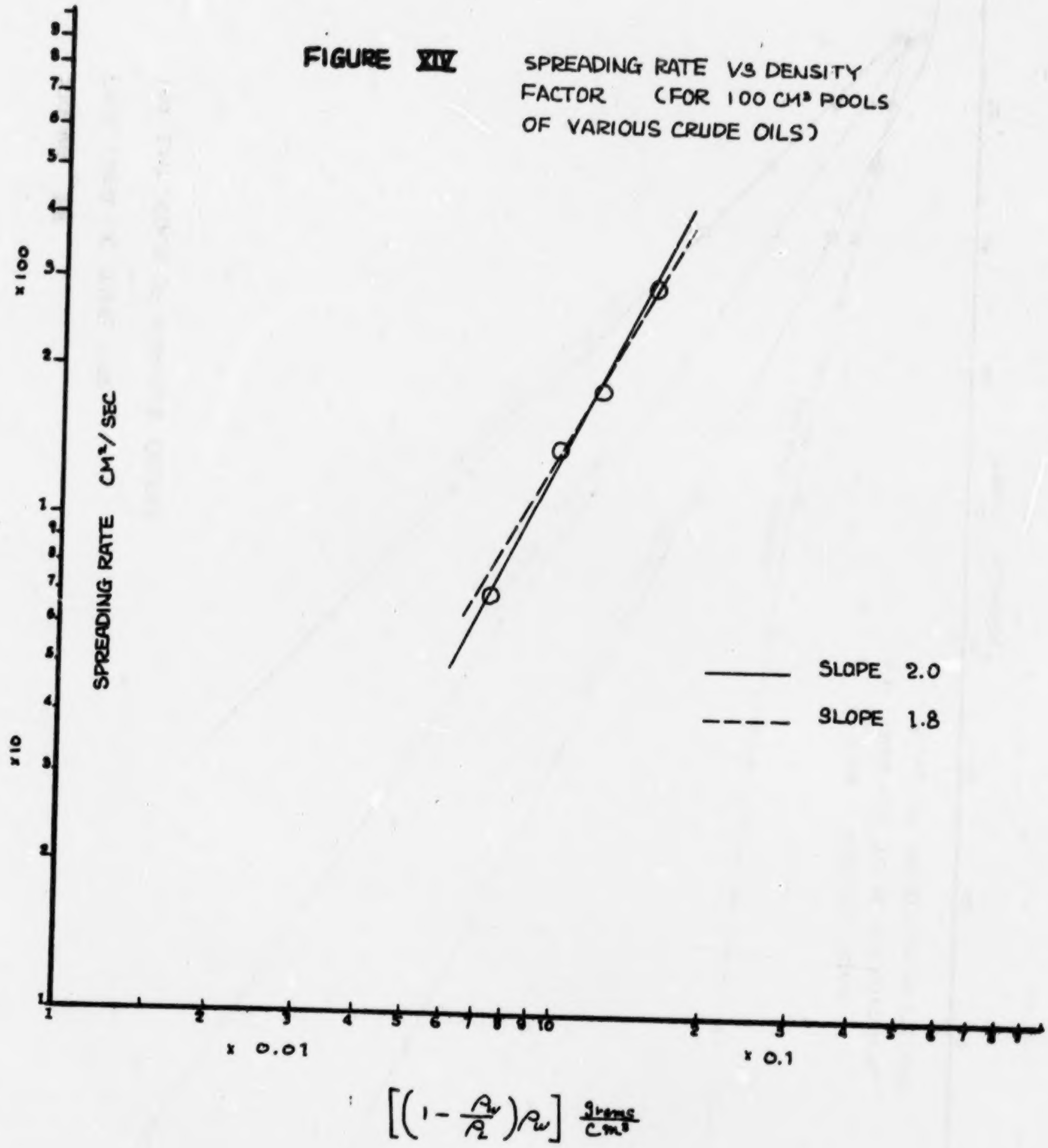

FIGURE XIV SPREADING RATE VS DENSITY FACTOR (FOR 100 CM³ POOLS OF VARIOUS CRUDE OILS)

Table 6. Area Spreading Rates as a Function of Oil Density

(100 cm^3 pools)

Type of Crude	$(1 - \frac{\rho_u}{\rho_L})\,\rho_u$ gr/cm^3	$[\,(1 - \frac{\rho_u}{\rho_L})\,\rho_u\,]^2$ gr^2/cm^6	$dA/d\theta$ Spreading Rate $cm^2/sec.$	$\frac{dA/d\theta}{[\,(1 - \frac{\rho_u}{\rho_L})\,\rho_u\,]^2}$ $cm^8\,/\,gr^2\ sec.$
Fullerton	.1545	.0239	291	12,200
Safaniya	.1213	.0147	181.3	12,350
Tia Juana	.09976	.00995	138.5	13,900
Urania	.07343	.005392	69.7	12,950

It can be seen that a line of slope 2.0 fits the points fairly well. Accordingly, the group $(dA/d\theta)_o \, / \left[\left(1 - \frac{\rho_u}{\rho_L}\right) \rho_u \right]^2$ remains fairly constant, the individual values deviating from the average value (12,850 $\text{cm}^8/\text{gram}^2$-sec.) by 8% at most and 4.6% on the average. Actually because a relatively short range of the quantity $\left[\left(1 - \frac{\rho_u}{\rho_L}\right) \rho_u \right]$ is covered it is difficult to decide on empirical grounds whether the exponent for $\left[\left(1 - \frac{\rho_u}{\rho_L}\right) \rho_u \right]$ should be 2.0, or some value close to 2.0. An exponent of 1.8 provides a slightly better fit than 2.0, the group $(dA/d\theta)_o \, / \left[\left(1 - \frac{\rho_u}{\rho_L}\right) \rho_u \right]^{1.8}$ deviating from its average value (8,230 $\text{cm}^{7.4}/\text{gram}^{1.8}$-sec.) by 4.2% on the average and 6.4% at most.

The effect of spill volume on spreading rate was tested. Fullerton crude, the least viscous, and therefore the crude whose pool volume could be controlled with the greatest precision, was used in these tests. Fullerton also had the advantage of being the least susceptible to lens formation and falling off in spreading rate. Spill volumes were varied from 25 cm^3 to 150 cm^3. The area vs time plots for these tests are shown in Figure XV. It can be seen that the spreading rate increases markedly as the volume increases. The area spreading rates are plotted vs pool volume in a log-log plot in Figure XVI. It can be seen that with the exception of the 25 cm^3 pool volume the points fall fairly well on a straight line of slope 1.8. It will be assumed that the 25 cm^3 point is in error. The $(dA/d\theta)_o \, / \, V^{1.8}$ values - excluding that for 25 cm^3 - deviate from their average value .1775/$\text{cm}^{3.4}$ sec., by 2% on the average and 4% at most. In more limited and less accurate tests with Urania crude a V exponent of 1.6 was obtained.

The excess hydrostatic pressure is equal to the hydrostatic force per unit length of pool cross section $\frac{\rho_u g}{2} \left[1 - \frac{\rho_u}{\rho_L} \right] t^2$ divided by the pool thickness t, i.e. $\frac{\rho_u g}{2} \left[1 - \frac{\rho_u}{\rho_L} \right] t$. When the pool has any given radius R, the thickness is equal to $V/\pi R^2$ where V is the pool volume. Thus for any given pool radius the excess

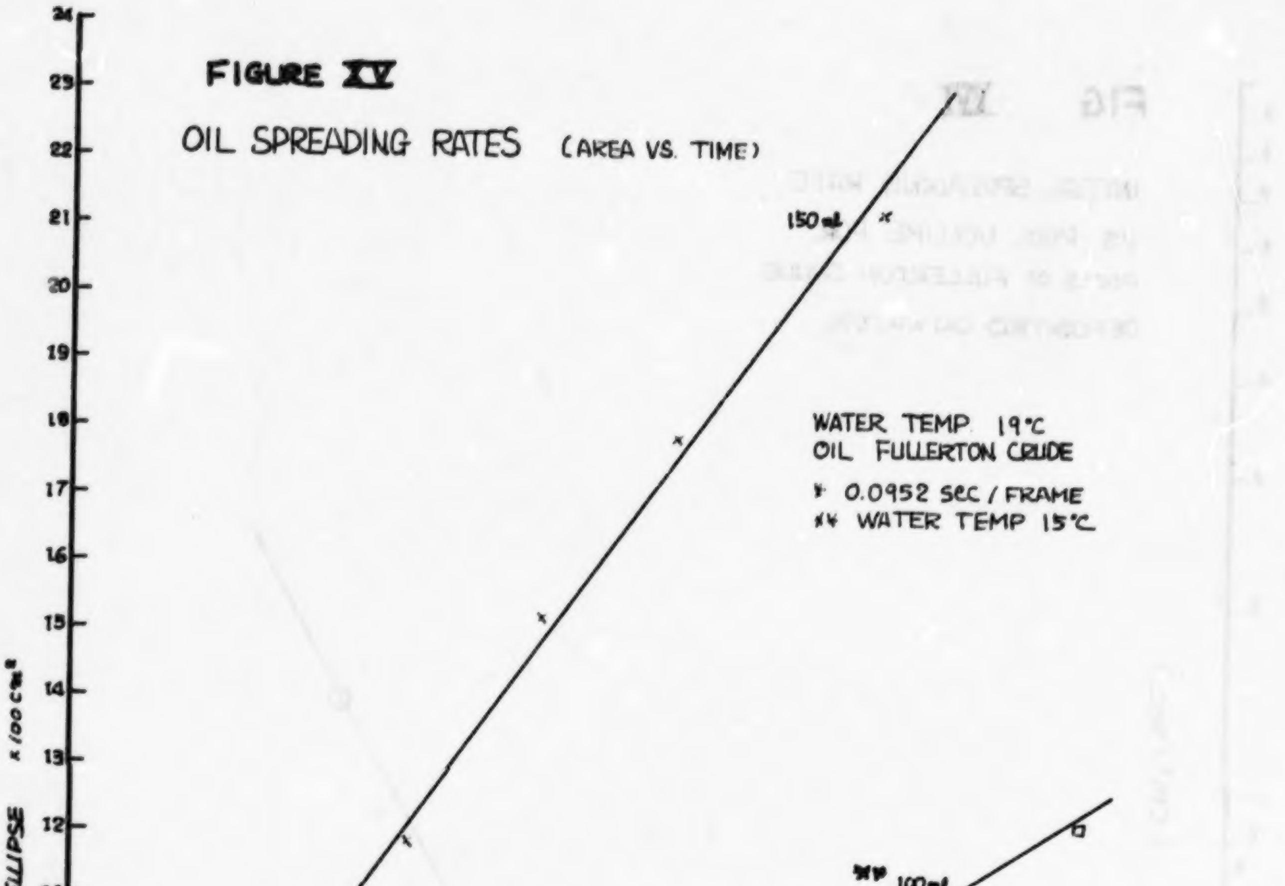

FIGURE XV

OIL SPREADING RATES (AREA VS. TIME)

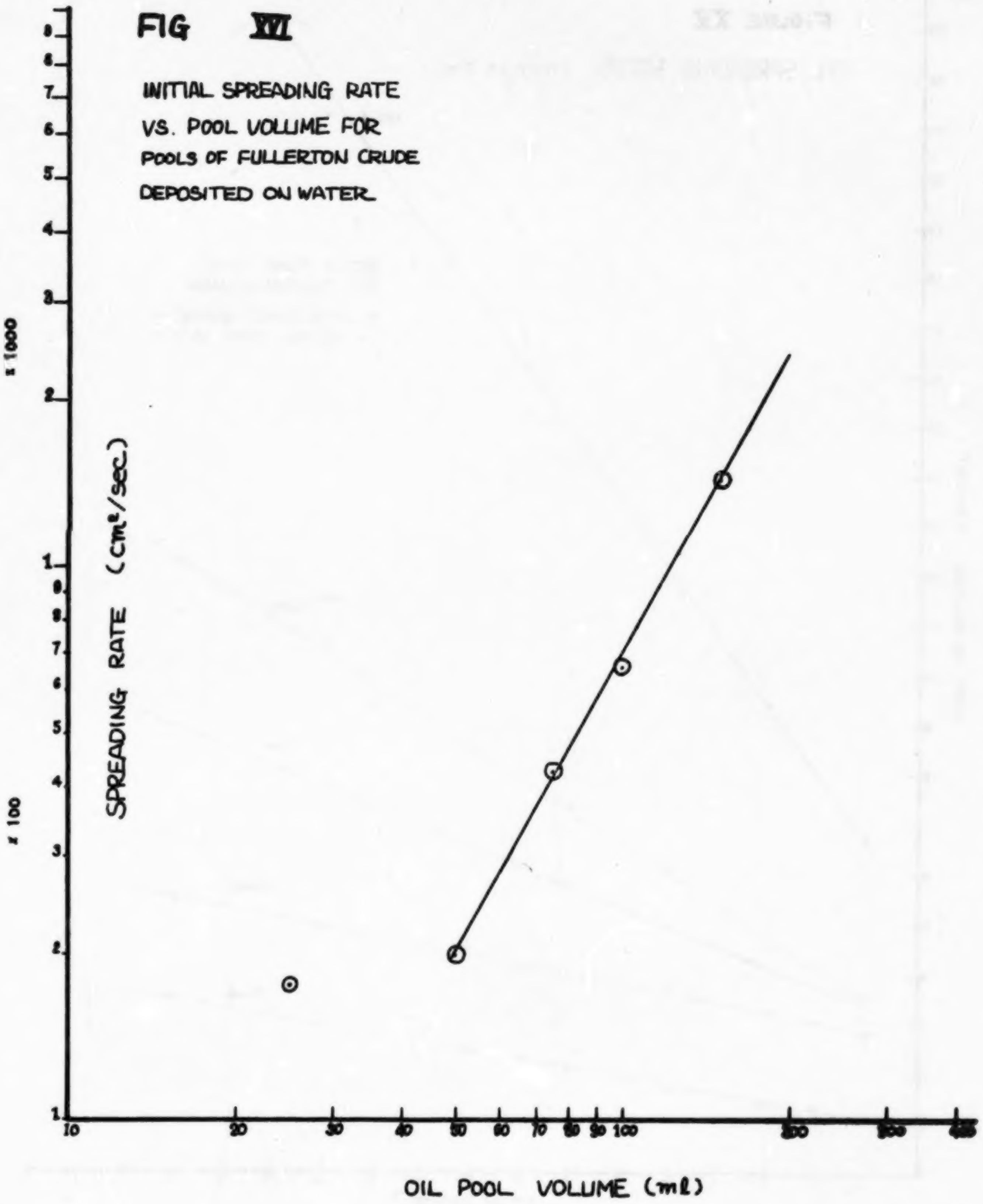

FIG XVI

INITIAL SPREADING RATE VS. POOL VOLUME FOR POOLS OF FULLERTON CRUDE DEPOSITED ON WATER.

hydrostatic pressure should be proportional to $(\rho_u g V/2\pi R^2)[1 - \rho_u/\rho_L]$.

This would imply that the grouping $\rho_u V [1 - \rho_u/\rho_L]$ might be a significant characteristic parameter in determining the spreading characteristics of a spill. Based on this inference and the closeness of the empirically determined exponents for the individual groups $\rho_u (1 - \rho_u/\rho_L)$ and V it will be assumed that both are raised to the same exponent. That is the initial rate of increase in pool area will be assumed proportional to $[\rho_u (1 - \rho_u/\rho_L) V]^n$ where n is approximately 1.8. R^{-2}, which varies as the pool spreads does not appear in this group, which therefore can be taken as a time invariant characteristic parameter. Essentially, it has been assumed that the area spreading rate is a function of the excess hydrostatic pressure, which in turn varies as R^{-2}. Yet the area spreading rate, which is constant, does not depend on R. Therefore, if our reasoning is correct, there must be some other factor, as yet undetermined, which exactly cancels out the dependency on R.

The various oils differ markedly in viscosity. The Urania is 50 times more viscous than the Fullerton. At the same time the group $\rho_u (1 - \rho_u/\rho_L)$ was varied, the viscosity also experienced a concomitant variation; and it is difficult to wholly separate the effects of these two variations. However it can be noted that for equal volume pools of Fullerton and Urania, the Fullerton spreads roughly four times as fast in area, has twice as high a value of $[1 - \rho_u/\rho_L]\rho_u$, and a forty-five times lower viscosity in the test temperature range. It thus appears that, if the oil viscosity is a variable affecting the rate of spreading, it must be a very weak one. There are two situations that could give rise to this situation. One is that the spreading process is turbulent in which case the influence of viscosity, though not completely negligible, would be weak. The second is that the flow resistance to spreading depends on flow induced in the water layer beneath the spreading oil. In such a case the viscosity of the water might influence the spreading rate. Fullerton spreading tests were carried out at three different water temperatures: 11°C, 15°C and 44°C. The spreading rates are tabulated below.

Table 7. Area Spreading Rates vs Temperature for 100 cm^3 pools of Fullerton Crude

Temperature	$(dA/d\theta)_o$ Spreading Rate cm^2 / sec.	μ_w Water Viscosity cps	$(dA/d\theta) \times \mu_w$
11°C	550	1.274	700
15°C	650	1.145	745
44°C	1060	0.608	644
		Average	696

The spreading rate is also plotted vs the viscosity of water on log-log paper in Figure XVII. It can be seen that the plot has a slope of roughly -1.0. That is the area spreading rate appears to be inversely proportional to the viscosity of the water on which the spreading is taking place. This is substantiated by the rough constancy of the term $(dA/d\theta)_o \times \mu_w$ in Table 7. This term has an average value of 696 cm^2/sec. cps, and the individual values deviate from this figure by only 5% on the average, and 7.5% at most. Empirically it appears that an even better fit is obtained using an exponent n of -0.8 or -0.9 for u_w, in which case the term $(dA/d\theta)_o \times \mu_w^{-n}$ varies from its average value by an average of 3%, and 4.5% at most. A relatively small range of viscosities has been covered and like the previously established exponents for V and $\left[\left(1 - \frac{\rho_u}{\rho_L}\right)\rho_u\right]$ the exponent n is not fixed with a high degree of accuracy. For this reason the simple correlation

$$\left(\frac{dA}{d\theta}\right)_o \propto \frac{1}{\mu_w} \tag{52}$$

will be used until the exponent for μ_w is fixed with greater certainty. Tests in which the viscosity of water is altered by a thickening agent may be suitable for extending the range over which u_w can be varied.

FIG XVIII SPREADING RATE FOR 100 CM³ POOLS OF FULLERTON CRUDE OIL VS VISCOSITY OF THE UNDERLYING WATER

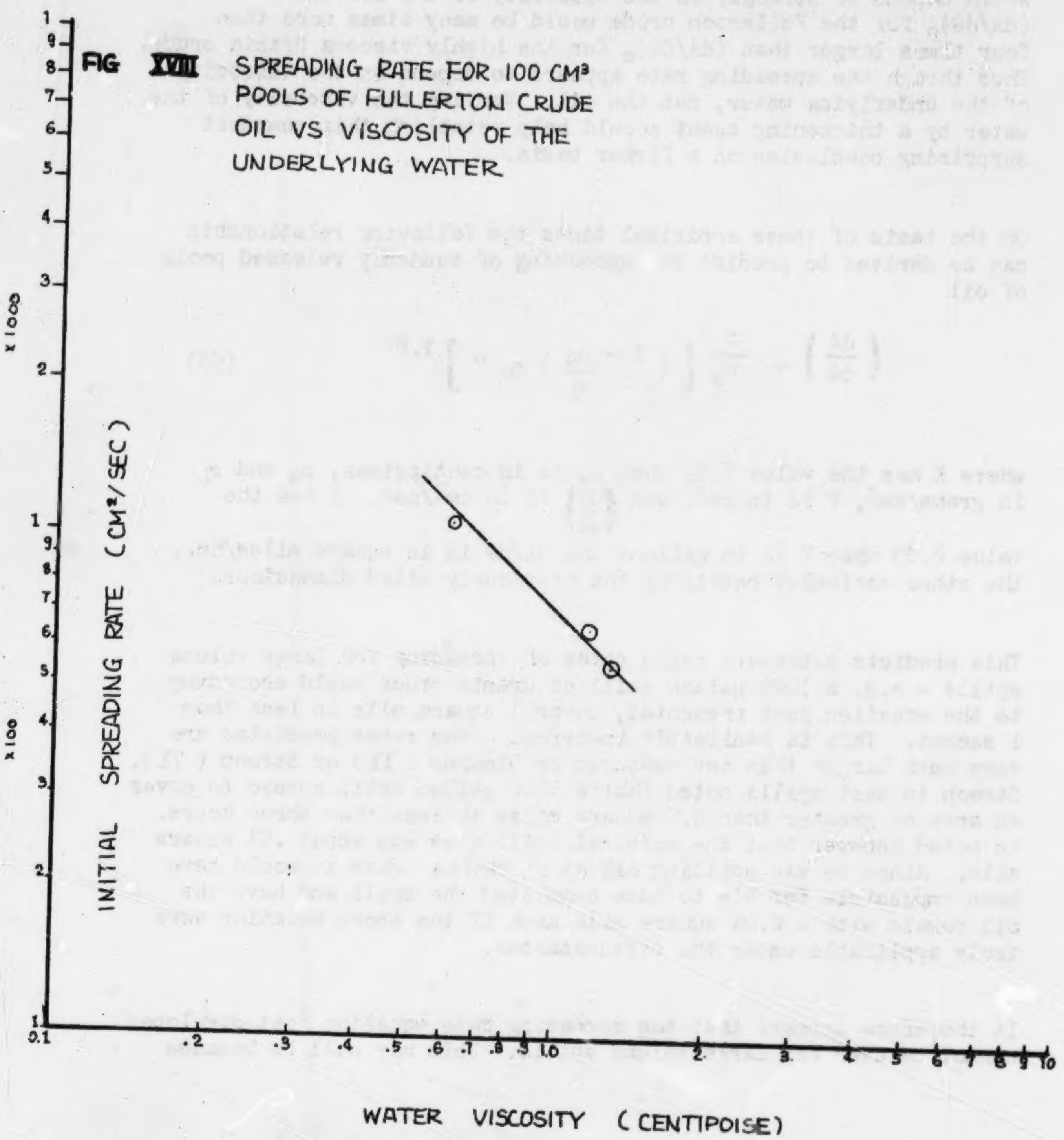

The change in temperature also causes a lesser change in the viscosity of the Fullerton crude. Thus it might appear that one could equally well assume that the spreading rate was a function of the viscosity of the oil. However if this were so, $(dA/d\theta)_o$ would depend so strongly on the viscosity of the oil that $(dA/d\theta)_o$ for the Fullerton crude would be many times more than four times larger than $(dA/d\theta)_o$ for the highly viscous Urania crude. Thus though the spreading rate appears to depend on the viscosity of the underlying water, not the oil. Varying the viscosity of the water by a thickening agent should help establish this somewhat surprising conclusion on a firmer basis.

On the basis of these empirical tests the following relationship can be derived to predict the spreading of suddenly released pools of oil

$$\left(\frac{dA}{d\theta}\right) = \frac{K}{\mu_w}\left[\left(1 - \frac{\rho_u}{\rho_L}\right)\rho_u V\right]^{1.8} \qquad (53)$$

where K has the value 5.35 when μ_w is in centipoises, ρ_u and ρ_L in grams/cm^3, V is in cm^3, and $\left(\frac{dA}{d\theta}\right)$ is in cm^2/sec. K has the value 2.03 when V is in gallons and $dA/d\theta$ is in square miles/hr., the other variables retaining the previously cited dimensions.

This predicts extremely rapid rates of spreading for large volume spills - e.g. a 1000 gallon spill of Urania crude would according to the equation just presented, cover 1 square mile in less than 1 second. This is manifestly incorrect - the rates predicted are very much larger than any measured by Blokker (11) or Stroop (71). Stroop in test spills noted that a 1260 gallon spill spread to cover an area of greater than 0.5 square miles in less than three hours. He noted however that the original spill area was about .01 square mile. Since he was spilling oil at a finite rate it would have been impossible for him to have completed the spill and have the oil remain with a 0.01 square mile area if the above equation were truly applicable under the circumstances.

It therefore appears that the spreading rate equation just developed cannot be used for large volume spills. This may well be because larger spills involve a different hydrodynamic regime. Since the small scale spreading rate depends strongly on the viscosity of water it must be a viscous or streamline regime. Larger spills probably fall within a turbulent flow regime, where the conditions regulating the rate of spread are different. It would be very desirable in future work to determine: whether the two regimes just postulated truly exist; what the critical conditions are which determine which regime spreading will take place; and what spreading correlation governs large scale spills. A third flow regime, where F_s the surface tension spreading force, rather than the excess hydrostatic pressure $\left[1 - \frac{\rho_u}{\rho_L}\right]\frac{\rho_u g t^2}{2}$, provides the driving forces may well exist when the pool becomes very thin. The rate of spread transition noted with Safaniya and Tia Juana crudes may represent the onset of surface tension driven spread. Thus Equation (53) may no longer apply when the pool thickness, as a result of spreading, falls below a critical value. Equation (53) probably no longer applies as the pool thickness approaches 0.001-in.- the approximate minimum thickness noted for films of spilled oil.

Equation (53) is wholly empirical and dimensionally inconsistent (except for the forced consistency imposed by the dimensions assigned to the constant K). As yet no hydrodynamic model, which might justify Equation 53 and provide insight as to the actual flow processes taking place, has been found. A wide variety of models have been explored but none has proved satisfactory.

Conservation of energy limits the maximum spreading rate. An energy balance can be readily obtained for a simple disc model of an oil pool such as shown below:

Figure XVIII

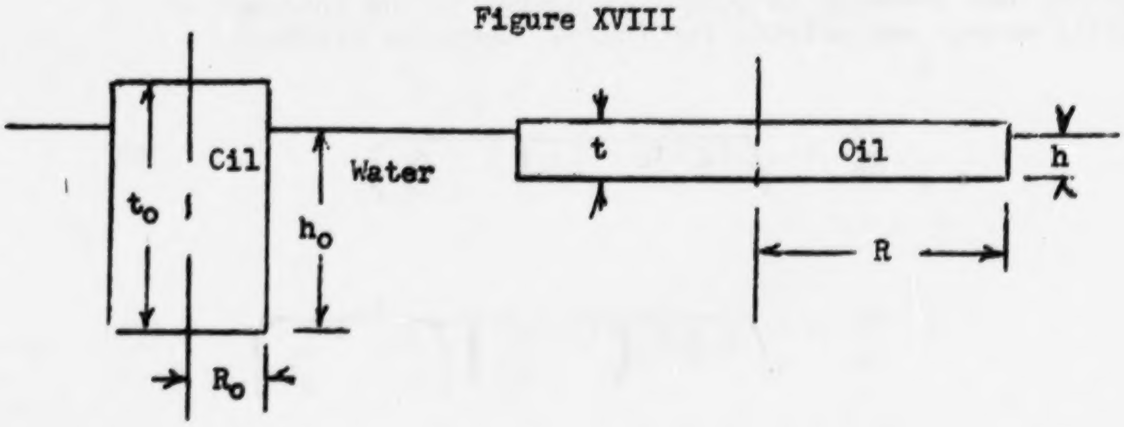

Neglecting surface energy, it can be shown that when a cylindrical disc like pool of oil of volume V spreads from an original radius R_o to a radius R, thereby decreasing its thickness from t_o to t and its submergence from h_o to h, the decrease in potential energy Δ PE will be equal to:

$$\Delta PE = V \rho_u \left(1 - \frac{\rho_u}{\rho_L} \right) g \left(\frac{t_o - t}{2} \right) \qquad (54)$$

The increase in kinetic energy Δ KE can be shown to be equal to

$$\Delta KE = \frac{\rho_u V}{4} \left(\frac{dR}{d\Theta} \right)^2 \qquad (55)$$

where, in deriving the above equation, use has been made of the fact that conservation of mass requires the local radial velocity U_r to be related to the boundary radial velocity by

$$U_r = \frac{r}{R} \left(\frac{dR}{d\Theta} \right) \qquad (56)$$

and that consequently

$$\overline{U}_r^{\,2} = \frac{1}{2} \left(\frac{dR}{d\Theta} \right)^2 \qquad (57)$$

Equating the decrease in potential energy to the increase in kinetic energy and solving for (dR/dΘ) there is obtained

$$\frac{dR}{d\Theta} = \sqrt{2 g \left(t_o - t \right) \left(1 - \frac{\rho_u}{\rho_L} \right)} \qquad (58)$$

or

$$\frac{dR}{d\Theta} = \sqrt{\frac{2 g V}{\pi} \left(1 - \frac{\rho_u}{\rho_L} \right) \left[\frac{1}{R_o^2} - \frac{1}{R^2} \right]} \qquad (59)$$

It can be seen from either of the last two expressions, when time $\theta = 0$, $R = R_o$ and $t = t_o$ the spreading rate should be equal to 0, i.e. less than the constant spreading rate predicted by Equation (53). The spreading rate thereafter rapidly increases until it is greater than that predicted by Equation (53). When Equation (59), obtained by considering the potential energy from which the kinetic energy of expansion is derived, predicts a lower velocity than Equation (53) the velocity obtained from energy conservation should, as a first approximation, be valid. However when Equation (53) predicts a lower velocity it, when otherwise applicable, should be valid. The critical time θ_c and the critical radius R_c at which the two predicted rates of spreading are equal can be obtained by solving Equations (53) and (59) simultaneously for R_c/R_o and integration of Equation (59) for θ_c using the previously obtained value of R_c/R_o and the assumed or given values of V, ρ_u and ρ_L. Solution for R_c/R_o yields

$$\frac{R_c}{R_o} = 1 + \frac{\sigma_o^{1.8}}{(8\,\pi\,g)^{0.5}} \left(\frac{K}{\mu}\right) \left[\left(1 - \frac{\rho_u}{\rho_L}\right) V \right]^{1.3} \qquad (60)$$

and for θ_c

$$\theta_c = R_o \sqrt{\frac{\pi}{2\,V\,g} \frac{(R^2 - R_o^2)}{(1 - \rho_u/\rho_L)}} \qquad (61)$$

When these equations are solved for θ_c and R_c, for typical values for V, R_o, ρ_u and ρ_L it is found that R_c and θ_c depend very much on V and R_o. For the case of a cylindrical pool which initially is as high as it is wide ($V = 2\,\pi\,R_o^3$) solutions obtained for values of $V = 100$ cm^3 and 1000 cm^3 with $\rho_u = 0.855$ and $\rho_L = 1.0$ indicate that $R_c/R_o = 1.30$ for $V = 100$ cm^3 and $R_c/R_o = 16.7$ for $V = 1000$ cm^3. Thus the range at which Equation (53) becomes applicable starts at very much larger radii as the spill volume increases. The corresponding values of θ_c are 0.16 seconds for 100 cm^3 and 5.0 sec. for 1000 cm^3. At 10 liters the corresponding values are $R_c/R_o = 338$ and $\theta_c = 54$ seconds. The critical time θ_c corresponds to an induction period during which expansion is slow and during which Equation (53) is not yet applicable. For 100 cm^3 spills the predicted θ_c, 0.16 sec., is roughly equal to the induction period of 0.2 seconds observed for test spills before the constant rate of expansion in area equation begins to become applicable. For a 1000 gallon spill the induction period would be 85 hours and R_c would be one nautical mile; but the film would probably have stopped expanding long before these conditions were reached. It appears likely that such a large spill would go from an energy conservation limited spreading rate to a turbulent resistance limited spreading rate for which the transitions might be significantly different than the critical transitions just calculated.

Wind Drift

Forty-five wind drift tests were carried out. In most of these, approximately ten oil pool drift rates were measured at a given set of operating conditions. Forty of the tests were made at a standardized wind duct height of 22 inches. Tests involving wind speeds of less than 19 ft./sec. were made using the attic fan, those greater than 19 ft./sec. - the industrial fan. The percentage drift, (oil pool velocity/wind velocity) x 100, for each of these tests was calculated using average wind velocity determined as described in the procedure section. While there was considerable scatter in the data it was noted that the percentage drift for the runs involving the attic fan averaged 3.2% while those involving the industrial fan averaged 2.8%. Since the industrial fan provided higher wind speeds this might appear to be a velocity dependent effect. Inspection showed however that the two different fans provided different wind velocity profiles. For the industrial fan, which had a large hub, the velocity at the vertical center line of the duct averaged 7% lower than the mean velocity in the duct, whereas for the attic fan the corresponding center velocity was 3.3% higher than the mean velocity. The oil pools moved down the center of the duct and therefore the percentage drift should be based on the center line wind velocity. Accordingly the average speeds for the industrial fan were multiplied by 0.93 and the attic fan speeds by 1.033 and the corresponding drift percentages calculated on the basis of these new velocities.

The resulting drift percentages and velocities are plotted vs each other in Figure XIX. While there is still a good deal of scatter in the data, the average percentage drift appears to remain fairly constant as the velocity varies. For the forty test the percentage drift averages 3.09%. The average relative deviation from this

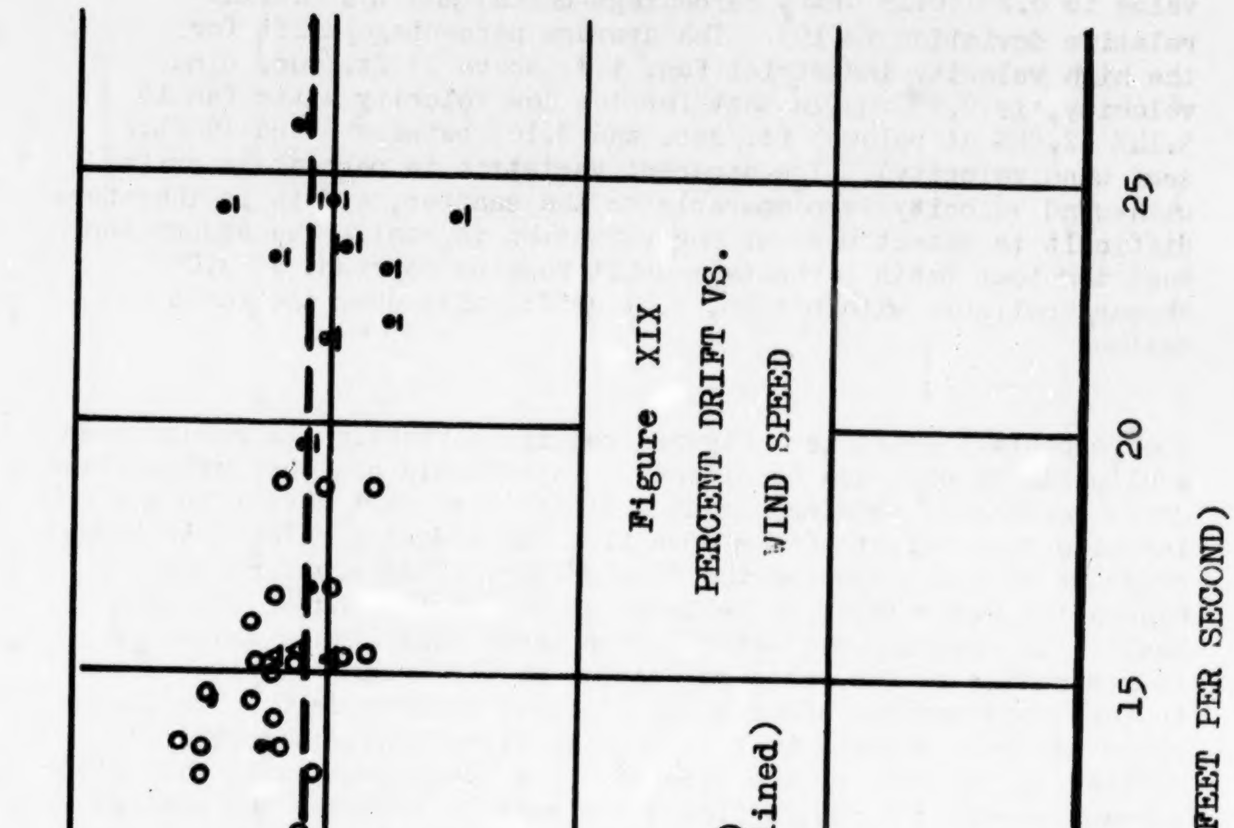
Figure XIX PERCENT DRIFT VS. WIND SPEED

value is 6.2% (0.19 drift percentage units) and the maximum relative deviation is 19%. The average percentage drift for the high velocity industrial fan, i.e. above 19 ft./sec. wind velocity, is 2.98% while that for the low velocity attic fan is 3.14% (2.88% at below 6 ft./sec. and 3.18% between 6 and 19 ft./sec. wind velocity). The apparent variation in percentage drift with wind velocity is comparable to the scatter, and it is therefore difficult to detect whether the variation is real. The assumption that the test basin percentage drift remains constant at 3.09% appears reliable within +.05, -.21 drift units over the range tested.

The percentage drift test figures require correction to render them applicable to open sea conditions. Essentially one must extrapolate drift conditions obtained using a finite wind duct height to the infinite duct height of the open air. In a duct a relatively large pressure drop accompanies the flow of air. This pressure drop causes the water level to be lower at the upwind end of the test basin. In essence, the water in the basin acts like a manometer in responding to the pressure drop. The difference in water level in turn produces two effects which oppose surface drift. One, a slope current, flowing in the opposite direction to the wind is created in the bulk of the liquid. In a closed end basin this slope current provides a return flow which exactly balances the surface drift, thereby satisfying the necessary condition of zero net mass flux. The return ducts accommodate some of the return flow and help minimize the end effects associated with return flow. The return flow is distributed over a larger area and thus has a much lower velocity than the surface flow, which, as will be shown later, is confined to a very thin layer. Since the surface layer is moving counter to the bulk flow the surface drift velocity should tend to be somewhat reduced by the return flow.

Secondly, the oil in moving on the water surface, is moving slightly uphill due to the difference in water level. This should also tend to slow down the oil movement.

A simple theory will help provide insight as to magnitude of the percentage drift and how the duct height correction might be applied. The wind in moving over the water creates a surface shear stress which is proportional to $f \rho_A U^2/2$ where f, the friction factor, is a function of the Reynolds number characterizing the flow, U is the velocity relative to the surface, and ρ_A is the density of the air. If the air is moving over water which is not moving below the surface (i.e. the return flow is distributed over such a wide area that its velocity may be assumed negligible) the velocity profile for the air-water system can be represented by the following sketch.

Figure XX

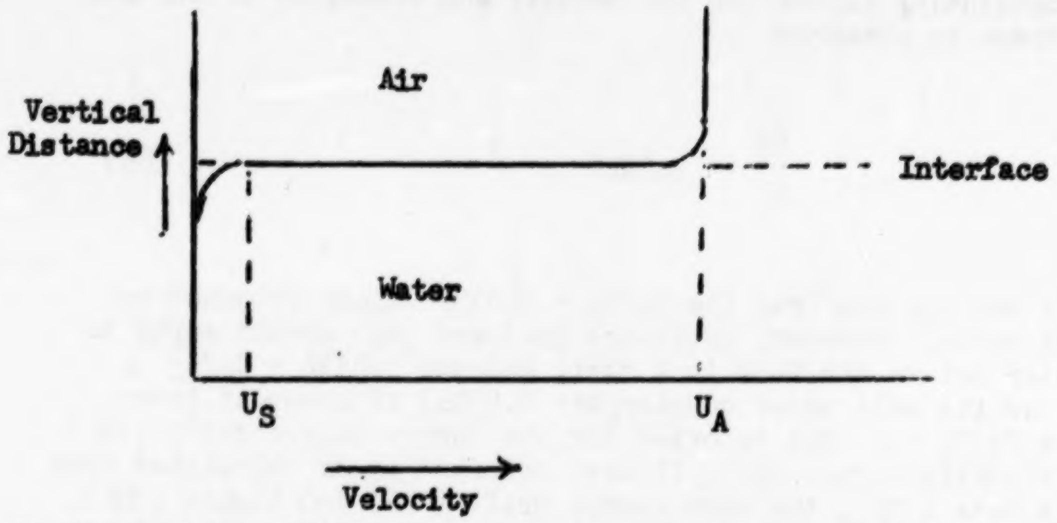

At the surface of the water the shear stress due to the air movement will cause a drift velocity U_S to develop. Relative to the surface of the water, the water appears as if it is moving backwards with a velocity $-U_S$, and the air forward with a velocity $(U_A - U_S)$. At equilibrium the shear stresses due to these two relative flows should be equal, i.e.

$$f_A \rho_A \frac{(U_A - U_S)^2}{2} = f_W \rho_W \frac{(-U_S)^2}{2} \qquad (62)$$

where f_A is the air friction factor, f_W the water friction factor, and ρ_W the water density. For turbulent flow over flat surfaces, the friction factor can be related to the Reynolds number by a simple equation of the form

$$f = K \left(\frac{L U \rho}{\mu} \right)^n \qquad (63)$$

where K is a constant, μ the viscosity, and n a characteristic exponent. For high flow Reynolds numbers, n equals - 1/7 (Falkner (29)). Substituting for f, using a n value of - 1/7, there is obtained upon rearrangement and cancellation of terms which appear on both sides the equation

$$\frac{U_S}{U_A} = \left(\frac{\mu_A}{\mu_W}\right)^{.077} \left(\frac{\rho_A}{\rho_W}\right)^{0.462} \Big/ \left[1 + \left(\frac{\mu_A}{\mu_W}\right)^{.077} \left(\frac{\rho_A}{\rho_W}\right)^{0.462}\right] \tag{64}$$

Upon substituting values for the density and viscosity of air and water, there is obtained

$$\frac{U_S}{U_A} = 0.0318 \tag{65}$$

which is not too far from the $U_S/U_A = 0.0309$ figure obtained in the test basin. However, Equations (64) and (65) should apply to open water not to air flow in a duct, and the $0.0318 = U_S/U_A$ figure (or its salt water counterpart 0.0314) is somewhat lower than the $U_S/U_A = 0.0341$ reported for the Torrey Canyon drift (66) or the slightly higher U_S/U_A figures reported by or calculated from Stroop's data (71), the Gerd Maersk drift (75) and Hughes (33). Equation (65) predicts U_S/U_A values which are significantly higher than those calculated from Thorade's drift equations (73) which appear to be in error.

The percentage drift is not very sensitive to the exact value of n used. For moderately high Reynolds numbers as contrasted to very high Reynolds number a value of -0.2 is sometimes used for n. In such a case U_S/U_A would equal 0.0311, and if n were 0, U_S/U_A would equal 0.0330 (both for fresh water). This insensitivity is due to the fact that the Reynold numbers for the air and water differ only by a factor of 1.8.

In previously considering duct height corrections it was postulated that these were ultimately due to air flow induced pressure drop. Since the flow regime is turbulent for both the water and the air, it will be assumed that the term $f_W \rho_W U_S^2/2$ in Equation (62) will have to be corrected by a term proportional to the air flow induced pressure drop. But this in turn is proportional to $f_A'(\frac{L}{D})\rho_A(\frac{U_A^2}{2})$ where f_A' is the appropriate friction factor for duct flow. Substituting this proportionality in Equation (62) and neglecting the small difference between U_A2 and $(U_A-U_S)^2$ in the left hand side there is obtained after some rearrangement

$$\rho_A U_A 2 \left(f_A - K f_A' \frac{L}{D} \right) = f_W \rho_W U_S 2 \qquad (66)$$

where K is the constant of proportionality in the correction term. Both friction factors f_A and f_A' should show similar functional dependence on the appropriate Reynolds numbers but the characteristic lengths in the Reynolds numbers should be different, D for f_A' and L for f_A. Substituting for f_A and f_A' in terms of these Reynolds numbers and assuming f is proportional to $R_e^{-1/7}$ there is obtained upon rearrangement:

$$\frac{U_S}{U_A} = \left(\frac{\rho_A}{\rho_W}\right)^{0.462} \left(\frac{\mu_A}{\mu_W}\right)^{0.077} \left[1 - K\left(\frac{L}{D}\right)^{1.143}\right]^{0.539} \qquad (67)$$

This is similar to Equation (64) with the correction term $\left[1 + \left(\frac{\rho_A}{\rho_W}\right)^{0.462} \left(\frac{\mu_A}{\mu_W}\right)^{0.077}\right]$ in the denominator dropped and the term $\left[1 - K\left(\frac{L}{D}\right)^{1.143}\right]^{0.539}$ which corrects for duct height added as a factor. It was previously noted that use of the factor $\left(\frac{\rho_A}{\rho_W}\right)^{0.462} \left(\frac{\mu_A}{\mu_W}\right)^{0.077}$ yielded percent drift estimates which were slightly lower than percent drifts measured at sea. Let us assume this factor requires correction and replace it by an unknown factor M. In our tests L the basin length was maintained constant. Introducing M and lumping all the constant terms in Equation (67) there is obtained:

$$\frac{U_S}{U_A} = M \left[1 - \frac{K'}{D^{1.143}} \right]^{0.539} \qquad (68)$$

This equation can be used to obtain both M , the open sea percentage drift, and K' if reliable experimental percentage drift data is available at two different duct heights. If reliable percentage drift data is available at three different duct heights, the validity of Equation (68) can also be checked. Assume U_S/U_A is known at two different duct heights D_1 and D_2. By dividing Equation (68) for case 1 by Equation (68) for case 2 there is obtained upon rearrangement

$$K' = \frac{(U_S/U_A)_1^{1.86} - (U_S/U_A)_2^{1.86}}{\dfrac{(U_S/U_A)_1^{1.86}}{D_2^{1.14}} - \dfrac{(U_S/U_A)_2^{1.86}}{D_1^{1.14}}} \qquad (69)$$

Equation (69) is solved for K' and K' is in turn substituted in Equation (68) where a particular experimental value of U_S/U_A and the corresponding value of D is used to solve for M . If the same values of K' and M are obtained using the different pairs of three different duct heights and corresponding U_S/U_A values Equation (68) would be verified.

Five tests were carried out at lower than normal duct heights. Since the average duct height for these tests did not vary greatly, and individual percentage drift measurements were subject to great variation, the overall average duct and average U_S/U_A value for the tests - 13.1 inches and 0.0259 respectively will be used in calculating K' and M . It can be seen that U_S/U_A at these lower duct heights is significantly smaller than U_S/U_A at the 22 inch duct height, and the duct height correction is therefore quite significant. Using 13.1 inches for D_2 and 0.0259 for $(U_S/U_A)_2$ and the standard duct height 22 inches for D_1 and the previously established value 0.0309 for $(U_S/U_A)_1$, Equation (69) was solved for K'. A value of 8.94 inches$^{1.14}$ was found for K'. This value, when substituted in Equation (68), yielded a value for M of 0.0366 when appropriate values of (U_S/U_A) and D were substituted. Error analysis accounting for the probable errors in the U_S/U_A values at both the low and high duct heights indicates that, based on this value of M, the open-ocean percentage drift should be 3.66% ± .17%. This figure is in quite good agreement with average field data.

It should be noted that the open ocean drift value obtained is only moderately sensitive to the exact method of scaling up to infinite duct height. For example assuming U_S/U_A varies linearly with 1/D and goes to M as 1/D goes to 0 yields a open-ocean percentage drift figure of 3.82 which is not too different from the 3.66 obtained by the present more elaborate procedure.

In contrast to wind duct height, the water depth had a negligible effect on wind drift rates. Three tests were carried out at water depths ranging from 3-1/2 inches to 5-1/2 inches - in contrast to the normal 8 to 10-1/2 inch depth. The average percentage drift for these three tests was 3.14%, which barely differs at all from the 3.09% average drift value for all the normal depth tests.

Similarly it appears that the drift rate is not greatly effected by the viscosity of the water or the oil. The percentage drift for heavy paraffin oil, which is much more viscous than light paraffin oil, averaged 3.11%, which scarcely differs from the normal 3.09% value. Two tests were carried out in which the water temperature was varied appreciably. In one test a temperature of 8.5°C was used and in the other 11°C. The percentage drift for these two tests averaged 3.21%, which is slightly higher than the normal 3.09% value. However the 0.12% difference between these low temperature results and the normal drift results (where the temperature averaged 19 to 25°C) is less than the 0.19% average deviation normally experienced in percentage drift tests, and less than the 0.135% deviation that would, on the basis of error analysis, occur on the average for any random sequence of two tests. In the range 8.5°C to 22°C, water viscosity changes by a factor of 1.4, and if water viscosity were to significantly effect drift, the change should be much more marked and of opposite sign than the slight change noted. Equation (64) indicates the water viscosity should affect the percentage drift. But, the predicted effect for a 1.4 fold change in water viscosity would be only 0.08 percentage drift units, which scarcely could be detected due to the normal scatter in the drift data.

The percentage drift for crude oil (Urania) averaged 2.98% and thus was slightly lower than the normal 3.09% value. However the great bulk of the crude oil tests were made at high velocities using the industrial fan and the difference can be mostly attributed to either the higher velocity or artifacts associated with the use of the industrial fan. Only Urania crude was used in these high velocity tests, because the paraffin oils provided less visual contrast and broke up into small pools, and thus could not be readily observed. In three low velocity tests in which Urania crude was used, the percentage drift averaged 3.08% which is virtually identical with the normal 3.09% figure. It thus appears that differences in percentage drift between crude oils and the paraffin oils used in most of the tests is negligibly small.

Based on the Urania crude tests, the paraffin oil tests, and limited tests with tetradecane the effect of F_s, the surface tension spreading pressure, on wind drift is negligibly small.

The use of salt water as opposed to fresh water had little effect on drift rates. In two tests carried out on 3.5% salt water using Urania crude and wind speeds close to 24.0 ft./sec. the percentage drift averaged 2.96%, which is virtually identical with the 2.98% average drift reported for all tests involving Urania crude and high wind speeds. Equation (64) indicates that a 0.04% reduction in percentage drift should have occurred upon switching from fresh water to salt water. Such a small change could not be detected in our tests. It appears that the test basin results which were mostly obtained with fresh water can equally well be applied to salt water with no significant error.

Tests were carried out at pool volumes different from the standard 50 cc volume. In two tests with paraffin oils at 100 cc volume the percentage drift averaged 2.99% and in one test at 200 cc volume 2.98%. While slightly lower than 3.09%, these results are well within the range of variation of individual tests and the deviation limits that would be expected on the basis of error analysis to occur for a random sequence of three tests. It thus appears that pool volume has a negligibly small effect on percentage drift.

In most tests, the test basin surface was kept fairly clean by sweeping off residual oil. In one wind drift test with paraffin oil, however, the basin surface was deliberately dirtied with crude oil. In this test the drift averaged 3.19%. This value is slightly higher than normal, but because of the large normal scatter in the drift data it is difficult to determine whether the difference is significant or accidental. It was observed that the oil suppressed wave formation and the slight increase in drift effect might be due to this wave suppression action.

It was noted that wave action significantly lowered wind drift. In four tests in which waves having a period of roughly 1 second, a wave length of roughly 45 inches and amplitudes of roughly 4 inches were used, the average percentage drift was 2.66%, as contrasted to the normal 3.09%. Drift caused by these waves alone was found to be small, roughly .01 ft./sec., as determined by tests. Such a drift could only influence the apparent percentage wind drift by 0.07% in the range tested. Therefore the decrease in apparent wind drift could not be due to an undetected wave drift, but must instead be due to increased resistance to wind induced drift, or less effective transfer of momentum from the wind to the oil floating on the water. This is further substantiated by the fact that waves moving in the direction of the wind and waves moving counter to the wind both produced the same reduction in wind drift.

It is believed that reduced efficiency of momentum transfer comes about because there are drag free stagnant zones in the lee of each wave crest. If this is so, longer waves and less sharply peaked waves may cause less reduction in wind drift. With such waves there would be fewer sheltered lee zones and, because the air flow diversion would be more gradual, the relative size of the sheltered areas would be smaller. The testing of this hypothesis through the use of longer period waves would be most desirable. Unfortunately because of limitation in the range of operation of the wave machine, and the depth of the basin, the desired longer period waves could not be generated, and important questions relating to wave wind-drift interaction remain unresolved.

The wind drift retarding effect of waves may explain the slight tendency towards lower drift at high wind speeds. More waves, and waves of greater amplitude were created in the test basin at these higher wind speeds. These wind created waves in turn should somewhat reduce the percentage wind drift - but whether the effect can in fact be reliably detected under the test conditions used is somewhat questionable. Since wind will generate similar waves, but of higher amplitude and greater wave length and spectral variety on the open sea - particularly as the fetch increases - the effects of wind and wave are inextricably bound together. This combined effect must be resolved if reasonable drift predictions are to be made.

Though a twenty foot test basin might appear adequately long, significant end effects are readily apparent. In wind drift tests using wood chips, the wood chip velocity peaked at roughly 5 to 7 feet downstream from the point where oil usually was deposited. Up to that distance the wood was accelerating and beyond it decelerating. This peak velocity sometimes was as much as 9% higher than the average velocity over the usual drift test length. With oil the peaking was less marked, the peak velocity being roughly 3% higher than the mean velocity in the test section. The deceleration is caused in part by approach to the end of the test basin. Because this deceleration starts so far upstream in the basin it is difficult to be certain that the wood chip or oil pool has reached its steady drift velocity prior to deceleration. A forty foot long test basin would increase the available drift test length by a factor of three or four and permit verification that steady state drift velocities had been reached. One complicating factor, which is not an end effect, also might contribute to drift rate reduction as the oil proceeds downstream in the basin. The wave amplitude increases in the downstream direction, and this increase in amplitude, because of the wave-wind drift interaction, could also cause a reduction in percentage drift. The detection, measurement, and correlation of this type of interaction would also be facilitated by a longer basin.

It was observed that wood chips drifted at rates that were significantly lower than those for oil pools at the same test conditions. The following table lists relative drift rates for wood chips and other drift tracers.

Table 8. Relative Drift Rates

	$\frac{\text{Marker Drift Velocity}}{\text{Oil Pool Velocity}}$
3/4" x 3/4" paper marker	.90
Xylene, Dibutyl Phthalate, Zinc Oxide mixture of specific gravity 1.00 floating just below surface	.91
3/4" x 3/4" x 3/32" thick wood chips	.85
3/4" x 3/4" x 3/16" wood chips	.78

It is somewhat remarkable that thin slips of paper floating on the surface and droplets of specific gravity 1.00 liquid floating just below the surface move at a lower velocity than the oil. The reason for this is not known.

The progressive decrease in drift rate with increasing wood chip thickness indicates that the surface drift is confined to an extremely thin layer. A simple model for this surface flow is a velocity profile in which the velocity exponentially decays as the depth below surface increases, i.e.

$$U_D = U_S \; e^{-kZ} \qquad (70)$$

where Z is the depth below the surface, U_D the drift velocity at that depth, U_S the surface drift velocity and k the decay constant. The wood chip data in table three indicates that for such a model k should equal roughly 1.9 in.$^{-1}$. For this k value, the local drift velocity should equal only 10% of the surface drift velocity at a water depth of 1.2 inches.

The average velocity $\overline{U}_D$ over a given depth for this model is given by the formula

$$\overline{U}_D = \frac{U_S}{kZ} [1 - e^{-kZ}] \qquad (71)$$

This formula indicates that for a floating object 1.2 inches deep the drift velocity should be only 39% of the surface drift velocity.

This apparent reduction of drift velocity with depth suggested that the use of shallow drogues or subsurface draggers might markedly reduce wind induced oil pool drift. Accordingly draggers having the configurations shown in Figure XXI were constructed and tested.

In case A, the dragger was dropped to the center of the oil pool. The dragger percent drift was 1.63%, much less than normal oil drift, but most of the pool of oil pulled away from the dragger. In case B, a similar reduction in drift was noted but here much more of the oil was retained by the dragger. In case C no oil was lost, and the percent drift was 1.51%. The drift reductions are of the order of magnitude that might be expected through the use of Equation (71) with a k value of 1.9 in.$^{-1}$.

These tests indicate the technical feasibility of reducing wind drift by a factor of two or more through the use of draggers. A slight degree of confinement is apparently necessary to prevent oil from pulling away from the dragger. The economic feasibility of using draggers depends on developing cheap simply produced draggers which can be readily disseminated.

It is noteworthy that configuration C also prevented crude oil from spreading and thus effectively confined the spill to an area many times smaller than it would normally occupy. It is quite possible that a floating net like array made up of foamed plastic strands could be used to provide a similar type of confinement for large oil spills.

Wave Drift

It was previously noted that wave drifts of 0.01 ft./sec. were noted for wave action alone. This is markedly less than predicted

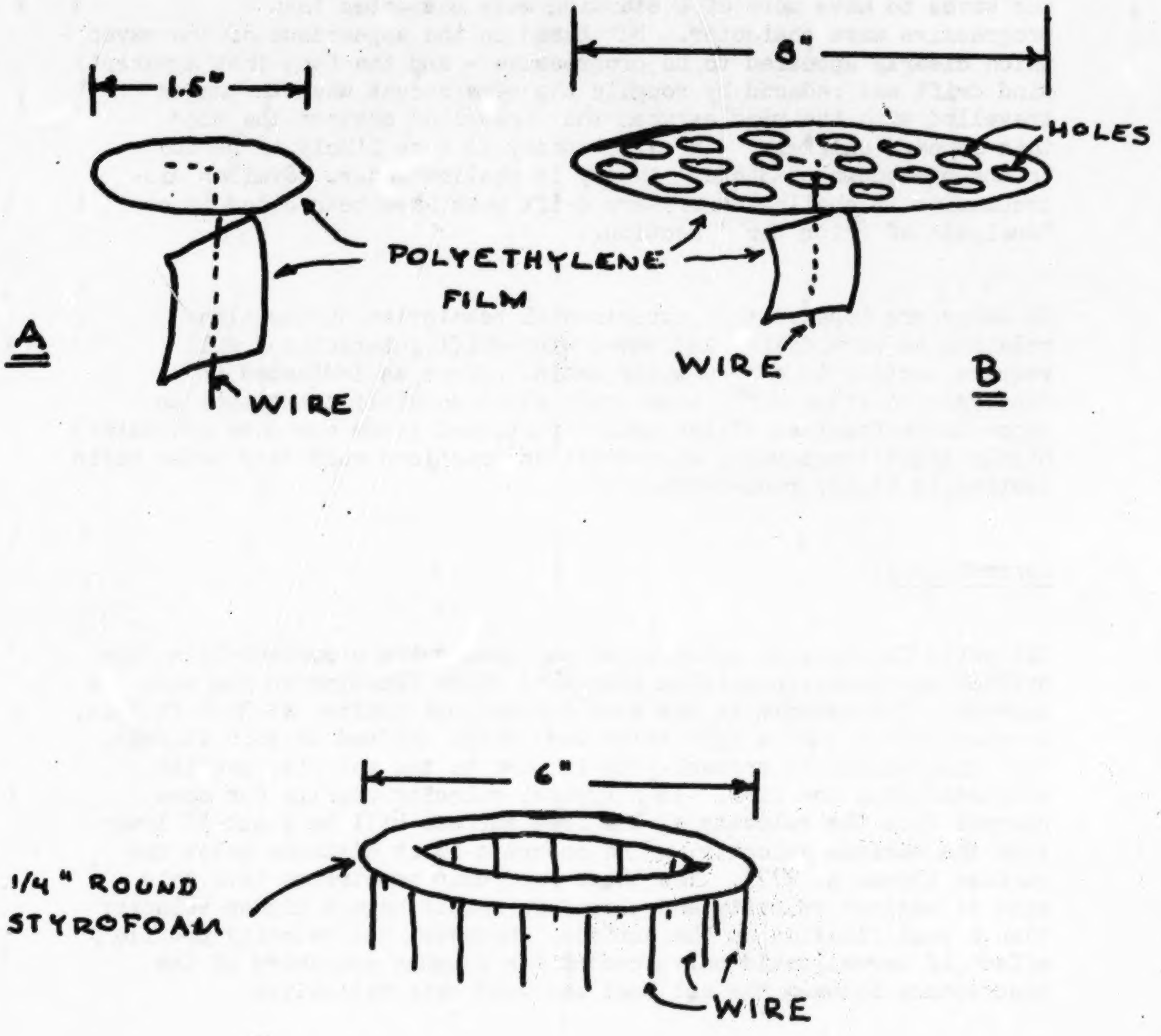
1.5"
8"
HOLES
POLYETHYLENE FILM
A
WIRE
WIRE
B
6"
1/4" ROUND STYROFOAM
WIRE
C

FIGURE XVI

DRAGGERS

by Stokes' correlation, Equation (30), which indicates a wave drift of 0.2 ft./sec. In part this discrepancy may be due to inadequate dampening of wave reflection, which could have caused the waves to have more of a standing wave character than a progressive wave character. But based on the appearance of the waves - which clearly appeared to be progressive - and the fact that apparent wind drift was reduced by roughly the same amount when the waves travelled with the wind as when they travelled against the wind this appears unlikely. The discrepancy is more likely to be due to the breakdown of Stokes' theory in shallow water. Similar discrepancies in shallow water wave drift work have been cited in our "Analysis of Prior Work" section.

It therefore appears that experimental resolution of questions relating to wave drift, and wave, wind-drift interactions will require testing in a deep water basin. Since, as indicated in "Analysis of Prior Work", wave drift might possibly constitute an appreciable fraction of the total drift, and since our work indicates highly significant wave, wind-drift interactions such deep water basin testing is highly recommended.

Current Drift

Oil pools floating on water which was undergoing a current-like flow drifted at slower velocities than wood chips floating in the same current. For example, in the same current, oil drifted at 30.6 ft./min. whereas 3/4" x 3/4" x 1/4" thick wood chips drifted at 36.0 ft./min. This discrepancy is probably due in part to the velocity profile characterizing the flow. In a typical velocity profile for open channel flow the velocity at the free surface will be about 5% lower than the maximum velocity, which occurs a short distance below the surface (Rouse p. 277). The thick wood chip penetrates into this zone of maximum velocity and therefore should have a higher velocity than a pool floating on the surface. However, the velocity profile effect, if normal, would only account for roughly one-third of the discrepancy between the oil pool and wood chip velocities.

When machine made waves (having the characteristics previously described) are superimposed on the current like flow, the oil pool drift and the wood chip drift become virtually identical - the difference in drift being less than 1% of the drift velocity. This may well be due to wave induced uniformity in the velocity profile. Since conditions at sea are wavy it appears valid to assume that oil pools will experience a current induced drift equal to surface drift associated with the current.

The surface currents are not uniform in the length direction in the test basin. For distances moderately removed from the downstream end of the test basin the surface current increases in the downstream direction. This is probably due to a transition from the uniform velocity profile imposed by the flow distributor grid at the upstream end of the test basin to the normal flow profile which is peaked near the free surface.

Combined Wind-Current Drift

Sixteen tests were carried out in which floating oil pools were subjected to both wind and current action. The results of these tests are tabulated in Table 9. In these tests the wind drift was measured in the absence of currents, and the current drift measured in the absence of the wind, and then the combined drift for the same current pumping speed, and fan speed was measured.

In all cases the contribution of the current to the combined drift was less than the current drift in the absence of wind. This result is very startling and contrary to prior expectations and the usual assumption of the simple vector additivity of drifts. The combined drift T is very roughly correlated by the equation

$$T = W + 0.557\,C \qquad (72)$$

Although the average deviation from this equation was only 6.4% and the maximum deviation 13.4%, the agreement is only fortuitous and the equation can not in general be correct. It is obvious that as W goes to zero, T should approach C, not $.557\,C$ as indicated by the equation. This requirement implies that the coefficient for C should increase as W decreases, but the data provides no indication of such an increase. The cause for the lack of additivity of the wind and current drifts has not been determined in spite of considerable effort.

Table 9. **Combined Wind and Current Drift**

Wind Velocity	W Wind Drift	C Current Drift	W+C Sum of Drifts	T Actual Combined Drift	W+C-T	(W+C-T)/C
(		ft./sec.		)		
7.93	.220	.294	.514	.379	.135	.469
10.36	.248	.270	.518	.365	.153	.566
16.25	.466	.293	.759	.591	.168	.572
12.55	.396	.149	.545	.470	.075	.503
10.55	.321	.149	.470	.395	.075	.503
25.87	.604	.322	.926	.756	.171	.528
26.62	.774	.342	1.116	.898	.218	.637
25.95	.831	.327	1.158	.889	.266	.813
23.68	.600	.330	.930	.845	.085	.258
23.24	.650	.330	.980	.881	.099	.300
21.01	.597	.370	.967	.750	.217	.586
25.04	.750	.351	1.101	1.000	.101	.288
24.80	.639	.351	.990	.889	.101	.288
25.23	.686	.380	1.069	1.020	.049	.129
24.95	.697	.373	1.070	.970	.100	.268
22.20	.598	-.191	.407	.444	-.037	.193
					Average	.443

There is no marked trend in the additivity behavior as the wind velocity or wind-drift, current drift ratio varies. This combined drift result is at such variance with the anticipated simple additivity, and the limiting relationship that must hold when W equals zero, that it must be viewed with suspicion.

It is possible that current induced turbulence could increase the shear stress friction factor on the water side of the air-water interface. If this were the case the wind induced drift would be reduced and the combined drift would be less than the sum of the individual drift.

It should be noted that only one test was run with the current opposing the wind. In that test there was a large scatter in the current drift data, and the deviation from Equation (72) was fairly large. However even in this case the contribution of the current drift to the combined drift was less than the current drift in the absence of wind.

References

(1) Abbot, M.B., La Houille Blanche, No. 5, pp 622-628, (Oct. 1961), No. 6, pp 827-846, (Dec. 1961).

(2) Adam, N.K., Proc. Roy. Soc. (London), B122, p 134(1937).

(3) Adam, N.K., "The Physics and Chemistry of Surfaces", pp 7-10, 209-215, 363-389, Dover, New York (1968).

(4) Anon., Clearing up the Oil, Petroleum, p 95, May/June 1967.

(5) Bagnold, R.A., J. Instn. Civ. Engrs., 27, p 467 (1947).

(6) Barrillon, E., and P. Woog, Ann. Off. Nat. Combustible Liquide, 2, p 274.

(7) Bashforth, F., and J.C. Adams, "An Attempt to Test the Theory of Capillary Action", (Cambridge), London (1883).

(8) Battelle Memorial Institute, "Oil Spillage Study, Literature Search and Critical Evaluation for Selection of Promising Techniques to Control and Prevent Damage" to Dept. of Transportation, U.S. Coast Guard, Nov. 20, 1967, AD 666 282.

(9) Benyon, L.R., "The Torrey Canyon Incident - A Review of Events", the British Petroleum Company Limited (Sept. 1967).

(10) Benyon, L.R., Filtration and Separation, 5, p 360, (1968); Oil and Gas International, 8, p 52, (June 1968).

(11) Blokker, P.C., "Spreading and Evaporation of Petroelum Products on Water", 4th International Harbor Conference, Antwerp, Belgium, June 1964.

(12) Blokker, P.C., Deutsche Gewesserkundl. Mitt. 10, pp 112-114 (1966).

(13) Bradley, R.S., Trans. Faraday Soc., 36, p 199 (1940).

(14) Brinkman,R.Biochem. Z. 139, p 274 (1923).

(15) Cary, A. and E.K. Rideal, Proc. Roy. Soc. A109, p 312 (1925).

(16) Chang, M.S., Jour. of Geophysical Research, 74, pp 1515-1536 (1969).

(17) Chin, H. and W.J. Pierson, "Sixth Symposium on Military Oceanography", (in print 1969).

(18) Coghill, W.H. and C.O. Anderson, "U.S. Bureau of Mines Tech. Paper 262" (1923).

(19) Coligny, A.F.H., Compt. Rend. Acad. Sci. Paris, 52, p 1309 (1861); 87, p 10 (1878).

(20) Costin, M., P. David, R. Gerard, and B. Katz, Report CU 2-63, Lamont Geological Observatory, Palisades, N.Y. (1963).

(21) Cowan, E., "Oil and Water, The Torrey Canyon Disaster", Lippincott (1968).

(22) Defant, A., Ann. d. Hydr. u. Marit. Meteorol., 46, p 78 (1918).

(23) Dennis, J.V., "Oil Pollution Survey of the United States Atlantic Coast", Amer. Petr. Inst., (May 15, 1955).

(24) Dennis, J.V., "Oil Pollution Survey of the Great Lakes within the United States Territorial Limits", Amer. Petr. Inst. (Jan. 15, 1960).
(25) Dennis, J.V., "Oil Pollution Conditions of the Florida East Coast", Amer. Petr. Inst., (May 15, 1960).
(26) Dennis, J.V., "The Relationship of Ocean Currents to Oil Pollution off the Southeastern Coast of New England", Amer. Petr. Inst., (Jan. 23, 1961).
(27) Dorsey, N.E., J. Washington Acad. Sci., 18, p 505 (1928).
(28) Ekman, V.W., Ark. f. Mat. Astron. och Fysik, 2, No. 11, pp 1-53, (1905).
(29) Falkner, V.M., Aircraft Eng., 15, p 65, (1943).
(30) Foxworthy, J.C., R.B. Tibby, and G.M. Barsom, Jour. Water Poll. Control Fed., 37, p 1170, (1966).
(31) Garrett, W.D., "Factors Effecting the Use of Monomolecular Films to Control Oil Pollution on Water", presented to Div. of Waste Chemistry, Amer. Chem. Soc., Minneapolis, Minn., April 15, 1969.
(32) Hardy, W.B., Proc. Roy. Soc., A88, p 313, (1913); A86, p 610 (1912).
(33) Hughes, P., Q. Jnl. R. Met. Soc., 82, pp 494-502, (1956).
(34) Joseph, J., and H. Sendner, Deut. Hydrogr. Zeit., 11, No. 2, pp 49-77 (1958).
(35) Koningliijk Neederlandsch Meteorologisch Institut, De Bilt, "Oceanog. Meteolg. Waaremingen, Atlantische Oceaan", No. 111 Karter, (1918).
(36) Krummel, O., "Handbuch der Ozeanographie" Vol. I (1907); Vol. II (1911), J. Engelhorn, Stuttgart.
(37) Langmuir, I., J. Chem. Phys., 1, p 756 (1933).
(38) Lippok, W., Deutsche Gewasserkundl. Mitt., 10, pp. 145-57 (1966).
(39) Lippok, W., ibid., 10, pp 105-112 (1966).
(40) Longuet-Higgins, M.S., Phil. Trans. Roy. Soc., A245, pp 535-581 (1953).
(41) Lyons, C.G., Trans. J. Chem. Soc.(London), p 623 (1930).
(42) Ministry of Transport and Civil Aviation, "Report of the Committee on the Prevention of Pollution of the Sea by Oil", London, H.M. Stationery Office, (1953).
(43) Mitchim, W.F., M. Sc. Dissertation, Univ. of California (1939).
(44) Morlock, R., "Recherches sur les Champs de Force Superficiels at l'etalement des Liquides", Thesis, Marseille (1947).
(45) Moskowitz, L., J. Geophys. Res., 69, No. 24, pp 5161-5179 (1964).

(46) Moss, J., "Character and Control of Sea Pollution by Oil", Amer. Petr. Inst. (1963-1965).

(47) Neumann, G., Ann. d. Hydr. u. Marit. Meteorol., 67, p 82 (1939).

(48) Neumann, G., and W.P. Pierson, "Principles of Physical Oceanography", Prentice-Hall, Englewood Cliffs, N.J. (1966), p 146, 147, 209.

(49) Obukhov, A.M., Advances in Geophysics, 6, No. 113, Academic Press, (1959).

(50) Okubo, A., Tech. Rept. 30, Ref. 62-29, Chesapeake Bay Inst. Johns Hopkins Univ., (1962).

(51) Okubo, A. and D.W. Pritchard, "Disposal of Radioactive Wastes, II, p 229, Int. Atomic Energy Agency, Vienna (1960).

(52) Ozmidov, R.V., Dokl. Akad. Nauk. S.S.S.R., 120, p 761 (1958).

(53) Pattison, D.A., Chemical Engineering, 76, p 50 (Feb. 10, 1969).

(54) Pierson, W.J. and L. Moskowitz, J. Geophys. Res., 69, No. 24, pp 5181-5190 (1964).

(55) Pierson, W.J., G. Neumann, and R.W. James, H.O. Publ. 603, U.S. Navy Hydrographic Office, Washington, D.C., (1955).

(56) Pierson, W.J., Tech. Rept. Contr. Nonr 285(03), College of Eng. Res. Div. New York Univ., (1961).

(57) Pilpel, N., Endeavour, XXVII, p 11, (Jan. 1968).

(58) Poisson, S.D., cited in "Handbuch der Exp. Physik", Vol. VI, p 98 (1928).

(59) Porter, A.W., Phil. Mag., 15, p 163 (1933).

(60) Purchas, D.B., Filtration and Separation, 5, p 360 (1968).

(61) Ramdas, L.A., Proc. Indian Assoc. Cult. Science, 10, p 1 (1926).

(62) Reynolds, O., "Works", Volume I, British Assoc. Report, p 410 (1881).

(63) Rouse, H., "Fluid Mechanics for Hydraulic Engineers", Dover, New York (1961).

(64) Schumacher, A., Ann. d. Hydr. u. Marit. Meteorol., 68, p 109 (1940).

(65) Sigwalt, R., Compte Rend., 259, p 56 (1964).

(66) Smith, J.E., '"Torrey Canyon" Pollution and Marine Life', Cambridge (1968).

(67) Smith, J.W., "The Torrey Canyon Disaster", British Assoc. for the Advancement of Science Annual Meeting, Leeds, England, Sept. 6, 1967.

(68) Spooner, M.F., and G.M. Spooner, "The Problem of Oil Spills at Sea", Marine Biological Assoc. of the United Kingdom, the Laboratory, Citadel Hill, Plymouth, England.

(69) Stehr, E., "Berechnungsgrundlagen fur Pressluft Olsperren", Mitt. Hannov. Ver. Ans. f. Grundbau. u. Wasserbau, Franzius Instit., Hannover, (1959).

(70) Stokes, G.G., Trans. Camb. Phil. Soc., 8, p 441 (1847).

(71) Stroop, D.V., "Report on Oil Pollution Experiments, Behaviour of Fuel Oil on the Surface of the Sea", Bureau of Standards, Dept. of Commerce, Washington, D.C. (Dec. 1927).

(72) Sugden, S., J. Amer. Chem. Soc., 121, p 858, (1922); 125, p 27 (1924).

(73) Thorade, H., Ann. d. Hydr. u. Marit. Meteorol., 42, p 379, (1914).

(74) Tick, L.J., J. Math. Mech., 8, pp 643-652 (1959).

(75) Tomczak, G., Ozeanographie, 10, pp 129-130 (1964).

(76) U.S. Beach Erosion Board, Technical Report No. 1 (1941), Washington, D.C., U.S. Government Printing Office.

(77) Witting, R., Ann. d. Hydr. u. Marit. Meteorol., 37, p 193 (1909).

(78) Woog, P., "Contribution a l'etude du graissage", p 87, Paris, (1926).

(79) Woog, P., "Graissage, Onctuosite, Influence Moleculaire", p 88, Paris (1926).

(80) ZoBell, C.Z., Int. J. Air Wat. Poll., 7, p 173-198 (1963).

(81) Zuckerman, S., "Report of the Committee of Scientists on the Scientific Aspects of the Torrey Canyon Disaster", H.M. Stationery Office, London (1967).

(82) Zuidema, H.H., and Waters, G.W., Ind. Eng. Chem. Anal. Ed., 13, p 313 (1941).

Notation

In carrying out this project, reference is made to work in several different disciplines, and by many different authors. In such work, traditional commonly accepted systems of notation have developed. In the present work these commonly accepted systems of notation have been retained for the most part. This serves to prevent confusion in comparing the present and prior work. However it has led to the same letter symbol having different meanings depending on its context. In all cases the correct meaning should be clear from the context involved, but to prevent any confusion where multiple definitions are provided for the same letter, each multiple definition in the following table is referred back to the first equation of a given sequence in which it is used.

A	Angle at edge of lens (Figure II, Equations 9, 10)
A	Wave amplitude (Equation 29)
A	Spill Area (Equations 52, 53)
a	Capillary constant $[2\sigma / g(\rho_2 - \rho_1)]^{1/2}$
B	Angle at edge of lens relative to extended edge surface of water
b	Channel width
C	Concentration (Equation 26)
C	Current Drift Velocity (Equation 72)
D	Pool Diameter (Equation 8)
D	Duct Height (Equation 66)
f	Linear tension (Equation 18)
f	Friction factor (Equation 62)
F	Force
F_s	Spreading force $(\sigma_L - \sigma_u - \sigma_i)$
g	Acceleration of gravity
H	Height of Wind Duct (Equation 37)

h	Lens submergence (Figure I, Equation 3)
h	Water depth (Equations 29, 30)
K	Effective diffusivity (Equation 26)
K	Constant in friction factor relationship (Equation 63)
K'	Duct height correction factor (Equation 68)
K	Spreading rate coefficient (Equations 23, 53)
k	Attenuation vs depth factor for surface drift (Equation 79)
KE	Kinetic energy
L	Length of duct, length of wind path
ℓ	Spill length
M	Wind drift proportionality factor (Equation 68)
n	Exponent
P	Hydrostatic pressure
PE	Potential energy
R	Radius of curvature (Equation 1)
R	Lens or pool radius (Equations 19, 22, 55)
r	Distance from center of pool (Equation 26)
S	Spectral distribution function for wave energy
T	Total drift velocity (Equation 72)
T	Basin Depth (Equation 37)
T	Wave period (Equation 32)
T	Period of oscillation (Equation 22)
t	Lens thickness (Figure I, Equation 2)

U_S	**Water surface velocity due to wind shear (Figure XX, Equation 62)**
U_A	**Air velocity (Figure XX, Equation 62)**
U_D	**Water velocity below free surface (Equation 72)**
$\overline{U}$	**Mean forward velocity due to wave motion (Equation 29)**
U_r	**Radial velocity (Equation 56)**
V	**Surface drift velocity (Equation 26)**
$\overline{V}_w$	**Average wind velocity over water (Equation 37)**
$\overline{V}_D$	**Average wind velocity in duct (Equation 37)**
$\overline{V}_o$	**Average oil velocity (page 41)**
V	**Spill volume (Equations 7, 24, 38, 53)**
W	**Wind drift velocity (Equation 72)**
W	**Wind speed (Equation 26)**
W	**Depth of water in basin (Equation 37)**
z	**Depth below free surface of liquid (Equation 2)**
Z	**Depth below mean free surface (Equation 29)**

Greek Letters

α	**Angle between wind path and drift path**
θ	**Latitude**
Δ	**Difference**
Θ	**Time**
λ	**Wave length**
ρ	**Density**
σ	**Surface or interfacial tension**
ω	**Angular frequency of wave motion**
μ	**Viscosity**

Subscripts

A	Air
C	Critical or transition between types of spreading
D	Subsurface (Equation 70)
D	In duct (Equation 37)
i	Interfacial
L	Lower layer (eng. water) in lens system (Equation 3)
L	Acting to the left (Equation 3)
o	Original (Figure XVIII, Equation 54)
o	At the free surface (Equation 30)
o	Oil (page 41)
P	Due to hydrostatic pressure
R	Acting to the right
r	Radial
u	Upper layer (e.g. oil) in lens system
z	In vertical direction
w	Water, over water
1	Above interface, major
2	Below interface, minor
100	For 100 cm^3 volume
∞	Limiting case for large lenses or fully spread spill